NUMERICAL SIMULATION OF TWO-PHASE FLOW IN DISCRETE FRACTURES USING RAYLEIGH-RITZ FINITE ELEMENT METHOD

A Thesis

by

SANDEEP P. KAUL

Submitted to the Office of Graduate Studies of
Texas A&M University
in partial fulfillment of the requirements for the degree of

MASTER OF SCIENCE

December 2003

Major Subject: Petroleum Engineering

NUMERICAL SIMULATION OF TWO-PHASE FLOW IN DISCRETE FRACTURES USING RAYLEIGH-RITZ FINITE ELEMENT METHOD

A Thesis

by

SANDEEP P. KAUL

Submitted to the Office of Graduate Studies of
Texas A&M University
in partial fulfillment of the requirements for the degree of

MASTER OF SCIENCE

Approved as to style and content by:

David S. Schechter (Chair of Committee)	Robert A Wattenbarger (Member)
Wayne Ahr (Member)	Hans Juvkam-Wold (Head of Department)

December 2003

Major Subject: Petroleum Engineering

ABSTRACT

Numerical Simulation of Two-Phase Flow in Discrete Fractures Using Rayleigh-Ritz Finite Element Method.

(December 2003)

Sandeep P. Kaul, B. Tech., G. B. Pant University, India;

B.A.P.E.T., Southern Alberta Institute of Technology, Canada

Chair of Advisory Committee: Dr. David. S. Schechter

Spontaneous imbibition plays a very important role in the displacement mechanism of non-wetting fluid in naturally fractured reservoirs. We developed a new 2D two-phase finite element numerical model, as available commercial simulators cannot be used to model small-scale experiments with different boundary conditions as well as complex boundary conditions such as fractures and vugs. Starting with the basic equation of fluid flow, we derived the non-linear diffusion saturation equation. This equation cannot be put in weighted-integral weak variational form and hence Rayleigh-Ritz finite element method (FEM) cannot be applied. Traditionally, the way around it is to use higher order interpolation functions and use Galerkin FEM or reduce the differentiability requirement and use Mixed FEM formulation. Other FEM methods can also be used, but iterative nature of those methods makes them unsuitable for solving large-scale field problems. But if we truncate the non-linear terms and decouple the dependent variables, from the spatial as well as the temporal domains of the primary variable to solve them analytically, the non-linear FEM problem reduces to a simple weighted integral form, which can be put into its corresponding weak form. The advantage of using Rayleigh-Ritz method is that it has immediate effect on the computation time required to solve a particular problem apart from incorporating complex boundary conditions. We compared our numerical models with the analytical solution of this diffusion equation. We validated the FDM numerical model using X-Ray

Tomography (CT) experimental data from the single-phase spontaneous imbibition experiment, where two simultaneously varying parameters of weight gain and CT water saturation were used and then went ahead and compared the results of FEM model to that of FDM model. A two-phase field size example was taken and results from a commercial simulator were compared to the FEM model to bring out the limitations of this approach.

DEDICATION

To my beloved parents, my sister and her lovely family for their love, care, and continued inspiration.

ACKNOWLEDGMENTS

I would like to express my deepest gratitude and appreciation to Dr. David S. Schechter, chair of my advisory committee for his continuous trust and encouragement – two virtues which kept me going when I had very well decided in the middle of the course work to permanently wind down my degree because of financial concerns and student visa regulations. This is the product of his vision, patience and support.

I would also like to thank Dr. Robert A. Wattenbarger and Dr. Wayne Ahr for serving as committee members and helping me in my research.

I would also like to thank Dr. Thomas A. Blasingame for his personal effort and trust in my abilities and giving me admission to this department at a short notice of five days.

I would like to thank Dr. Erwinsyah Putra for his unflinching support and constructive technical critique. Without his support this challenging work would not have reached to its logical conclusion.

I would like to thank Dr. Arun Khargoria for his support and technical help even though more than once he could have flatly refused because of his Ph. D defense.

Finally, I want to thank my friends in the naturally fractured reservoir group, Zuher Syihab, for his technical help and especially his software skills, Vivek Muralidharan, for his experimental work, Deepak Chakravarthy, for programming the intricate fracture network schemes, Prasanna K. Tellapaneni, for helping me with valuable suggestions on reservoir simulation and help run *CMG*® files, Deepak Devegowda, for suggesting solution of mobility equation, Manoj Sarfare and Jesus Galaviz, for introducing me to the wonderful world of *Mathematica*® and *Maple*®, Manmeet Vedi, for clarifying the basics of finite element analysis when I had none. Last, but certainly not the least, I would like to thank my friends in Canada, Robert Vaz, Ravinder Reddy, Satpal Chawla and Shashi Bellihal, whose help went a long way to help me set foot in College Station. I would also thank all others whom I have not mentioned for making my years as a graduate student pleasurable, rewarding and my

pure inability to appreciate their support, because of a lack of realization during my stay here. I would also like to acknowledge the guidance provided by the faculty of the Department of Petroleum Engineering, Texas A&M University and the Department of Energy, United States Government, under whose aegis this work was carried out.

Thank you very much.

TABLE OF CONTENTS

Page

CHAPTER Page

CHAPTER Page

LIST OF FIGURES

FIGURE Page

LIST OF TABLES

CHAPTER I

INTRODUCTION AND LITERATURE REVIEW

1.1 Introduction

The quest to produce more oil has led various researchers to evaluate more complex reservoirs such as naturally fractured ones. The complexity of fluid flow in these types of reservoirs arises from the fact that there are two media, which can allow fluids to flow through them. This leads to the logical conclusion that there are two principal media of fluid flow. The first is through the porous medium called the matrix flow and the other is the flow through the fracture network. At the heart of this phenomenon lies the problem of interaction of these two flow media with each other. In naturally fractured reservoirs the matrix acts as a source where hydrocarbons are present whereas the fractures facilitate in fast recovery of these hydrocarbons. Hence it is important to study what makes the matrix produce more oil. Water is used as a means to efficiently displace oil as discussed in detail by Craig[1]. But fluid flow in porous media, which is determined primarily by capillary force, is relatively difficult phenomenon to quantify and there has been much research effort directed in this direction like that of Handy[2], Garg *et al.*[3], Babadagli and Ershaghi[4], Li and Horne[5], Akin and Kovscek[6], Reis and Cil[7], Zhou *et al.*[8], to name a few. Also, depending on the geometry of the fracture, there may or may not be any capillary force in the fracture network. This imparts spontaneity to fluid flow within naturally fractured reservoirs. Given the complexity of quantifying the spread of fractures, it is even difficult to ascertain the limits where the fracture flow acts as an independent flow entity instead of being a part of porous matrix.

Although very wide in its scope, fluid flow studies in fractured media, as we have narrowed it down, deals exclusively with the study of this spontaneous phenomenon that helps displace oil out of matrix. This paper deals with quantifying, with the help of a numerical model, the experimental study of spontaneous imbibition

---

This thesis follows the style and format of *Journal of Petroleum Technology*.

process in both unfractured and fractured cores having negligible capillary pressure in the fracture.

The challenge associated with undertaking such experimental studies, on a laboratory scale, is that commercially available simulation softwares have some limitations. They are not designed for such a task. Out of the two popular softwares available to us, one has to have aquifer as a constant pressure boundary condition, whereas the other would not run without wells in place, thus undermining the spontaneity of the process of fluid flow. This made it amply clear to us that, if we had to understand the spontaneous imbibition process on the laboratory scale then, we would have to come up with our own numerical model which would have to be flexible enough so that the affect of various parameters on spontaneous imbibition process can be studied in-depth. As a tool to verify this numerical model, we used X-Ray Tomography, as it is the best tool available to study fluid flow in porous media.

1.2 Reservoir Engineering Fundamentals Pertaining to Simulation

There are various fundamental properties which need to be evaluated before reservoir simulation can be carried out. These properties impact reservoir simulation to a very large extent and are classified as:

1. Rock Properties
2. Fluid Properties

1.2.1 Reservoir Rock Properties

Rocks are generally filled with fluids such as oil, water or gas or combinations of these fluids. Our aim is to quantify the fluids contained in these rocks, their transmissibility, and other related properties. What is common in these properties and their distribution is that they all depend on the rock and its type. The rock properties which are relevant to us are:

1. Porosity
2. Permeability
3. Fluid Saturation

Porosity is the volume of pore space within the rock as compared to the total bulk volume. This gives us an idea about the portion of rock that is composed of interconnected spaces. Porosity is classified according to the mode of origin as (*a*) original and (*b*) induced. Original porosity is present on account of the geology of the place and typically represents the intergranular space in the rock. The induced porosity is represented by that part which develops on account of interplay of various geological forces acting at a particular place. Fractures and Vugs are the most common type of such porosity. Depending on the geological environment, the rocks may have cementing material or may be filled with other types of fillers. Thus both the above types of porosities may be represented by (i) total porosity and (ii) effective porosity. This depends on the amount of sealing of the pore spaces achieved by the cementing or sealing material. This differentiation is more prevalent in case of natural fractures where these are filled with crystalline or mineralized material. From reservoir engineering point of view, effective porosity is the important parameter as it represents the space which is occupied by mobile fluids.

Permeability, more specifically absolute permeability, is the ability of the rock to allow one particular type of fluid to pass through it. It gives the measure of those interconnected spaces that are connected throughout instead of those terminating into a dead end inside the rock. The latter ones act as small storage spaces for the fluid. Thus it is the measure of the capacity of a porous medium to transmit fluids. Thus permeability, like porosity, can be defined by two parameters; (a) Absolute permeability and (b) Effective permeability. The significance of the latter comes to light in case of more than one type of fluid being present in the pore spaces. A detailed analysis is discussed in the relative permeability section. Many researchers have tried to classify permeability for porous rocks as a bunch of tubes and the accompanying fluid flow by Poiseuille's equation. In the like manner, the fluid flow in fractures is assumed to be take place between a set of parallel plates each at rest. Thus it is not uncommon to find the permeability of rocks to be in millidarcys whereas in case of a fracture it ranges in several darcys. In case of oil reservoirs permeability exists in layers that is, in three

dimensions, permeability is almost the same in a plane but different in the perpendicular direction to that plane. Hence we have different forms of permeability averaging in order to arrive at a particular value of permeability.

Fluid saturation is another important factor to be considered because it gives an idea of storage of fluids, both hydrocarbons and water, as well as conduction capacity of the porous rock. When we try to recover hydrocarbons, we change the fluid saturation levels in the reservoir rock. Not all of it can be recovered and it difficult to demarcate exactly the fluid saturation in the reservoir, but it is important to know how much accumulation is present down there initially. Thus in order to determine the quantity of hydrocarbons present, it is important to determine the fluid saturation of oil, water and gas with reasonable amount of accuracy present initially.

1.2.2 Reservoir Fluid Properties

As discussed previously, the fluid saturations are important to whole process of recovery of hydrocarbons. If only one fluid be present in the pore spaces then there is only one set of force present, namely the force of attraction between the rock and the fluid. When two or more fluids are present in the reservoir, then they interact with each other. For it, apart from the force of attraction between the rock and each of the fluids, there is interaction between the fluid molecules. The net resultant attractive force on the molecule is zero but at the interface the forces are unbalanced and give rise to interfacial tension. Thus for two or more fluids in the pore spaces, there are at least three sets of forces which effect the fluid movement. This gives rise to the following phenomena:

1. Wettability
2. Capillary Pressure
3. Relative Permeability

Wettability is defined as the tendency of one fluid to adhere to a solid surface. Thus the idea directly follows that different fluids will adhere to different type of rock material differently. The conceptual idea of wettability is illustrated by Young-Dupre equation, as given in Craig[1], and illustrated in **fig. 1.1**.

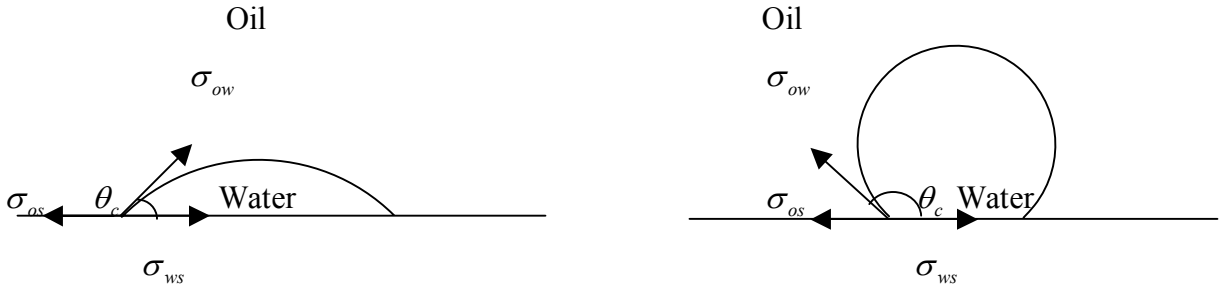

Figure 1.1 – Conceptual Representation of Wettability, (a) Water-wet Rock, (b) Oil-wet Rock after Reference 1

As can be seen from the above figure, wettability is expressed as an angle θ_c. The balance of three forces, namely σ_{os} - interfacial tension between the solid and the lighter fluid; σ_{ws} - interfacial tension between solid and denser fluid; and σ_{ow} - interfacial tension between the fluids, determines this angle. For angles less than 90^o, the rock is considered to be water wet whereas for angles greater than 90^o, it is known as oil wet. For angles near 90^o it is referred to as mixed wet. What can be made out of the measured angle is the fact that the wetting fluid which has affinity towards the rock tries completely to spread over the surface of the rock. Hence the angle for strongly water wet rock nears zero and for strongly oil wet rock it is nearer to 180^o. It order to understand the full impact of wettability, it is a good idea to refer to **fig. 1.2**, as per reference 1, showing the work of Raza *et al*. This figure clearly illustrates the importance of efficiency of displacement of oil with water is directly dependent on wettability. The first figure illustrates the drainage process because the rock is oil wet and water is forcing itself in order to displace oil. The second figure illustrates imbibition process, since the rock is water wet and water imbibes rather than forces through the pores to displace oil. Wettability is also measured with the help of Amott Wettability Index, where a scale ranges from -1(Oil wet) to 1(Water wet). All mixed wet rocks have wettability index around zero.

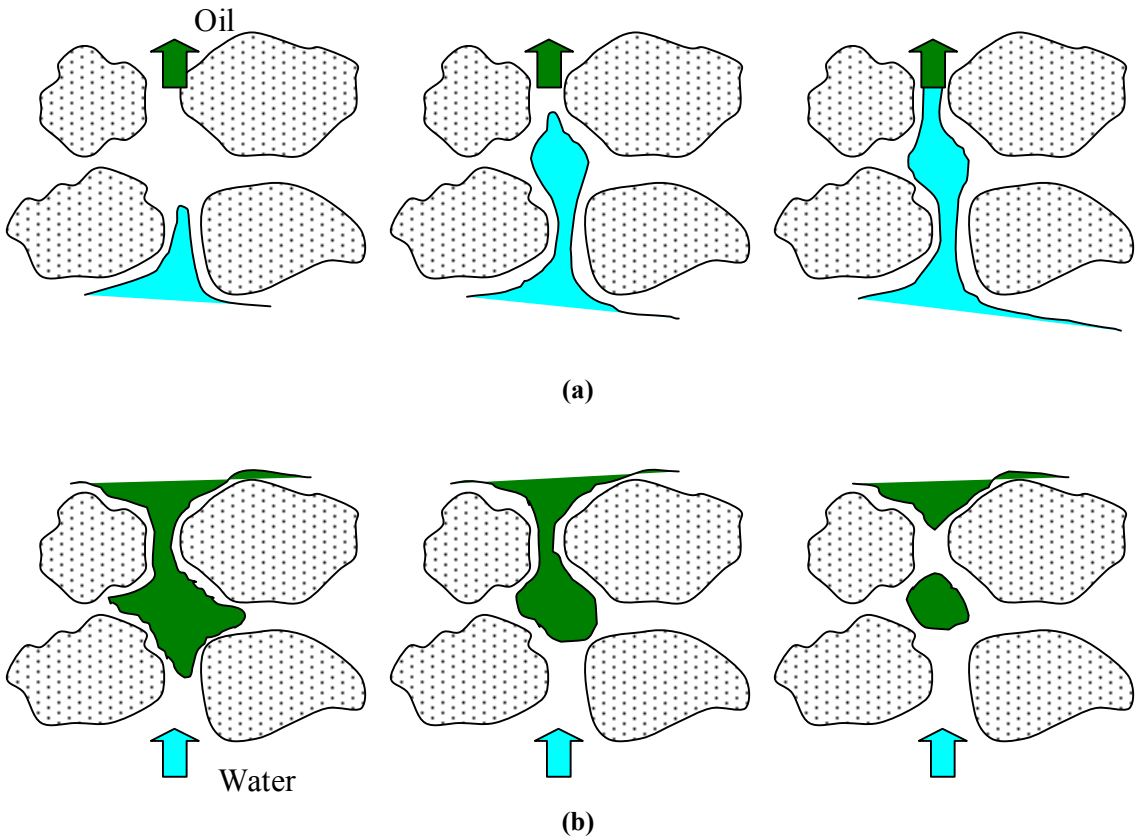

Figure 1.2 – Conceptual Representation of Effect of Wettability, (a) Oil-wet Rock, (b) Water-wet Rock after Raza *et al*

Capillary Pressure, the other important factor, is defined as the difference of pressures between the non-wetting phase and the wetting phase. It gives us the idea how the fluids, both wetting and non-wetting, behave with respect to the surrounding rock and the geometric dimensions of the pore spaces. Capillary Pressure is the major factor in controlling imbibition in the rock. But capillary pressure is found to be dependent on the direction of saturation change, phenomenon called Hysteresis. This gives rise to drainage capillary pressure curve, whereby wetting phase is displaced by (desaturates) non-wetting phase and imbibition capillary pressure curve, wherein non-wetting phase is displaced by imbibition (resaturates) of wetting phase, both results generated in a water wet core. Spontaneity to imbibition process is controlled by the magnitude of this variable. When pressure is employed in order for imbibition to take place then it is called forced imbibition. Also, in order that the drainage process can start, we have to

overcome the threshold capillary pressure. This is the reason drainage capillary pressure starts from a higher magnitude than zero. Also the slope of the capillary pressure curve gives the qualitative measure of the grain-size distribution. Flatter the curve, less capillary pressure change required to move the fluids beyond threshold pressure and more uniform is the grain size. The work of Killins *et al*, as it appears in reference 1, is reproduced here to show the difference in capillary pressure curves of oil wet and water wet rocks. (**fig. 1.3**)

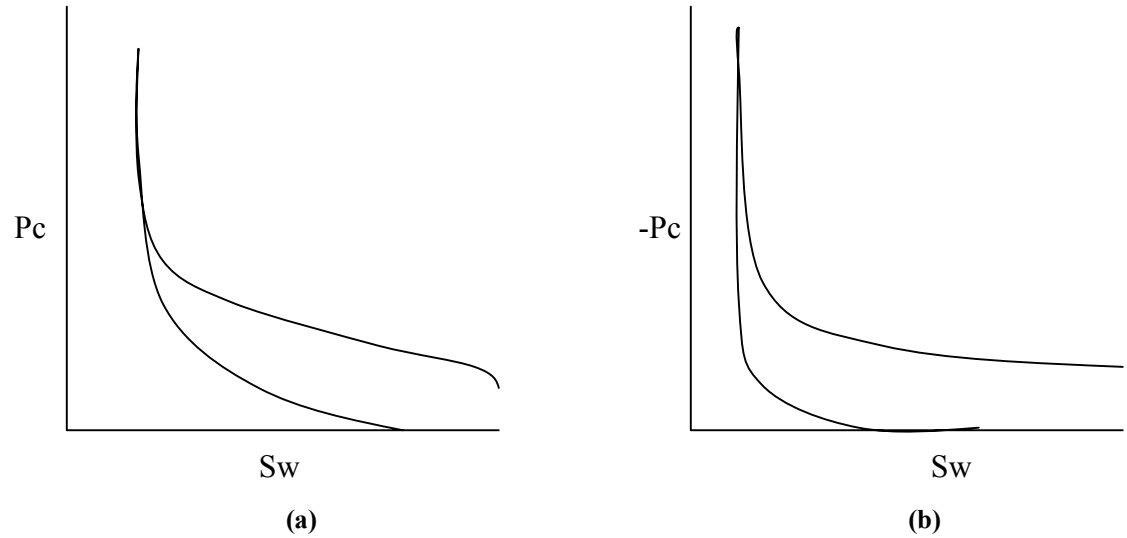

Figure 1.3 – Conceptual Representation of Capillary Pressure, (a) Water-wet Rock, (b) Oil-wet Rock
after Killins *et al*

Relative permeability is a direct measure of the ability of the porous media to allow one fluid to pass through when another is also present, both fluids considered immiscible. Effective Permeability quantifies the relative measure of this conductance when another fluid is also present in the pore spaces. As in case of capillary pressure, relative permeability also exhibits Hysteresis effect. This discussion is reproduced from reference 1, wherein the wetting phase, in strongly water wet system, retraces the drainage relative permeability during the imbibition process but this does not occur for the non-wetting phase. Also, the distinction between the relative permeability curves of water wet and oil wet rocks has been shown in **fig. 1.4**, from reference 1.

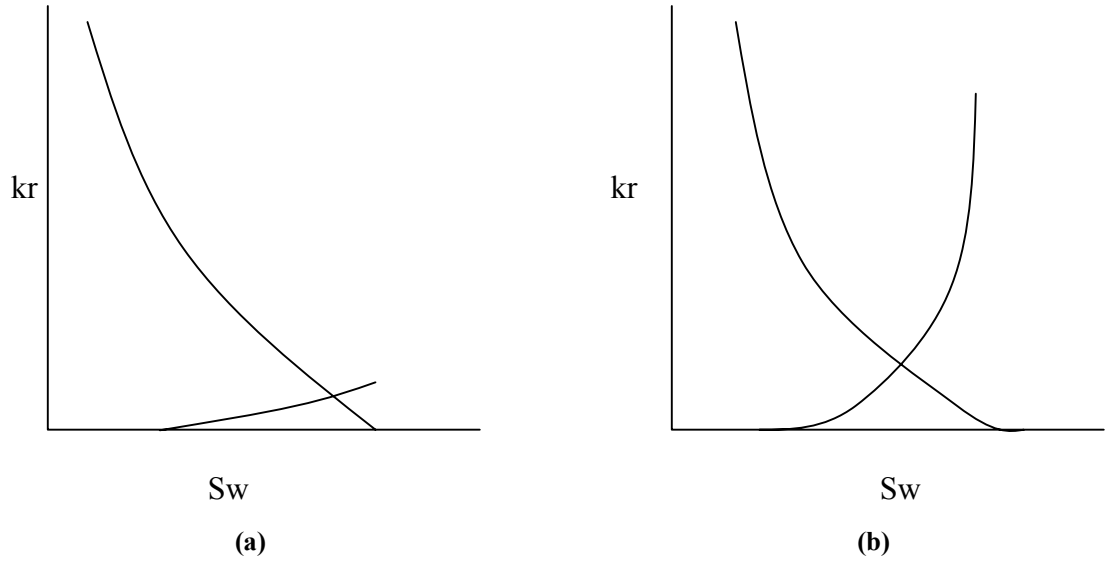

Figure 1.4 – Conceptual Representation of Relative Permeability, (a) Water-wet Rock, (b) Oil-wet Rock after Reference 1

Relative permeability together with the capillary pressure curve encompasses the wettability of the rock in all types of reservoir simulation.

1.3 Spontaneous Imbibition in Porous Media – A Literature Review

In the absence of pressure differential, fluid movement in porous rocks is governed by differential created by capillary pressure. This process is called spontaneous imbibition. This is particularly important in fractured and vugular reservoirs were the wetting fluid fills up the crevices and subsequently interacts with the surrounding porous media thereby displacing the non-wetting fluid inside it with the help of spontaneous imbibition. The non-wetting fluid then moves along these fractures and interconnected vugs to be recovered subsequently. Also, owing to the size of the reservoir and the orientation of fractures and permeability of the reservoir, the pressure differential would just cause movement of fluids in these paths of least resistance. It does not directly contribute in recovery of hydrocarbons from these highly heterogeneous reservoirs. The point which comes to light is the fact that in case of heterogeneous reservoirs, the matrix acts as the source whereas the fractures and the vugs act as temporary storage of

hydrocarbons. With the conventional hydrocarbon reservoirs tending towards steep decline, it becomes inevitable that we turn our attention to these types of reservoirs.

Spontaneous imbibition has been a topic of research of many researchers. Handy[2], Garg *et al.*[3], Babadagli and Ershaghi[4], Li and Horne[5], Akin and Kovscek[6], Reis and Cil[7], Zhou *et al.*[8], are some of the few who have contributed significantly to the study of spontaneous imbibition. In the following pages we will chronologically discuss the works, both experimental and scaling theories, of these researchers.

1.3.1 Handy's Experimental Procedure (1956)

For immiscible displacement in porous media, Handy[2] was one of the early researchers who, based on assumptions, showed that square of the spontaneous imbibition volume linearly depended on time, shown in equation (1.1). These assumptions are that there is a piston like displacement of the water front, the effect of gravity is neglected, wetting phase is continuous behind the imbibing front, pressure gradient of the non-wetting phase (gas in this case) is negligible, and capillary forces play a dominant part in determining the flow as opposed to viscous forces. As a result of this the spontaneous imbibition equation, derived from Darcy's law and Continuity equations, follow a diffusion type of process. As a result of his analytical approach, spontaneous imbibition was quantified

$$Q_w^2 = \left(\frac{2P_c k_w \phi A^2 S_w}{\mu_w} \right) t \qquad \text{…….(1.1)}$$

both in case of experimental study done on Boise sandstone and limestone cores. Although spontaneous imbibition follows a linear trend initially in an experiment, this assumption breaks down when sufficient quantity of wetting phase has imbibed and viscous and gravity forces begin to affect spontaneous imbibition. After such a time, spontaneous imbibition follows a non-linear trend and given sufficient time it levels off. In our simulators, both finite difference and finite element, we have proved this point.

1.3.2 Warren and Root (1962)

Although not directly related to spontaneous imbibition, this theory forms the basis of dual-porosity simulation and hence needs to be reviewed in order to apply the idea of spontaneous imbibition to naturally fractured reservoirs. According to these researchers, naturally fractured and vugular reservoirs contribute greatly to the pore volume but their contribution to the flow capacity is negligible. They developed their theory based Barenblatt *et al*[9] model where transfer potential between matrix and fracture was based on their pressure differential, without taking into account the specific storage of the fracture. This model accounts for fracture storativity. They idealized the reservoir, as shown in **fig. 1.5(a)**, with **fig. 1.5(b)** with the assumption that fracture network can be represented by orthogonal, continuous and parallel to the principle axis of permeability.

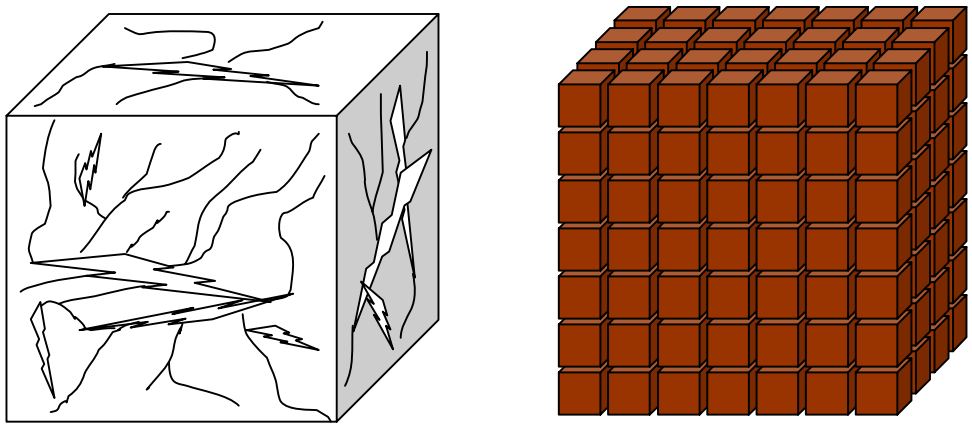

(a) **(b)**

Figure 1.5 – Conceptual Representation of Naturally Fractured Reservoir after Warren and Root

The size of all the matrix blocks is the same. This gave rise to shape factor for single phase flow. Warren and Root[10] model is also used to model vugular reservoirs as well. Two parameters were defined with the help of which fractured reservoirs are characterized. They are the dimensionless parameters, λ, called the interporosity flow coefficient and ω_f, the fracture storativity/capacitance. Pseudo-steady state flow was assumed in the matrix and late time data was used for it.

1.3.3 Mattax and Kyte (1962)

Mattax and Kyte[11] are credited with scaling laws of spontaneous imbibition from cores to reservoir sized matrix blocks in case of fractured, water-drive reservoirs. This was over and above two methods presented for scaling. They verified their method with the help of experiments performed both in 1D and 3D. For all experiments, plots of oil recovery versus time and a dimensionless scaling parameter, t_D, were given which was defined as:

$$t_D = t\sqrt{\frac{k}{\phi}}\frac{\sigma}{\mu_w L^2} \qquad \text{…….(1.2)}$$

is the extension of the imbibition theory and could be used, with certain assumptions, to quantify oil recovery from a large reservoir matrix block in fractured water-drive reservoirs based on imbibition tests performed on small size reservoir cores. Thus the cumulative recovery at any time is an exponential function of the scaling parameter and can be shown to be represented by:

$$R = R_\infty\left(1 - e^{-\lambda t}\right) \qquad \text{…….(1.3)}$$

1.3.4 De Swaan (1976)

De Swaan[12] removed the pseudo-steady state assumption and introduced transient flow between matrix and the fracture. According to him oil recovery from naturally fractured reservoirs is a compromise between water injection and cumulative oil produced. At higher injection rates, the matrix blocks are exposed to higher water saturation sooner which results in higher water-oil ratio. As opposed to this, if lower injection rates are maintained then even though more oil is produced and water cut is lowered, the time period for oil recovery may be inconveniently large. The basic assumption which he makes in his theory is that there is a homogeneous distribution of matrix blocks along the fracture. He compared his results with experimental and numerical simulation results found in the literature and found that there was a good

agreement between the two. He put forth an analytical transient solution of saturation in fractures using convolution. The rate of water imbibition per unitary fracture length is given by:

$$W'_{Iu} = \frac{N_{maRu}}{\tau_I} \int_0^t e^{-(t-\theta)/\tau_I} \frac{\partial S_w}{\partial \theta} d\theta \qquad \text{…….(1.4)}$$

1.3.5 Kazemi et al (1976)

Kazemi *et al*[13] developed a conceptual model of 3D numerical simulation based on the single phase flow equations derived by Warren and Root[10]. Before the advent of their simulation model, a segment of the reservoir was simulated and the results were extrapolated to the whole field. According to their theory, fractures formed the boundaries of the matrix block and both of them were coupled with the help of a transfer function based on Warren and Root[10] theory. This mathematical formulation was then applied to the reservoir as a whole using finite difference method. A typical grid cell of the reservoir was composed of several matrix blocks. Saturation and pressure were assumed to be constant within a particular grid cell containing the matrix blocks. Gravity segregation within matrix blocks was not carried out but overall segregation was accounted for. Similar provision was kept for the relative mobility and other reservoir properties. For 3D case they developed a new shape factor based on pseudo-steady state condition in the matrix and given by:

$$\sigma = 4\left(\frac{1}{L_x^2} + \frac{1}{L_y^2} + \frac{1}{L_z^2}\right) \qquad \text{…….(1.5)}$$

They tested their simulator with two field cases, one a regular five spot quarter-section and other a five-well fractured model.

1.3.6 Firoozabadi and Hauge (1989)

Firoozabadi and Hauge[14] put forth a new model based on the fact that there could be a high capillary pressure in the fracture and the imbibition of the drained liquid by the low lying block because of gravity and the consequent change in the fluid distribution. The controlling factors as far as the capillary pressure of the fracture are the fracture aperture, fracture surface roughness and the number of contact points between the adjacent fracture faces. Since they could not match production data using parallel plate theory, they assumed that the fracture surface was made up of large number sequence of cones. They assumed that the apex of one side of the cone was in contact with the apex on the other side. Thus these cones represented the variable fracture aperture and fracture surface roughness. The magnitude of fracture capillary pressure was calculated using the above geometry of the roughness and basic equation of capillarity, the Young-Laplace equation To support the other aspect of their theory, they conducted an experiment on an oil saturated outcrop rock sample and put it in the centrifuge. At the end of this experiment, the rock sample was taken and divided into several blocks, which were stacked and the same experiment performed under identical conditions. In both cases the volume of drained liquid was recorded against time and block saturation were measured. The conclusions drawn as a result of this experiment were that oil recovery got adversely affected by the increase in the number of blocks.

1.3.7 Kazemi, Gilman and Elsharkawy (1992)

Kazemi, Gilman and Elsharkawy[15] used empirical transfer functions to predict the performance of 3D reservoir by scaling data from laboratory results. His cumulative recovery was of the form:

$$R = R_{\infty}\left(1 - e^{-\lambda_D t_D}\right) \qquad \text{…….(1.6)}$$

The value of λ_D and t_D were given by the following expressions:

$$\lambda_D = \left[\sqrt{\frac{\phi}{k}}\left(\frac{\mu_w}{\sigma F_s}\right)\right]\lambda \qquad \text{…….(1.7)}$$

$$t_D = \left[\sqrt{\frac{k}{\phi}}\left(\frac{\sigma F_s}{\mu_w}\right)\right]t \qquad \text{…….(1.8)}$$

The matrix block shape factor was defined by:

$$F_s = \frac{1}{V_{ma}}\sum\frac{A_{ma}}{d_{ma}} \qquad \text{…….(1.9)}$$

This gives the idea of the amount of area which is in contact with the fluid with respect to distance from the center of the block to the face. It is the measure of the shape factor as given by equation (1.5).

1.3.8 Babadagli and Ershaghi (1992)

Babadagli and Ershaghi[4] conducted experimental imbibition study on low and high permeability cores. They considered Austin chalk and Colton sandstone which are the best representation of matrix characteristics for naturally fractured reservoirs and a core sample of Berea sandstone. At the heart of their research was the idea that in case of naturally fractured reservoirs most of the displacement of both wetting and non-wetting fluids occurs in the fracture and hence fracture transmissivity needed to be elaborated on. The straight line relative permeability of fractures was not a good assumption. Flow experiments performed using an elaborate setup the details of which are in the paper and X-Ray CT scanner was used to measure the saturation profiles. As a result of their experiments, they got a set of relative permeability curves which the authors refer to as effective relative permeability. They also presented the plots of PV versus time and a few schematics of position of water saturation front as measured with the help of CT scanner. The CT schematics clearly showed that at low rate displacement was faster in

the matrix than in the fracture whereas at higher rate it was faster in the fracture. Also, the matrix imbibition was controlled by the coefficient of the effective relative permeability equation. With the help of these curves, they claim, the dual porosity simulation can be reduced to fracture network modeling.

1.3.9 Guzman and Aziz (1992)

Guzman and Aziz[16] presented a sensitivity analysis of fine grid simulation performed on fractured rock. Key variables, such as fracture relative permeability, matrix-fracture capillary pressure and matrix wettability were used to design experiments such that their effect on simulation could be studied. Results of this paper were presented in the form of dimensionless capillary number, N_{cap}, which is the ratio of capillary forces to that of the viscous forces. The effect of fracture relative permeability was illustrated in plots of water cut versus PV injected at various capillary numbers. The effect of this parameter was not significant at high and medium capillary number, but in case of low capillary number when the viscous forces were dominant, the influence was quite strong. For this there is a limiting value of $N_{cap} \approx 20$ which, according to them, was regardless of the shape of capillary pressure curve. The effect of matrix capillary pressure was also studied. The results were very much predictable, that is for a weakly water wet matrix for which the capillary number is also low, early breakthrough was seen. For strongly water wet rock for which capillary number was also high, breakthrough time was also considerably higher than the earlier case. But the only thing which was opposite to their prediction was that in case of high capillary number rock water moved faster in the matrix as compared to that in the fracture. The effect of matrix-fracture capillary pressure was studied with respect to base case of zero capillary pressure in the matrix. They found out that capillary imbibition is controlled by the pressure differential between the matrix and the fracture. In case of high fracture capillary pressure, water flow from the matrix to the fracture thereby decreasing the oil recovery.

1.3.10 Civan (1993)

Civan[17] solved one dimensional Buckley-Leverett water displacement equation for naturally fractured reservoirs using method of differential quadrature. He included a new term for compressible fluids and showed that some empirical transfer functions can be derived theoretically.

1.3.11 Garg et al (1996)

Garg *et al*[3] solved the spontaneous imbibition equation for one-dimension and analyzed saturation data measured with the help of X-ray CT. They setup a mechanism with which they could simultaneously measure the weight of the water imbibed and measure the water saturation with the help of CT scanner. It was a unique experiment wherein the core was in constant contact with the surface of water and water, with the help of spontaneous imbibition, constantly imbibed into it. The immediate issue of the experimental setup was that buoyancy played and important part in corrupting the data for initial time period. The solution to the 1D spontaneous imbibition equation was arrived at by assuming a Corey type relative permeability variation and a logarithmic variation for capillary pressure. Finite difference method was employed in the design of 1D numerical simulator. The numerical simulation was conducted for two values of saturation exponents and saturation profile was obtained for each. The weight gain data was also matched. This experiment was chosen to validate our numerical code.

1.3.12 Reis and Cil (1998)

Reis and Cil[7] performed experimental and derived analytical transfer functions for counter-current imbibition, which according to them is the most important oil recovery mechanism in naturally fractured reservoirs. Again counter-current imbibition, according to them, is controlled by eight important characteristics which were observed with the help of experiments conducted on single matrix blocks surrounded by fractures. The effect of each of these characteristics has been documented to support their point. The unique observation of their experiments was that air (gas) was compressed by water within the matrix block until a threshold pressure is reached. Also for 3D imbibition, the unique characteristic was that all the recovery curves fell in a narrow band when the time

axis was normalized by transition time, a useful thing for scaling experimental recovery from cores. It was found that initial water saturation of up to 20% did not affect recovery rates significantly. They also proposed three new types of transfer functions.

1.3.13 Akin and Kovscek (1998)

Akin and Kovscek[6] conducted experimental study on diatomite rock, which is a high porosity and low permeability siliceous rock. Very little data or literature was available for these types of rocks at the time of their study. Though the authors do not give any specific reason, it is believed that spontaneous imbibition happened as a result of cocurrent imbibition. For this they set up an elaborate experiment where the ends of the porous media were left deliberately open to facilitate cocurrent imbibition and the saturation was measured with the help of X-Ray CT scanner. The paper had plots of CT derived water saturation. Experiments were conducted for air-water imbibition and water-oil imbibition. As a verification task, similar experiments were conducted in Berea sandstone also. They found that the saturation moved with a very sharp front suggesting that pores of all sizes and which are well interconnected fill at the same time. Although diatomite is a different rock than sandstone, it exhibited similar trends in saturation profiles and dimensionless weight gain versus time function. Relative permeability and capillary pressure data was derived from the experimental data.

1.3.14 Schechter and Guo (1998)

Schechter and Guo[18] integrated fracture characteristics with results obtained from experimental study of transfer mechanism in the design of 10 acre CO_2 pilot in naturally fractured Spraberry Trend Area. Both matrix and fracture were characterized with the help of vertical and horizontal well core and log data. Working along the lines of Mattax and Kyte[11], they used an empirical exponential relation to fit the experimental data of water imbibition in oil saturated rocks. They found that the scaled imbibition rate in Spraberry cores was significantly slower than in strongly water-wet Berea cores. Also, previously held notion that CO_2 would breakthrough because of channeling towards producing well, has been refuted with the help of experimental results.

1.3.15 Zhou et al (2001)

Zhou *et al.*[8], performed experimental study of counter-current imbibition on diatomite rock samples. What they did different from Akin and Kovscek[6] was that in their experimental setup they sealed the other end of the core with an end cap allowing water to flow out from a slit as compared to an end cap having a spider web type channeling which encouraged cocurrent imbibition. They found that, in case of counter-current imbibition, oil recovery is approximately proportional to square root of time during the infinite acting period. Also scaling of the simulation demonstrated that end point mobility ratio, which is the measure of wettability, was an important factor. They also have attempted the answer as to whether cocurrent or counter-current imbibition would be a preferred mechanism of oil recovery in low permeability rocks. Their experiments and simulation result indicated that cocurrent imbibition reaches residual oil saturation faster than counter-current imbibition. But if the viscosity of the oil is more then counter-current imbibition has larger recovery.

1.3.16 Li and Horne (2001)

Li and Horne[5] developed a method of characterizing the process of spontaneous imbibition in gas saturated rocks. They found a linear relationship between imbibition rate and reciprocal of gas recovery by spontaneous water imbibition and with no effect of initial water saturation on residual gas saturation. This finding, according to them can be used to characterize spontaneous imbibition gas-saturated porous media. Also, they addressed a difficult problem of characterizing imbibition process in gas-liquid systems by providing an analytical solution to calculate effective water permeability and capillary pressure. They found that for a water-wet porous media, if the imbibition height is less than the height corresponding to $P(S_w)$ then only one point of capillary pressure and relative permeability governs spontaneous water imbibition. They also developed a method of calculating capillary pressure and relative permeability of water phase behind the saturation front from the imbibition data which is consistent with experimental data.

1.4 Finite Elements – An Overview

Finite element is a technique of numerical analysis which helps in evaluating complex physical phenomena. It is particularly useful in performing numerical simulation of physical processes such as fluid flow.

1.4.1 Comparison of Finite Difference with Finite Elements

All numerical methods try to determine the approximate solution of a differential equation, which represents some physical phenomena. This is because the exact solution of that differential equation with the help of analytical methods cannot be sought.

In case of finite difference method, the differential equation is approximated by difference quotients which are truncated expansions of Taylor series for derivatives reference 19. A set of algebraic equations is then arrived at, which are then solved at discrete mesh points with the help of boundary conditions to yield particular solution at those mesh points.

As opposed to this, finite elements as per reference 20, tries to arrive at a particular solution, which is of the form, $u \approx \sum_{j=1}^{n} u_j \psi_j$ with the help of three fundamental steps:

1. The problem domain is divided into a set of simple domains of various shapes which are called finite elements.
2. The differential equation is then put in a particular form, called equivalent weighted integral form. The solution is approximated, on each element, with interpolation functions. This creates an expression of the discrete differential equation together with its boundary condition for each element.
3. These set of equations are assembled using the principle of continuity, where it is assumed that the solution is continuous at the interelement boundaries.

These assembled discrete equations are subjected to boundary and initial conditions and are then solved over the whole domain. By far the most important advantage of finite elements over finite difference is that it can model irregular boundaries also.

It is not always possible to represent a differential equation in weighted integral form, also called the Rayleigh-Ritz finite element method. It is then put into nearest weighted integral form and the residue generated is then successively reduced and a solution sought. This is called the weighted residual method and popular weighted residual methods are the Galerkin method, Least-Square method, and Collocation method.

1.4.2 Different Finite Element Methods

As per reference 20 and we reproduce the discussion from it, finite element methods are divided into two broad categories:

1. Weighted Integral Method
   a) Rayleigh-Ritz Method: Following the three fundamental steps, a particular differential equation is put into weighted integral form, given by:

$$I = \frac{1}{2} B(w,u) - l(w) \qquad \text{.....(1.10)}$$

The solution is of the form:

$$u_N = \sum_{j=1}^{N} c_j \phi_j + \phi_o \qquad \text{.....(1.11)}$$

which satisfies the homogeneous part of the differential equation through ϕ_j and the non-homogeneous part through ϕ_o. If we were to consider, for example, any differential equation of the form:

$$-\frac{d}{dx}\left(a\frac{du}{dx}\right) + cu = f \qquad \text{.....(1.12)}$$

as:

$$A(u) = f \qquad \text{.....(1.13)}$$

where A is an operator, linear or non-linear, then the Rayleigh-Ritz method is:

$$A(u_N) - f = A\left(\sum_{j=1}^{N} c_j \phi_j + \phi_o\right) - f = 0 \qquad \text{.....(1.14)}$$

2. Weighted Residual Methods: For these, the above equation generates a residue:

$$R \equiv A(u_N) - f = A\left(\sum_{j=1}^{N} c_j \phi_j + \phi_o\right) - f \neq 0 \qquad \text{.....(1.15)}$$

This residue, after putting in weighted integral, is made to vanish as:

$$\int_{\Omega} \psi_i(x,y) R(x,y,c_j)\, dxdy = 0 \qquad \text{for all } i = 1,2,\ldots\ldots N$$

.....(1.16)

The value of the weight function ψ_i is not necessarily same as the approximating function ϕ_i.

a) Galerkin Method: If the choice of the weight function ψ_i is equal to approximating function ϕ_i then the residual method is known as Galerkin method. Thus,

$$\sum_{j=1}^{N} \left[\int_{\Omega} \phi_i A(\phi_j)\, dxdy\right] c_j - \int_{\Omega} \phi_i [f - A(\phi_o)]\, dxdy = 0 \qquad \text{.....(1.17)}$$

b) Least Square Method: In this method, we minimize the square of the residual.

c) Collocation Method: In this method, we try to select the approximate solution u_N by requiring the residual to be zero at the same time.

3. Mixed Finite Element Formulations:

   In this case, especially in differential equations which are of higher order we reduce the differentiability requirement on the weight function by converting it into another parameter so that lower order equations are formed.

Thus Rayleigh-Ritz method is a direct method which does not require any iterative effort to reach a solution if required boundary conditions are there. Weighted Residual method may be iterative as we are trying to reduce the residual. Hence more computation time is required to reach a solution.

1.4.3 Computation Time of Multiphase Flow

Multiphase flow in porous media and its simulation is a unique problem in itself. This arises from the fact that we are trying to find the solution of problem which, typically for a field scale problem, runs for 10-15 years in order to do a history match and other 10 years to do the forecasting. Numerical Simulators thus are required to perform simulation in minutes, hours, days and years depending on whether experimental data or field data is being simulated. In multiphase flow, for spontaneous imbibition, we seek to find solution of the differential equation represented by the following expression:

$$\frac{\partial S_w}{\partial t} = \frac{\partial}{\partial x}\left[\frac{k k_{rw} k_{ro}}{\phi(\mu_w k_{ro} + \mu_o k_{rw})}\right]\left[-\left(\frac{\partial P_c}{\partial S_w}\frac{\partial S_w}{\partial x}\right) + g\Delta\rho\sin\alpha\right]$$

$$+\left[\frac{k k_{rw} k_{ro}}{\phi(\mu_w k_{ro} + \mu_o k_{rw})}\right]\frac{\partial}{\partial x}\left[-\left(\frac{\partial P_c}{\partial S_w}\frac{\partial S_w}{\partial x}\right) + g\Delta\rho\sin\alpha\right] \quad \text{.....(1.18)}$$

The derivation of this equation is left for a little later time. In this equation the primary variable is saturation, S_w, which varies both in space and time. The other dependent variables for two phase flow are:

1. Relative permeability of water, k_{rw}
2. Relative permeability of oil, k_{ro}

3. Capillary pressure, P_c
4. Change in depth gradient, $\sin\alpha = \frac{dz}{dx}$

Apart from these four main variables which change drastically, the other variables which are considered fairly constant are:

5. Viscosity of water, μ_w
6. Viscosity of oil, μ_o
7. Porosity of the rock, ϕ

The most accurate solution of the equation (1.18) can be derived by taking into consideration the variation of all the seven variables. But each of these variables adds a degree of non-linearity of this equation. Hence, in order that we solve this equation with the resources of a desktop computer, we assume the last three to be constant. This leaves us with finding the solution with the help of five variables.

We can further reduce the number of variables in this equation by finding the relations of each of them with saturation. This reduces the computation time and the solution is sought by direct substitution into these equations. In case of relative permeabilities, for wetting and non-wetting fluids, we follow the relations of Brooks and Corey[22] which are given by:

$$S_{we} = \frac{S - S_{wi}}{1 - S_{wi} - S_{oi}}$$

$$k_{rw} = k_w S_{we}^n$$

$$k_{ro} = k_o \left(1 - S_{we}\right)^2 \left(1 - S_{we}^{\gamma}\right) \qquad \text{.....(1.19)}$$

$$n = \frac{2 + 3\lambda}{\lambda} \qquad \text{…....(1.20)}$$

$$\gamma = \frac{2+\lambda}{\lambda} \qquad \text{.....(1.21)}$$

where λ is called pore size distribution index and for typical porous rocks has a value of 2 and n is the saturation exponent. For our purpose, $S_{we} \approx S_w$ and is used interchangeably.

For capillary pressure, we use the following relation:

$$P_c = -P_{c0}S_w^3 + P_{c1}S_w^2 - P_{c2}S_w + C_c \qquad \text{.....(1.22)}$$

Again, the change in depth gradient can be assumed to be very small and the term neglected, but in our case we will carry it through, since we are interested in knowing the effect of gravity forces as well.

In all the numerical methods we employ, be it finite difference or finite elements, we will have a set of algebraic equations per element represented by following matrix form:

$$\begin{bmatrix} C_1 & 0 & 0 \\ 0 & C_2 & 0 \\ 0 & 0 & C_3 \end{bmatrix} \begin{bmatrix} S_{i-1}^{m+1} \\ S_i^{m+1} \\ S_{i+1}^{m+1} \end{bmatrix} = \frac{1}{\Delta t} \begin{bmatrix} S_{i-1}^{m} \\ S_i^{m} \\ S_{i+1}^{m} \end{bmatrix} \qquad \text{.....(1.23)}$$

where C_1, C_2 and C_3 are coefficients and their values are known at the beginning of the matrix operation. These matrix-type of equations are solved by carrying out the matrix inversion and for which we employ Gauss Elimination method. For finite difference method, when equations from all the elements are assembled they form a tridiagonal matrix for single phase flow and pentadiagonal matrix for two phase flow. A typical pentadiagonal global matrix of all the elements assembled looks like equation (1.24).

$$\begin{bmatrix} b_1 & c_1 & & & d_1 & & & & \\ a_2 & b_2 & c_2 & & & d_2 & & & \\ & a_3 & b_3 & c_3 & & & d_3 & & \\ & & . & . & . & & & . & \\ e_i & & & a_i & b_i & c_i & & & d_i \\ & . & & & . & . & . & & \\ & & e_{N-2} & & & . & . & . & \\ & & & e_{N-1} & & & . & . & . \\ & & & & e_N & & & a_N & b_N \end{bmatrix} \begin{bmatrix} \\ S_{i-1}^{m+1} \\ S_i^{m+1} \\ S_{i+1}^{m+1} \\ \\ \\ \\ \\ \end{bmatrix} = \frac{1}{(\Delta t)} \begin{bmatrix} \\ S_{i-1}^{m} \\ S_i^{m} \\ S_{i+1}^{m} \\ \\ \\ \\ \\ \end{bmatrix} \quad \text{.....(1.24)}$$

Finite element (FEM) matrix is also almost similar to this, except that for a nine-node element, the element contributions make each of the coefficients *a*, *b*, *c*, *d* and *e* much more mathematically involved. We are using nine-node element, because for fluid dynamics and porous media flow type of problems, this type of element gives much more accurate result, as per reference 21. The major difference between finite difference and finite element (Galerkin Method) arises from the fact that in the case of former, all the coefficients are linear and direct solvers such as Gauss elimination can be readily applied whereas in the latter, we have to use iterative solvers to ascertain the values of these coefficients before actual inversion can take place. As a result we have to settle for Newton-Raphson method in order to solve the system of algebraic equations as it is one of the fast methods for solving these equations. If we assume that it takes 3-5 iterations per element to solve for the coefficients and make a final run per time step, then the finite element program has to run roughly five times in a single time step for each element. This is a fair assumption since the rate of convergence of this method is high. Also, the complexity of the differential equation represented by equation (1.18) is such that Galerkin or any other weighted residue finite element method can only be employed for a solution. Rayleigh-Ritz method cannot be applied to equation (1.18). A more elaborate reasoning about non-applicability of this method will be discussed in subsequent chapter.

Multiphase flow in oil/gas reservoirs are generally run for 10-15 years and then another 10 years is generally used for forecasting the life of the field. Thus the average span of typical reservoir simulation is around 25 years (25 X 365 days ≈ 10,000 days). In effect we are trying to get 50,000 (10,000 X 5 iterations/day) iterations in order to reach a solution. Assuming that for a million grid cells (extreme case scenario) if we arbitrarily choose 200 nano-seconds (200E-09 seconds) as the time required for solving single iteration of the pentadiagonal matrix, then:

$$\text{Time for one computation run by FEM} = \frac{5 \times 50{,}0000 \times 1{,}000{,}000}{2 \times 10^{7}} \approx 12{,}500\,\text{sec} \approx 3.5\ \text{hrs.}$$

As against this, the direct solution for finite difference method (FDM) is:

$$\text{Time for one computation run by FDM} = \frac{5 \times 10{,}0000 \times 1{,}000{,}000}{2 \times 10^{7}} \approx 2{,}500\,\text{sec} \approx 42\ \text{mins.}$$

If we were to plot this data against time, as shown in **fig. 1.6**, we can better visualize the problem associated with computation time associated with execution of finite element computer program. This is the reason why finite elements have not been that successful as compared to finite difference in multiphase flow problems as it severely taxes the computer resources. As a general rule finite element program for reservoir simulation type of problem can only be run on a mini or a main frame computer.

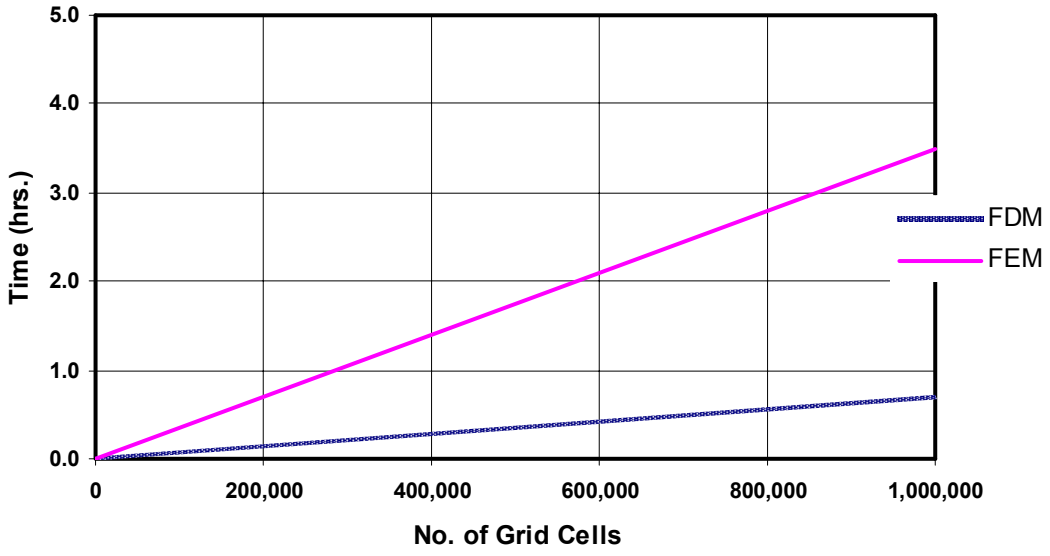

Figure 1.6 – Comparison of Execution Time for FDM and FEM

1.5 Statement of the Problem

Thus we reach a conclusion that as long as there is Galerkin type of formulation, finite element would be time consuming and computer memory taxing. Thus an attempt has been made to use Rayleigh-Ritz method so that finite element method can be solved directly rather than iteratively. The direct advantage of this is that we can integrate all the geological and geophysical details into an efficient mathematical model which is less mathematically intensive than existing finite element methods and can simulate fluid flow in porous media without having to resort to large refinements in order to capture details as done by finite difference method.

1.6 Finite Elements in Reservoir Simulation – An Overview

The use of finite elements in reservoir simulation is not new. This section presents some of the previous work done by researchers in the past. Some of the early researchers were Asfari and Witherspoon[23], Settari *et al*[24], Young[25], McMichael and Thomas[26] etc. Invariably these researchers have approached the simulation problem from Galerkin finite element method. Some of the early researchers, such as Darlow *et al*[27], Chavent *et al*[28], Ewing *et al*[29] etc., have formulated the multiphase problem with the help of mixed finite element formulations. Finite element method, as applied to naturally fractured reservoirs, has also been subject of study of many researchers. Some of them are Asfari and Witherspoon[30], Bhatia *et al*[31], Naji and Kazemi[32], Sutopo *et al*[33], Karimi-Fard and Firoozabadi[34], etc. The work of Iqbal and Civan[35] and Dalen[36] deserves a special mention as they have worked along almost similar lines so as to simplify the method like us, but former used finite analytic method to solve Buckley-Leverett one-dimensional problem and the latter used compatibility relaxation, capacity lumping, and upstream mobility weighing to represent finite elements as a finite difference model. Outside the realm of petroleum engineering, water resources engineering uses finite elements extensively.

CHAPTER II

PRINCIPLES OF X-RAY TOMOGRAPHY AND FLUID FLOW IN FRACTURES

2.1 Principles of X-Ray Tomography

2.1.1 Introduction

X-Ray Computer Tomography (X-Ray CT) is a method in the area of non-destructive testing (NDT). It was developed during the seventies for medical purposes and was subsequently introduced for industrial applications in the latter part of the eighties. It is the imaging technique, similar to X-ray radiography, the only difference being the way X-ray radiation penetrates an object. Most of the information which follows has been borrowed from Haung[37]. **Fig. 2.1** shows the basic difference between X-Ray CT and X-Ray radiography. A CT image generates a slice through the object in a true geometrical manner whereas X-ray radiography image projects a three-dimensional picture into two-dimension. Thus the CT image shows maps of the amount of radiation that is taken away (attenuated) in the form of linear attenuation coefficient, μ, from a beam of X-Ray at each point (voxel -3D value) of the object. The value of μ depends on the density and the atomic composition of the matter in which X-ray propagates. In contrast, the X-Ray radiographic image pixel values are proportional to

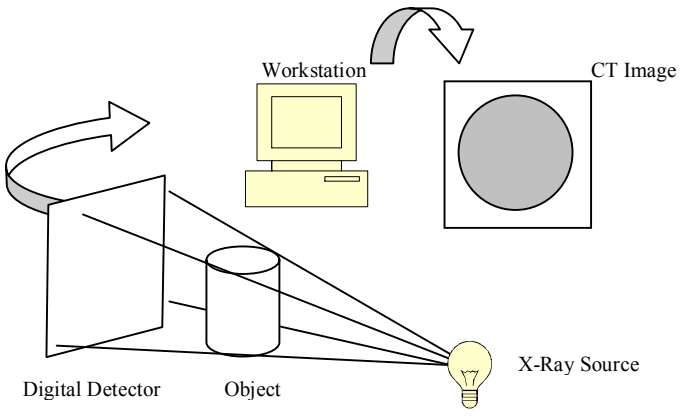

Fig. 2.1 – Conceptual Representation X-Ray Radiography and X-Ray Tomography

the radiation attenuated along the line from the X-ray source to the detector element (film in most cases but a digital detector in the **fig**. **2.1**). Although radiography is faster as compared to CT scanning, but it is inferior in revealing interior details of the imaged object.

In our experiments we are taking CT images of cores and rock objects, which give the projection of internal structures. Sometimes the over-laying grains obscure certain important details, which need study. By using slice-imaging techniques (tomography), we can selective have a layer by layer structural detail of the given core sample. With computerized tomography, CT scan, we can see sequence images of thin consecutive slices of the cores or rock object in three dimensions. Unlike conventional, classical tomography, computerized tomography does not suffer from interference from structures in the object outside the slice being imaged. This is done by irradiating only thin slices of the object with a fan-shaped beam. Also, the CT images (tomograms) of the object's structure can give more selective information within the object than conventional planar projection radiographs. Compared to planar radiography, CT images have superior contrast resolution, i.e., they are capable of distinguishing very small differences in attenuation (contrasts), but have inferior spatial resolution. The maximum spatial resolution of X-ray scan is 0.5 mm, which implies that the smallest details in the image that can be resolved, must be separated at least 0.5 mm. This drawback in X-Ray CT has lead to the refinement in X-Ray microtomography. In X-Ray microtomography, the spatial resolution of 2 micron (2 thousandths of a millimeter) and below can be achieved.

X-ray CT scanners used nowadays are either third- generation or fourth-generation. **Fig. 2.1**(**a**) shows a third-generation CT scanner. The X-ray tube and the receptor array are located on opposite sides of the object and both rotate around the object during data acquisition. **Fig. 2.2**(**b**) is a fourth-generation CT scanner. Here, only the X-ray tube rotates around the object; the receptor array, which is situated in the outside of the scanning frame, remains stationary. The receptors are made from solid-state material and can be as many as 4000. CT scanners are also available in which the

X-ray tube circles the object while the table moves continuously, so that the X-ray tube moves in a spiral orbit around the object. These are called spiral CT scanners. Department of Petroleum Engineering, Texas A&M University, now has a fourth generation spiral CT scanner.

2.1.2 Principles of Operation

In order to generate a CT image two steps are necessary. Firstly we should have physical measurements of the attenuation of X-rays along the core in different directions, and secondly we have to make mathematical calculations of the linear attenuation coefficients, μ, all over the slice. A fan-shaped beam, wide enough to pass on both sides of the core or rock object, is used. The image receptor is an array of several hundred small separate receptors. Readings from the receptors are fed into a computer, which after numerous calculations produces a tomogram of the object, i.e., a map of linear attenuation coefficients, μ. The data acquisition time is a few seconds and a 512 pixel x 512 pixel image matrix. Typically medical CT scanners today use a fan-beam, ones which are having about 700 receptors (3rd generation) or 4000 receptors (4th generation), complete data acquisition in approximately 1-2 seconds and within a few

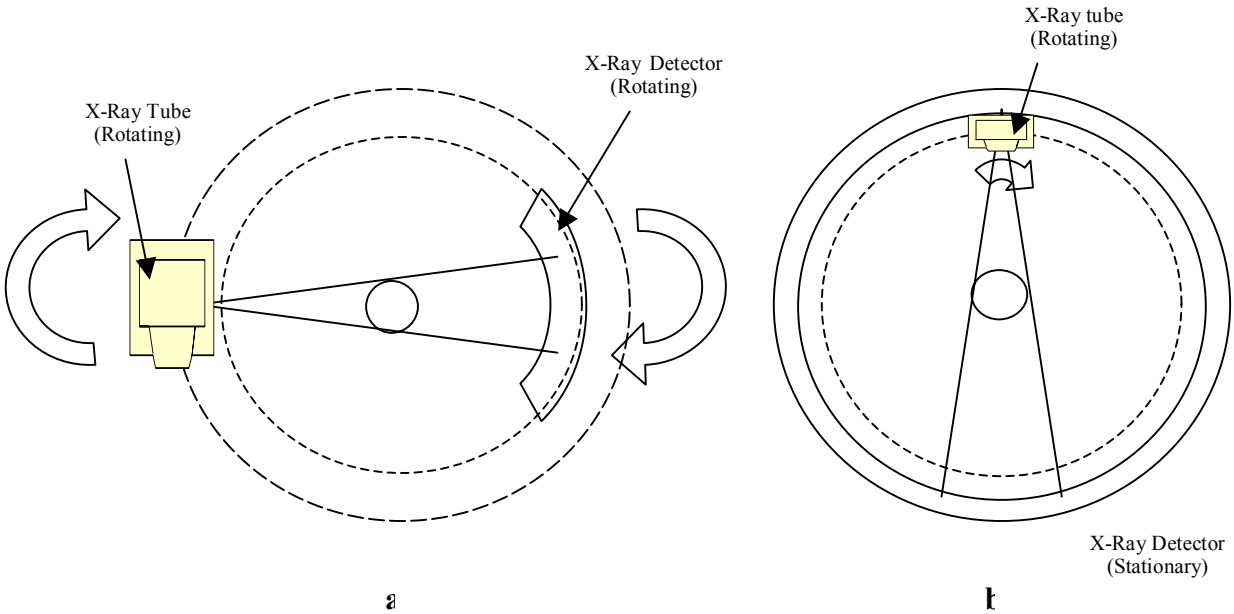

Fig. 2.2 – Conceptual Representation of 3rd Generation and 4th Generation X-Ray CT Scanner

seconds to reconstruct the 512x512 image matrix with 12 or 16 bits depth. X-Ray CT is one of the forms of digital radiology. When X-rays interact with matter, there are three primary interaction modes: photoelectric, Compton and coherent. When photoelectric effect occurs, a photon from the incident beam disappears, and an electron is ejected

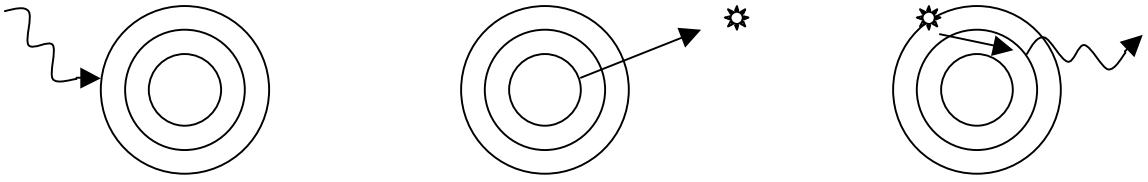

Fig. 2.3 – Photoelectric Effect

from the inner shell of an atom. As shown in **fig. 2.3**(**a**) an incident photon loses all its energy on entering an atom, being absorbed in the process. The atom responds, **fig. 2.3**(**b**) by ejecting an inner shell electron, which becomes a photoelectron. The atom reaches an excited state and an electron from a higher energy level fills the vacancy and emits a characteristic x-ray photon **fig. 2.3**(**c**).

In Compton scattering, **fig. 2.4**, a photon from the incident beam collides with an electron, loses some of its energy and is deflected from its original direction.

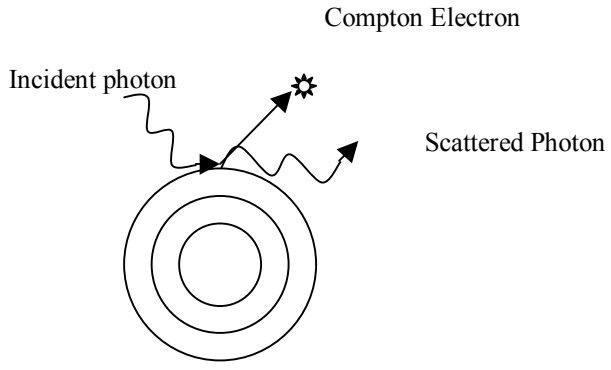

Fig. 2.4 – Compton Effect

In coherent (or Rayleigh) scattering, **fig. 2.5**, an incident photon is scattered by bound atomic electrons without losing energy and the atom is neither ionized nor excited. Thus, when a narrow beam of monoenergetic photons passes through a medium of thickness *x*, the beam will be attenuated and scattered because of the three above cited effects. The receptors measure the X-rays passing through a slice of the object in different positions. This forms one projection of the object. Its reading gives us a measure of the attenuation in the object along the path of a particular ray.

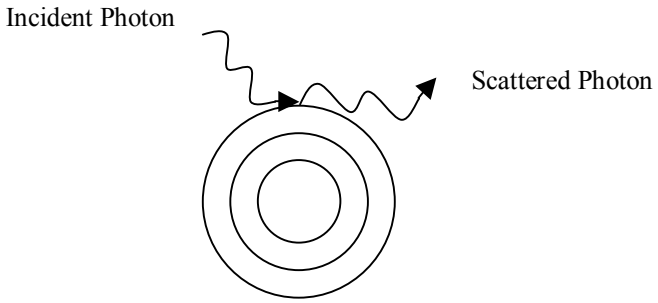

Fig. 2.5 – Rayleigh Scattering

For a homogeneous object, the receptor reading, as stated by reference 37, is given by:

$$I = I_0 e^{-\mu x} \qquad \ldots\ldots \quad (2.1)$$

where,

I_0 is the receptor reading without the object,

μ the linear attenuation coefficient for the object,

x is the object thickness along the path of that ray, and

e the base of the natural logarithm (e = 2.718).

For an inhomogeneous object such as a core or a rock, the product μx is a sum over all the different grains/crystal types, i, $\Sigma \mu_i x_i$. After the readings from one of the receptors have been stored in the computer, the tube is rotated to another angle and a new projection profile measured. This procedure, called reconstruction, is applied

whereby the data from sets of projection profiles through all volume elements (voxels) and for all rotation angles (projections), in a slice of the object, an average linear attenuation coefficient, μ, for each voxel is calculated. Each value of μ is assigned a grey scale value on the display-monitor and is presented in a square picture element (pixel) of the image.

2.1.3 Reconstruction Algorithms

The computer reconstructs an image, a matrix of μ-values for all voxels in a slice perpendicular to the rotation axis. The procedure to reconstruct the image is made with the help of reconstruction algorithm. The objective of this algorithm is to find the μ-values in each voxel based on all the measured data in the projection profiles. A filtering procedure helps in removing the smearing-out of the detail.

2.1.4 Display of CT Numbers, N_{CT}

In the digital display computer monitor, the measured μ - values is distributed over a grey scale with the lowest values of μ black and the highest white. A CT number, N_{CT} , is defined as:

$$N_{CT} = \mu \frac{\mu - \mu_w}{\mu_w} \quad \ldots. \quad (2.2)$$

where,

μ is the average linear attenuation coefficient for the material in a given voxel

μ_w that for water, and

N_{CT} is given in the dimensionless unit, *Hounsfield number*

The CT number scale has two fixed values independent of photon energy. For vacuum, air or body gas,

$$N_{CT} = -1000$$

and for water,

$$N_{CT} = 0.$$

The common method used for calculating porosity from CT images is:

$$\phi = \frac{N_{CT100\%Sat} - N_{CTDry}}{N_{CTWater} - N_{CTAir}} \quad \ldots. \ (2.3)$$

For water displacing air in the core, then saturation is given by:

$$S_w = \frac{N_{CTMat} - N_{CTDry}}{N_{CT100\%Sat} - N_{CTDry}} \quad \ldots. \ (2.4)$$

For oil-water phase, the saturation is calculated with the help of the following relation:

$$S_w = \frac{N_{CTMat} - N_{CT100\%Sat}}{\phi\left(N_{CTOil} - N_{CTWater}\right)} \quad \ldots. \ (2.5)$$

where,

$N_{CT100\%Sat}$ is the CT number of 100% saturated voxel,

N_{CTDry} is the CT number of dry voxel,

$N_{CTWater}$ is the CT number of Water = 0.0,

N_{CTAir} is the number of Air = -1000.0,

N_{CTMat} is the CT number of the matrix,

N_{CTOil} is the CT number of Oil.

2.1.5 Image Display

In order to give contrast to the object, we give a narrow interval of the CT numbers, called the window, to the entire grey scale on the display-monitor. The entire range of CT numbers is displayed on this grey scale, called the 'window width' and the average attenuation value is the 'window level'. Changes in window width, as shown in **fig. 2.6** alter the contrast and changes in window level help in selecting the structures in the image, displayed on the grey scale. As the window width is made narrower, the structure is assisted with higher contrast. Structures that are on the lower and higher sides of the window width (low and high CT numbers) are either completely black or

white. As the window width is made even narrower, the contrast of the structures displayed increases. Combinations of these techniques enable small differences in attenuations at various points in the object and its composition to be visualized.

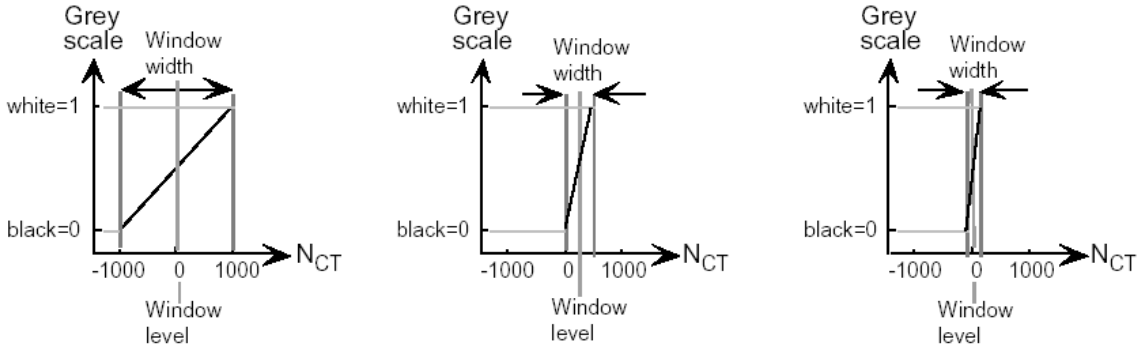

Fig. 2.6 – Effect of Window Width and Window Level after *Huang*

2.1.6 Artefacts

Computerized tomography is based on physical measurements followed by mathematical computations. These computations are based on idealized assumptions that do not entirely correspond to physical reality. This creates artefacts or errors in the measurement and reconstruction of the μ - values. Artefacts in the image are patterns that do not correspond to the object's structure. Beam hardening artifacts, as for example, are found when a spectrum of photon energies is used and is the most common form of artifact.

2.2 Theory of Fluid Flow in Fractures - A Background

The concept of flow between fractures was based on the idea of parallel-plate concept. It was believed that flow models could be developed both for a single fracture as well as network of fractures. According to Snow[38], the flow along fractures can be regarded as being projection of a field gradient which can be assumed to be parallel to neither of the fracture axes. This gradient gave rise to flow rate which was described by a second order tensor, representing the permeability of a continuous rock mass, with the same flow rate as the fractured rock under the same hydraulic gradient and laminar flow conditions. In order to arrive at the flow equation through a set of parallel plates, we derive it from the first principles.

2.2.1 Flow of Single Fluid Between Parallel Plates

The derivation of flow of single fluid between parallel plates can be found in any standard textbook of fluid mechanics, such as Bird *et al*[39]. An incompressible fluid is flowing in the *z*-direction, as shown in **fig. 2.7**, in a horizontal thin slit of length L and unit width under the influence of a horizontal pressure gradient $(p_0 - p_L)/L$. Let the distance between the plates is b. Let us consider that the flow is laminar and a small rectangular fluid element of length δz and height δx is present at a distance x from the lower plate. The velocity at the lower face of the element is v whereas it is $v+\delta v$ on the upper face. If δv is positive then the faster moving fluid exerts a forward force on the upper face whereas the fluid at the lower face tends to retard the fluid element. This generates shear stresses, which are:

$$\text{Stress on the upper face} = \left(\tau + \frac{\delta\tau}{\delta x}\delta x\right)$$

$$\text{Stress on the lower face} = (\tau)$$

Similarly, pressure on either of the faces of this element is given by:

$$\text{Pressure on the right face} = \left(p + \frac{\delta p}{\delta z} \delta z \right)$$

$$\text{Pressure on the left face} = \left(p \right)$$

In order that the flow to be steady and uniform the force on the fluid element should be zero which leads to:

$$\left[p - \left(p + \frac{\delta p}{\delta z} \delta z \right) \right] \delta x \delta y + \left[\left(\tau + \frac{\delta \tau}{\delta x} \delta x \right) - \tau \right] \delta y \delta z = 0$$

The force balance equation when divided by elemental volume $\delta x \delta y \delta z$ leads to the following differential equation for momentum flux:

$$\frac{\delta \tau_{xz}}{\delta x} = \frac{\delta p}{\delta z} = \frac{p_0 - p_L}{L} \qquad \ldots\ldots\ldots \quad (2.6)$$

Integration of the above equation gives:

$$\tau_{xz} = \left(\frac{p_0 - p_L}{L} \right) x + C_1 \qquad \ldots\ldots \quad (2.7)$$

Applying Newton's law of viscosity, we get:

$$-\mu \frac{dv_z}{dx} = \left(\frac{p_0 - p_L}{L} \right) x + C_1$$

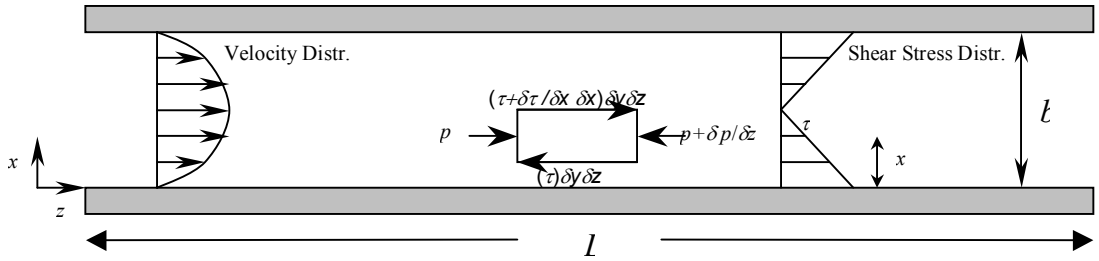

Figure 2.7 – Derivation of Equation of Flow between Parallel Plates

Integrating this equation yields:

$$v_z = -\left(\frac{p_0 - p_L}{2\mu L}\right)x^2 - \frac{C_1}{\mu}x + C_2 \qquad \ldots\ldots \quad (2.8)$$

With the help of following two boundary conditions we have:

B.C. 1: at $x = 0$, $v_z = 0$ $C_2 = 0$

B.C. 2: at $x = b$, $v_z = 0$

$$0 = -\left(\frac{p_0 - p_L}{2\mu L}\right)b^2 - \frac{C_1}{\mu}b$$

Substituting the value of C_1 in equation (2.8) we get:

$$v_z = \left(\frac{p_0 - p_L}{2\mu L}\right)\left(bx - x^2\right) \qquad \ldots\ldots\ldots \quad (2.9)$$

Since the velocity distribution is parabolic, the average velocity is obtained by integrating along the entire width and using equation (2.8).

$$\langle v_z \rangle = \frac{1}{b}\int_0^b v_z dx = \frac{b^2}{12\mu}\frac{(p_0 - p_L)}{L} \qquad \ldots\ldots\ldots \quad (2.10)$$

This equation is often used to represent flow in fractures as well wherein *b* is treated as the aperture width. The flow rate equation, known as the 'cubic law', is then given by:

$$q = \frac{b^3}{12\mu}\frac{(p_0 - p_L)}{L} \qquad \ldots\ldots \quad (2.11)$$

Comparing this equation with Darcy's law we have the value of the permeability given by:

$$k = \frac{b^2}{12} \qquad \ldots\ldots \quad (2.12)$$

Iwai[40] and many other researchers found out that cubic law ceases to be valid when high effective pressures were used. Some rock mechanics researchers, such as Cornwell and Murphy[41] have found that for large scale roughness ($\varepsilon/D > 1$) the maximum laminar limit is as low as Reynolds Number, Re = 100. Also others have found that equation (2.12) transforms under such large-scale roughness conditions to:

$$q = C\frac{b^3}{12\mu f}\frac{(p_0 - p_L)}{L} \qquad \ldots\ldots\ldots \quad (2.13)$$

Comparing this equation with the Darcy's law we get the general expression for permeability, *k*, in rough fractures as:

$$k = C\frac{b^2}{12f} \qquad \ldots\ldots \quad (2.14)$$

Results of experimental data done on fractures clearly show that cubic law was valid down to 0.2 μm aperture.

2.3 Application of X-Ray CAT Scan

X-ray Computerized Axial Tomography or CT Scan, over the years, has become a good tool to carry out measurements of various parameters of fluids inside the cores. Below is described a procedure which will be implemented by us.

2.3.1 Porosity Determination

Porosity distribution in the core is determined using CT-analysis method using simple correlations presented by Qadeer[42]. Each CT image is in the matrix form, in which each element, a voxel, represents a volume of 0.5 x 0.5 x 2.0 mm^3. As previously defined in equation (2.2), CT numbers are taken along the entire cross section of the core. For a dry unfractured core, for average CT numbers, we have:

$$N_{CTdry} = (1-\phi)N_{CTmatrix} + \phi N_{CTAir} \qquad \ldots\ldots \quad (2.15)$$

The dry core is then flooded with brine. The resulting CT image can be represented by the following relationship:

$$N_{CT100\%Brine} = (1-\phi)N_{CTmatrix} + \phi N_{CTBrine} \qquad \ldots\ldots \quad (2.16)$$

Subtracting equation (2.16) from equation (2.15), we have:

$$N_{CT100\%Brine} - N_{CTdry} = \phi\left(N_{CTBrine} - N_{CTAir}\right) \qquad \ldots. \quad (2.17)$$

Rearranging, we derive the relation to determine the porosity of the core as:

$$\phi = \frac{N_{CT100\%Brine} - N_{CTDry}}{N_{CTBrine} - N_{CTAir}} \qquad \ldots\ldots \quad (2.18)$$

2.3.2 Saturation Determination

We apply the same concept in determining the saturation of the core. If there is a mixture of two fluids in the core which is scanned, then:

$$N_{CTmixture} = (1-\phi)N_{CTmatrix} + \phi S_{FluidA} N_{CTFluidA} + \phi(1-S_{FluidA})N_{CTFluidB} \quad \ldots\ldots \quad (2.19)$$

Rearranging,

$$N_{CTmixture} = (1-\phi)N_{CTmatrix} + \phi S_{FluidA}(N_{CTFluidA} - N_{CTFluidB}) + \phi N_{CTFluidB} \quad \ldots\ldots \quad (2.20)$$

Subtracting equation (2.15) from equation (2.20), we have:

$$N_{CTdry} - N_{CTmixture} = \phi N_{CTAir} - \phi S_{FluidA}(N_{CTFluidA} - N_{CTFluidB}) - \phi N_{CTFluidB} \quad \ldots\ldots \quad (2.21)$$

Rearranging,

$$S_{FliudA} = \frac{N_{CTdry} - N_{CTmixture} + \phi(N_{CTFluidB} - N_{CTAir})}{\phi(N_{CTFluidA} - N_{CTFluidB})} \quad \ldots\ldots \quad (2.22)$$

From equation (2.18), for fluid B we have:

$$\phi = \frac{N_{CTMat} - N_{CTDry}}{N_{CTFluidB} - N_{CTAir}} \quad \ldots\ldots \quad (2.23)$$

Substituting this in equation (2.22) we have equation (2.5) as given previously.

CHAPTER III

MATHEMATICAL THEORY OF SPONTANEOUS IMBIBITION

In order to arrive at a mathematical model, we have to start from the basic equations. We take a control volume approach in this case. Let us assume a control volume of dimensions Δx, Δy, and Δz. Fluid flow occurring across this control volume obeys three basic laws of physics, namely:

1. Law of Conservation of Mass – also known as Continuity Equation.
2. Law of Conservation of Momentum – represented by Darcy's Law.
3. Law of Conservation of Energy.

3.1 Formulation of Continuity Equation

We apply the law of conservation of mass to this control volume. For this we follow a simple concept which is represented by:

Rate of increase of mass in the CV = Rate at which mass enters the four boundaries

From **fig. 3.1**, for one-dimensional case and for wetting phase, we can deduce the following:

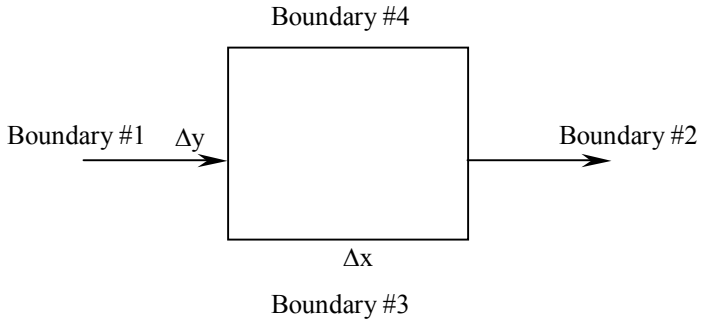

Figure 3.1- Control Volume Representation

Mass entering the element $= q_w \rho_w \big|_x$

Mass leaving the element $= q_w \rho_w \big|_{x+\Delta x}$

Mass accumulation $= A\phi\Delta x \dfrac{\partial}{\partial t}(S_w \rho_w)$

Mass balance equation is then given by combing the above expressions:

$$q_w \rho_w \big|_x - q_w \rho_w \big|_{x+\Delta x} = A\phi\Delta x \frac{\partial}{\partial t}(S_w \rho_w) \qquad \text{…….... (3.1)}$$

Assuming that there is a source, q_{ws}, which is producing water (wetting phase) from the control volume, the above equation then changes to:

$$q_w \rho_w \big|_x - q_w \rho_w \big|_{x+\Delta x} = A\phi\Delta x \frac{\partial}{\partial t}(S_w \rho_w) - q_{ws}\rho_w \qquad \text{…….... (3.2)}$$

According to the definition of the derivative of any given function, $F(x,t)$, for an increment Δx we have:

$$F(x,t) - F(x+\Delta x,t) = -\left(\frac{\partial F}{\partial x}\right)_t \Delta x \qquad \text{…….... (3.3)}$$

Combing equations (3.1) and (3.2), we have:

$$-\frac{\partial}{\partial x}(q_w \rho_w)\Delta x - A\phi\Delta x \frac{\partial}{\partial t}(S_w \rho_w) = -q_{ws}\rho_w \qquad \text{…….... (3.4)}$$

For incompressible fluids ρ_w is constant, hence:

$$-\frac{\partial}{\partial x}(q_w) - A\phi\frac{\partial}{\partial t}(S_w) = -q_{ws} \qquad \text{…….... (3.5)}$$

But according to the definition of flow rate, we have:

$$q_w = u_w A$$

and

$$\partial q_w = A\partial u_w \qquad \text{…….... (3.6)}$$

Substituting this in equation (3.5) we have:

$$\frac{\partial u_w}{\partial x} + \phi\frac{\partial S_w}{\partial t} = \frac{q_{ws}}{A} \qquad \text{…….... (3.7)}$$

We get a similar equation for the non-wetting phase as well. This is given by:

$$\frac{\partial u_o}{\partial x} + \phi\frac{\partial S_o}{\partial t} = 0 \qquad \text{…….... (3.8)}$$

3.2 Darcy's Law

Darcy's Law is an empirical relation. It can be proved that this law is a special case of the general momentum equation given by Navier-Stokes. There is a very simple proof of this, given by Sahimi[43], and we begin with the Navier-Stokes equation represented thus:

$$\rho\frac{D\overline{V}}{Dt} = \rho g - \nabla p + \mu\nabla^2\overline{V} \qquad \text{…….... (3.9)}$$

This can be rewritten in the form of flow potential, Φ, as following:

$$\rho \frac{D\overline{V}}{Dt} = \nabla \Phi + \mu \nabla^2 \overline{V} \qquad \text{……..... (3.10)}$$

where the flow potential is given by,

$$\nabla \Phi = -\frac{\nabla p}{\rho} + g \qquad \text{……..... (3.11)}$$

In the equation (3.10), $\overline{V}$ is the microscopic flow velocity. The left hand side of equation (3.10) is the inertia term. With regards to flow in porous media the inertia term, represented by the left hand side of the equation (3.10) is negligibly small as compared to the right hand side. Also we assume, for porous media the Reynolds number is small. Combining these two assumptions, we have:

$$\mu \nabla^2 \overline{V} = -\nabla \Phi \qquad \text{……..... (3.12)}$$

Rearranging, we have:

$$\nabla^2 \overline{V} = -\frac{1}{\mu} \nabla \Phi \qquad \text{……..... (3.13)}$$

Left hand side of equation (3.13) represents the change of the microscopic flow velocity with distance. Since details regarding the structure of the porous medium are unknown, we have to use suitable statistical averaging the terms in equation (3.13) over a large volume as compared to the individual pores and this leads to:

$$\bar{v} = -\frac{k}{\mu}\nabla\Phi \qquad \text{……..... (3.14)}$$

Detailed proof is given by reference 44 and has not been reproduced here. This is Darcy's law. The need for such a derivation pins from the fact that when we go to solve the Darcy's law we are essentially solving the momentum equation.

In case of multiphase flow, where two different types of fluids are present in the pores, we can write the Darcy's law for each component of the fluid as:

Oil: $$u_o = -\frac{kk_{ro}}{\mu_o}\left(\frac{\partial p_o}{\partial x} + g\rho_o \sin\alpha\right) \qquad \text{……..... (3.15)}$$

Water: $$u_w = -\frac{kk_{rw}}{\mu_w}\left(\frac{\partial p_w}{\partial x} + g\rho_w \sin\alpha\right) \qquad \text{……..... (3.16)}$$

Here we are assuming that the wetting fluid is water, having density ρ_w, and the non-wetting fluid is oil, having density ρ_o. The relative permeability takes into account the amount of pore space occupied by each of the components of the fluid. Gravity effect on fluid flow is included with angle, α, of the flow direction. Mathematically, this can also be represented by:

$$\sin\alpha = \frac{\partial z}{\partial x} \qquad \text{……..... (3.17)}$$

We can rearrange equations (3.15) and (3.16) as:

$$u_o \frac{\mu_o}{kk_{ro}} = -\left(\frac{\partial p_o}{\partial x} + g\rho_o \sin\alpha\right) \qquad \text{……..... (3.18)}$$

$$u_w \frac{\mu_w}{kk_{rw}} = -\left(\frac{\partial p_w}{\partial x} + g\rho_w \sin\alpha \right) \qquad \text{…….....} (3.19)$$

Subtracting equation (3.18) from equation (3.19), we have:

$$u_w \frac{\mu_w}{kk_{rw}} - u_o \frac{\mu_o}{kk_{ro}} = -\left(\frac{\partial p_w}{\partial x} - \frac{\partial p_o}{\partial x} \right) - g(\rho_w - \rho_o)\sin\alpha \qquad \text{…….....} (3.20)$$

Equation (3.20) is the Darcy's law as applied to two-phase flow. There are a lot of unknown variables in this equation and our effort is to reduce the number of these unknowns so as to solve the equation.

Going by the definition of capillary pressure, P_c, the pressure differential between the non-wetting fluid to wetting fluid, is given by:

$$P_c = p_o - p_w \qquad \text{…….....} (3.21)$$

and, let $\Delta\rho$, be the difference in the densities of wetting and non-wetting fluids represented by:

$$\Delta\rho = \rho_w - \rho_o \qquad \text{…….....} (3.22)$$

Combining equations (3.21) and (3.22) into equation (3.20) we have:

$$u_w \frac{\mu_w}{kk_{rw}} - u_o \frac{\mu_o}{kk_{ro}} = \left(\frac{\partial P_c}{\partial x} - g\Delta\rho \sin\alpha \right) \qquad \text{…….....} (3.23)$$

This is the momentum balance equation for two-phase flow in porous media.

3.3 Law of Conservation of Energy

According to this law, the sum of all energy gain or loss across the control volume is zero. Under normal circumstances, the whole fluid flow process is an adiabatic one since there is no heat flow between the control volume and its

surroundings. This makes the sum of heat flow including sum of internal heat generation zero. Assuming no other form of energy enters or leaves the control volume, we can altogether do away with the law of conservation of energy. But in reservoir simulation, as is with other fluid flow processes, we assume the flow process to take place under isothermal conditions, meaning that the temperature remains constant or the change in internal heat generation or absorption can be assumed to be very small. As a result, we can relate change in pressure directly with change in volume. This means that for system where there is variable density and viscosity we can use of equation of state and equation of viscosity. The former is represented by equation (3.24) which relates the density of the fluid to pressure and the latter is represented by equation (3.25), which relates the viscosity of the fluid to pressure. Thus, mathematically, we have:

$$\rho = \rho(p) \qquad \text{……..... (3.24)}$$

$$\mu = \mu(p) \qquad \text{……..... (3.25)}$$

This completes the application of all the fundamental laws to the given control volume.

3.4 Derivation of Spontaneous Imbibition Equation

To arrive at the governing equation of spontaneous imbibition, we have to combine equations (3.7), (3.8) and (3.23) and drop the term due to well (source/sink) production, since inclusion of this term negates the idea of spontaneous imbibition. If for some reason their inclusion becomes imperative, then in that case, the equation becomes a displacement equation. Out of the two possible approaches of spontaneous imbibition, we consider one of the approaches, called the counter-current imbibition, for which we have:

$$u_w = -u_o \qquad \text{..... (3.26)}$$

Hence from equations (3.23) and (3.26) we have:

$$u_w = \left(\frac{k k_{rw} k_{ro}}{\mu_w k_{ro} + \mu_o k_{rw}} \right) \left(\frac{\partial P_c}{\partial x} - g \Delta \rho \sin \alpha \right) \qquad \text{..... (3.27)}$$

Taking differential of equation (3.27) and combining it with equation (3.7) we have:

$$\frac{\partial S_w}{\partial t} = \frac{1}{\phi} \frac{\partial}{\partial x} \left[\left(\frac{k k_{rw} k_{ro}}{\mu_w k_{ro} + \mu_o k_{rw}} \right) \left(- \frac{\partial P_c}{\partial x} + g \Delta \rho \sin \alpha \right) \right] \qquad \text{..... (3.28)}$$

which transforms to:

$$\frac{\partial S_w}{\partial t} = \frac{\partial}{\partial x} \left[\frac{k k_{rw} k_{ro}}{\phi \left(\mu_w k_{ro} + \mu_o k_{rw} \right)} \left(- \left(\frac{\partial P_c}{\partial S_w} \right) \frac{\partial S_w}{\partial x} \right) \right] + \frac{\partial}{\partial x} \left[\frac{k k_{rw} k_{ro}}{\phi \left(\mu_w k_{ro} + \mu_o k_{rw} \right)} \right] g \Delta \rho \sin \alpha$$

..... (3.29)

Rearranging the above equation, leads to:

$$\frac{\partial S_w}{\partial t} = \frac{\partial}{\partial x}\left[\frac{kk_{rw}k_{ro}}{\phi(\mu_w k_{ro} + \mu_o k_{rw})}\right]\left[-\left(\frac{\partial P_c}{\partial S_w}\frac{\partial S_w}{\partial x}\right) + g\Delta\rho\sin\alpha\right]$$

$$+\left[\frac{kk_{rw}k_{ro}}{\phi(\mu_w k_{ro} + \mu_o k_{rw})}\right]\frac{\partial}{\partial x}\left[-\left(\frac{\partial P_c}{\partial S_w}\frac{\partial S_w}{\partial x}\right) + g\Delta\rho\sin\alpha\right]$$

……..... (3.30)

Equation (3.29) or (3.30) is the governing equation of spontaneous imbibition and is the non-linear diffusion saturation equation. The first part of equation (3.29) is the diffusion term [D], which is determined by capillary forces whereas the latter, gravity term [V] is determined by the gravitational forces. For simplicity, equation (3.29) is written in the form:

$$\phi\frac{\partial S_w}{\partial t} = -\frac{\partial}{\partial x}\left[D\left(\frac{\partial S_w}{\partial x}\right)\right] + \frac{\partial}{\partial x}[V]\sin\alpha \qquad \text{……..... (3.31)}$$

where,

$$[D] = \left[\frac{kk_{rw}k_{ro}}{(\mu_w k_{ro} + \mu_{mw} k_{rw})}\left(\frac{dP_c}{dS_w}\right)\right] \qquad \text{……..... (3.32)}$$

$$[V] = \left[\frac{kk_{rw}k_{ro}\Delta\rho}{(\mu_w k_{ro} + \mu_{nw} k_{rw})}\right]g \qquad \text{……..... (3.33)}$$

3.5 Derivation of General Displacement Equation

If general displacement is assumed then, for two-phase flow, we can derive the equation using the saturations. We know, in order to have mass balance at each point,

$$\rho_o \partial V_o + \rho_w \partial V_w = 0$$

$$\rho_o \partial S_o = -\rho_w \partial S_w \qquad \text{..... (3.34)}$$

Expressing the non-wetting phase saturation with the help of wetting phase saturation the continuity equation reduces to:

$$\frac{\partial u_o}{\partial x} - \phi \frac{\rho_w}{\rho_o} \frac{\partial S_w}{\partial t} = 0 \qquad \text{..... (3.35)}$$

Combining equations (3.7), (3.8) and (3.23), we have:

$$\left(-\phi \frac{\partial S_w}{\partial t} + \frac{q_{ws}}{A} \right) \frac{\mu_w}{k k_{rw}} - \phi \frac{\rho_w}{\rho_o} \frac{\partial S_w}{\partial t} \frac{\mu_o}{k k_{ro}} = \frac{\partial}{\partial x} \left[\left(\frac{\partial P_c}{\partial x} - g \Delta \rho \sin \alpha \right) \right] \qquad \text{..... (3.36)}$$

which reduces to:

$$\left(1 + \frac{\rho_w}{\rho_o} \right) \frac{\partial S_w}{\partial t} = \frac{1}{\phi} \frac{\partial}{\partial x} \left[\left(\frac{k k_{rw} k_{ro}}{\mu_w k_{ro} + \mu_o k_{rw}} \right) \left(-\frac{\partial P_c}{\partial x} + g \Delta \rho \sin \alpha \right) \right] + \left(\frac{k_{ro} \mu_w}{\mu_w k_{ro} + \mu_o k_{rw}} \right) \frac{q_{ws}}{\phi A}$$

..... (3.37)

and can be written as:

$$\left(1 + \frac{\rho_w}{\rho_o} \right) \frac{\partial S_w}{\partial t} = \frac{\partial}{\partial x} \left[\frac{k k_{rw} k_{ro}}{\phi (\mu_w k_{ro} + \mu_o k_{rw})} \left(-\left(\frac{\partial P_c}{\partial S_w} \right) \frac{\partial S_w}{\partial x} \right) \right] + \frac{\partial}{\partial x} \left[\frac{k k_{rw} k_{ro}}{\phi (\mu_w k_{ro} + \mu_o k_{rw})} \right] g \Delta \rho \sin \alpha$$

$$+ \left(\frac{k_{ro} \mu_w}{\mu_w k_{ro} + \mu_o k_{rw}} \right) \frac{q_{ws}}{\phi A} \qquad \text{..... (3.38)}$$

Rearranging the above equation, leads to:

$$\left(1+\frac{\rho_w}{\rho_o}\right)\frac{\partial S_w}{\partial t}=\frac{\partial}{\partial x}\left[\frac{kk_{rw}k_{ro}}{\phi\left(\mu_w k_{ro}+\mu_o k_{rw}\right)}\right]\left[-\left(\frac{\partial P_c}{\partial S_w}\frac{\partial S_w}{\partial x}\right)+g\Delta\rho\sin\alpha\right]$$

$$+\left[\frac{kk_{rw}k_{ro}}{\phi\left(\mu_w k_{ro}+\mu_o k_{rw}\right)}\right]\frac{\partial}{\partial x}\left[-\left(\frac{\partial P_c}{\partial S_w}\frac{\partial S_w}{\partial x}\right)+g\Delta\rho\sin\alpha\right]+\left(\frac{k_{ro}\mu_w}{\mu_w k_{ro}+\mu_o k_{rw}}\right)\frac{q_{ws}}{\phi A}$$

……..... (3.39)

Equations (3.38) or (3.39) are used as governing equations for oil-water displacement. As can be seen they are different from equations (3.29) and (3.30) only in the way the source (producer) or sink (injector) terms are handled.

CHAPTER IV

FINITE DIFFERENCE NUMERICAL MODEL

The spontaneous imbibition equation derived in the previous chapter was for one dimension. Rewriting this equation here:

$$\phi\frac{\partial S_w}{\partial t}=\frac{\partial}{\partial x}\left[\frac{kk_{rw}k_{ro}}{(\mu_w k_{ro}+\mu_o k_{rw})}\left(-\left(\frac{\partial P_c}{\partial S_w}\right)\frac{\partial S_w}{\partial x}\right)\right]+\frac{\partial}{\partial x}\left[\frac{kk_{rw}k_{ro}}{(\mu_w k_{ro}+\mu_o k_{rw})}\right]g\Delta\rho\sin\alpha$$

……..... (3.29)

For two-dimensional case the above equation can be written as:

$$\phi\frac{\partial S_w}{\partial t}=\frac{\partial}{\partial x}\left[\frac{kk_{rw}k_{ro}}{(\mu_w k_{ro}+\mu_o k_{rw})}\left(-\left(\frac{\partial P_c}{\partial S_w}\right)\frac{\partial S_w}{\partial x}\right)\right]+\frac{\partial}{\partial x}\left[\frac{kk_{rw}k_{ro}}{(\mu_w k_{ro}+\mu_o k_{rw})}\right]g\Delta\rho\sin\alpha$$

$$+\frac{\partial}{\partial y}\left[\frac{kk_{rw}k_{ro}}{(\mu_w k_{ro}+\mu_o k_{rw})}\left(-\left(\frac{\partial P_c}{\partial S_w}\right)\frac{\partial S_w}{\partial y}\right)\right]+\frac{\partial}{\partial y}\left[\frac{kk_{rw}k_{ro}}{(\mu_w k_{ro}+\mu_o k_{rw})}\right]g\Delta\rho\sin\alpha \text{ ..... (4.1)}$$

This can be reduced to a simple form similar to equation (3.31) as:

$$\phi\frac{\partial S_w}{\partial t}=-\frac{\partial}{\partial x}\left[D\left(\frac{\partial S_w}{\partial x}\right)\right]-\frac{\partial}{\partial y}\left[D\left(\frac{\partial S_w}{\partial y}\right)\right]+\frac{\partial}{\partial x}[V]\sin\alpha+\frac{\partial}{\partial y}[V]\sin\alpha \text{ .. (4.2)}$$

where the values of [D] and [V] are reproduced from the previous chapter:

$$[D]=\left[\frac{kk_{rw}k_{ro}}{(\mu_w k_{ro}+\mu_o k_{rw})}\left(\frac{dP_c}{dS_w}\right)\right] \qquad \text{……..... (3.32)}$$

$$[V]=\left[\frac{kk_{rw}k_{ro}\Delta\rho}{(\mu_w k_{ro}+\mu_o k_{rw})}\right]g \qquad \text{..... (3.33)}$$

For experimental purposes, a further simplification of this equation is carried out by assuming the effect of gravity to be negligible. This equation then takes the form:

$$\phi\frac{\partial S_w}{\partial t}=-\frac{\partial}{\partial x}\left[D\left(\frac{\partial S_w}{\partial x}\right)\right]-\frac{\partial}{\partial y}\left[D\left(\frac{\partial S_w}{\partial y}\right)\right] \qquad \text{..... (4.3)}$$

Equation (4.3) forms the basis of numerical code for finite difference simulation.

4.1 Finite Difference Discretization

For discretizing the above equation we start with basics of finite difference scheme. It can be recalled that for a given function, $F(x,t)$, the finite difference expansion for space and time are:

$$\frac{\partial F}{\partial x}=\frac{\left(F^n_{i+1,j}-F^n_{i,j}\right)}{\Delta x}+\frac{\left(F^n_{i-1,j}-F^n_{i,j}\right)}{\Delta x} \qquad \text{..... (4.4)}$$

$$\frac{\partial F}{\partial y}=\frac{\left(F^n_{i,j+1}-F^n_{i,j}\right)}{\Delta y}+\frac{\left(F^n_{i,j-1}-F^n_{i,j}\right)}{\Delta y} \qquad \text{..... (4.5)}$$

$$\frac{\partial F}{\partial t}=\frac{\left(F^{n+1}_{i,j}-F^n_{i,j}\right)}{\Delta t} \qquad \text{..... (4.6)}$$

Here,

$$\Delta x=\Delta x_{i,j} \qquad \text{..... (4.7)}$$

and

$$\Delta y=\Delta x_{i,j} \qquad \text{..... (4.8)}$$

It is evident that we are using central difference in space and forward difference in time for the finite difference expansions. Substituting this in equation (4.3), the finite difference equivalent of equation (4.3) is given by:

$$\frac{D^n_{i-\frac{1}{2},j}}{\Delta x_{i-\frac{1}{2},j}}\frac{\left((S_w)^{n+1}_{i-1,j}-(S_w)^{n+1}_{i,j}\right)}{\Delta x_{i,j}}+\frac{D^n_{i+\frac{1}{2},j}}{\Delta x_{i+\frac{1}{2},j}}\frac{\left((S_w)^{n+1}_{i+1,j}-(S_w)^{n+1}_{i,j}\right)}{\Delta x_{i,j}}$$

$$+\frac{D^n_{i,j-\frac{1}{2}}}{\Delta x_{i,j-\frac{1}{2}}}\frac{\left((S_w)^{n+1}_{i,j-1}-(S_w)^{n+1}_{i,j}\right)}{\Delta x_{i,j}}+\frac{D^n_{i,j+\frac{1}{2}}}{\Delta x_{i,j+\frac{1}{2}}}\frac{\left((S_w)^{n+1}_{i,j+1}-(S_w)^{n+1}_{i,j}\right)}{\Delta x_{i,j}}=-\phi_{i,j}\frac{\left((S_w)^{n+1}_{i,j}-(S_w)^{n}_{i,j}\right)}{\Delta t}$$

…….... (4.9)

The diffusion term are calculated at the face of the grid block. The relative permeability value is the upstream value and we have used harmonic average of the permeability value. Thus for face at a distance of:

$$\Delta x_{i-\frac{1}{2},j}=\Delta x_{i,j}-\Delta x_{i-1,j} \qquad \text{…….... (4.10)}$$

the diffusion coefficient is given by:

$$D_{i-\frac{1}{2},j}=\frac{(k_w)_{i-\frac{1}{2},j}}{\mu_w}\left(\frac{dP_c}{dS_w}\right)_{i-\frac{1}{2},j} \qquad \text{…….... (4.11)}$$

in which the capillary pressure term is calculated thus:

$$\left(\frac{dP_c}{dS_w}\right)_{i-\frac{1}{2},j}\approx\left(\frac{P_c(S_w+\Delta S)-P_c(S_w)}{\Delta S}\right)_{i-1,j} \qquad \text{…….... (4.12)}$$

CHAPTER V

FINITE ELEMENT NUMERICAL MODEL

In order to derive the finite element model of equation (3.30) or equation (3.39) we have to know the reason as why the classical Rayleigh-Ritz cannot be applied to these two equations. Before we answer that question we have to know the background as to how a particular differential equation becomes linear or non-linear.

5.1 Condition of Linearity

An operator *L*, is said to be linear if it satisfies all the listed criteria, as per reference 19:

1. $L(0) = 0$
2. $L(cu) = cL(u)$
3. $L(u+v) = L(u) + L(v)$

If any of the above criteria are not satisfied then the equation becomes a non-linear one. Consider for example:

$$L(x) = x^2 \qquad \text{…….... (5.1)}$$

Applying the above criteria, we have:

1. $L(0) = 0$
2. $L(cx) = c^2x^2 = cL(x)$
3. $L(x+y) = (x+y)^2 = x^2 + 2xy + y^2 \neq L(x) + L(y)$

Hence that equation is a non-linear one. As a general rule, linear problems are easier to solve than non-linear ones. Where ever possible, the non-linear equation is first linearized and then solved. A classical example of non-linear equation that is linearized is the diffusivity equation as given by reference 19. The actual form of this equation, as derived by substituting Darcy's law in Continuity equation, is:

$$\nabla \bullet \rho\left(-\frac{k}{\mu}\nabla p\right) = -\frac{\partial(\phi\rho)}{\partial t} \qquad \text{…….....} (5.2)$$

which finally forms:

$$\rho\nabla \bullet \nabla p + (\nabla\rho)\bullet(\nabla p) = \frac{\mu}{k}\frac{\partial(\phi\rho)}{\partial t} \qquad \text{…….....} (5.3)$$

The above equation is linearized after neglecting the second term on the left-hand side. This is possible by assuming that compressibility as negligibly small and we get the final, and more common form of the diffusivity equation as:

$$\rho\nabla \bullet \nabla p = \frac{\mu}{k}\frac{\partial(\phi\rho)}{\partial t} \qquad \text{…….....} (5.4)$$

5.2 Applicability of Various Finite Element Methods

According to Reddy[20], if the governing differential equation contains derivatives of the even order then it is possible to form the weak form of that differential equation and hence apply the Rayleigh-Ritz finite element method. Thus the ability to construct the weak form is the key to application of this method. The weak form, which gives rise to the functional $I(u)$, is a representation of the total potential energy of the system. The functional follows from variational calculus and is given by:

$$I(u) = \frac{1}{2}B(w,u) - l(w) \qquad \text{…….....} (5.5)$$

What it essentially does is to weaken the differentiability of the governing differential equation. Any function *u*, which satisfies the weak form and makes the total potential energy as represented by the functional $I(u)$ minimum, also satisfies the differential

equation and its natural boundary condition. These definitions are more relevant to solid mechanics where the functional has the meaning of energy. For outside the scope of solid mechanics, such as fluid flow in porous media, the functional $I(u)$ may not have the meaning of energy, but this idea is still useful for mathematical analysis.

Rayleigh-Ritz method can also be applied to non-linear problems which can be structured into weak variational form. But it is not always possible to construct the weak form of the given differential equation. Under such circumstances we go in for the following two methods:

1. Weighted-Integral Method
2. Weighted-Residual Method
3. Mixed Formulation Method

In both top cases it is not necessary that the specified boundary condition of the differential equation be included in the weighted-integral form. This makes the choice of the interpolating functions such that both the Dirichlet (essential) and the Neumann (natural) boundary condition are satisfied together. Weighted-residual method is an iterative method in which we try to reduce the residue generated by putting the differential equation into its weighted-integral form. These requirements increase the order of the polynomial expression used in the weighted- integral or the weighted-residual method. The most common choices are:

a) Galerkin Method
b) Least-Square Method
c) Collocation Method

Sometimes, when dealing with higher-order differential equation, the weak form requires the use of higher order interpolation functions. As opposed to this, if we use weighted-residual finite element method then we have to use even a higher order interpolating function than used above. The way around it is to reduce the differentiability requirement on the nodal degree of freedom. Such method is called Mixed formulation method. A detailed review of all these methods is given by reference 20. It is important to know the distinction between the Rayleigh-Ritz method and the

Galerkin method. They are not the same. The former uses the weak variational form whereas the latter uses the weighted-integral form. Consequently, the approximation functions used in Galerkin method are of higher order than those in Rayleigh-Ritz method. Under some circumstances both these methods yield the same results as per reference 20.

5.3 Spontaneous Imbibition in Porous Media through Rayleigh-Ritz Finite Element Method

We begin by reproducing equation (3.30) which was derived previously for one dimension as:

$$\frac{\partial S_w}{\partial t} = \frac{\partial}{\partial x}\left[\frac{kk_{rw}k_{ro}}{\phi(\mu_w k_{ro} + \mu_o k_{rw})}\right]\left[-\left(\frac{\partial P_c}{\partial S_w}\frac{\partial S_w}{\partial x}\right) + g\Delta\rho\sin\alpha\right]$$

$$+\left[\frac{kk_{rw}k_{ro}}{\phi(\mu_w k_{ro} + \mu_o k_{rw})}\right]\frac{\partial}{\partial x}\left[-\left(\frac{\partial P_c}{\partial S_w}\frac{\partial S_w}{\partial x}\right) + g\Delta\rho\sin\alpha\right] \quad \text{..... (3.30)}$$

5.3.1 Formulation of the Governing Differential Equation in Two-Dimensions

Extending the above equation from one dimension to two dimensional flow, this equation converts to:

$$\frac{\partial S_w}{\partial t} = \frac{\partial}{\partial x}\left[\frac{kk_{rw}k_{ro}}{\phi(\mu_w k_{ro} + \mu_o k_{rw})}\right]\left[-\left(\frac{\partial P_c}{\partial S_w}\frac{\partial S_w}{\partial x}\right) + g\Delta\rho\sin\alpha\right]$$

$$+\left[\frac{kk_{rw}k_{ro}}{\phi(\mu_w k_{ro} + \mu_o k_{rw})}\right]\frac{\partial}{\partial x}\left[-\left(\frac{\partial P_c}{\partial S_w}\frac{\partial S_w}{\partial x}\right) + g\Delta\rho\sin\alpha\right]$$

$$+\frac{\partial}{\partial y}\left[\frac{kk_{rw}k_{ro}}{\phi(\mu_w k_{ro} + \mu_o k_{rw})}\right]\left[-\left(\frac{\partial P_c}{\partial S_w}\frac{\partial S_w}{\partial y}\right) + g\Delta\rho\sin\alpha\right]$$

$$+\left[\frac{kk_{rw}k_{ro}}{\phi(\mu_w k_{ro} + \mu_o k_{rw})}\right]\frac{\partial}{\partial y}\left[-\left(\frac{\partial P_c}{\partial S_w}\frac{\partial S_w}{\partial y}\right) + g\Delta\rho\sin\alpha\right] \quad \text{..... (5.6)}$$

The capillary potential is given by:

$$\Phi_c = P_c - \Delta\rho g \sin\alpha$$

and its gradient in x-direction is:

$$\frac{\partial \Phi_c}{\partial x} = \frac{\partial P_c}{\partial x} - \Delta\rho g \sin\alpha \qquad \text{…….... (5.7)}$$

Let us assume that the capillary potential can be represented by a forcing function F_α where $\alpha = 1$ or 2 depend on direction. Thus we have:

$$F_1 = \left[-\left(\frac{\partial P_c}{\partial x} \right) + g\Delta\rho \sin\alpha \right] = -\frac{\partial \Phi_c}{\partial x}$$

$$F_2 = \left[-\left(\frac{\partial P_c}{\partial y} \right) + g\Delta\rho \sin\alpha \right] = -\frac{\partial \Phi_c}{\partial y} \qquad \text{…….... (5.8)}$$

Substitution of equation (5.8) in equation (5.6) reduces it to:

$$0 = \frac{\partial S_w}{\partial t} - \frac{\partial}{\partial x}\left[\frac{kk_{rw}k_{ro}}{\phi(\mu_w k_{ro} + \mu_o k_{rw})} \right][F_1] - \left[\frac{kk_{rw}k_{ro}}{\phi(\mu_w k_{ro} + \mu_o k_{rw})} \right] \frac{\partial}{\partial x}[F_1]$$

$$- \frac{\partial}{\partial y}\left[\frac{kk_{rw}k_{ro}}{\phi(\mu_w k_{ro} + \mu_o k_{rw})} \right][F_2] - \left[\frac{kk_{rw}k_{ro}}{\phi(\mu_w k_{ro} + \mu_o k_{rw})} \right] \frac{\partial}{\partial y}[F_2] \qquad \text{…….... (5.9)}$$

which is the governing differential equation used to formulate the finite element model.

5.3.2 Formulation of the Variational Weak Form

In order to construct the weak form we multiply the governing equation with weight function w, and integrate over the domain to get:

$$0 = \int_{\Omega_e} w\left\{\frac{\partial S_w}{\partial t} - \frac{\partial}{\partial x}\left[\frac{kk_{rw}k_{ro}}{\phi(\mu_w k_{ro} + \mu_o k_{rw})}\right][F_1] - \left[\frac{kk_{rw}k_{ro}}{\phi(\mu_w k_{ro} + \mu_o k_{rw})}\right]\frac{\partial}{\partial x}[F_1]\right\}dxdy$$

$$-\int_{\Omega_e} w\left\{\frac{\partial}{\partial y}\left[\frac{kk_{rw}k_{ro}}{\phi(\mu_w k_{ro} + \mu_o k_{rw})}\right][F_2] + \left[\frac{kk_{rw}k_{ro}}{\phi(\mu_w k_{ro} + \mu_o k_{rw})}\right]\frac{\partial}{\partial y}[F_2]\right\}dxdy \quad \text{..... (5.10)}$$

Let,

$$M = \frac{kk_{rw}k_{ro}}{\phi(\mu_w k_{ro} + \mu_o k_{rw})}$$

For the operator, we have,

$$\frac{\partial}{\partial x}(wF_1) = \frac{\partial w}{\partial x}F_1 + w\frac{\partial F_1}{\partial x} \quad \Rightarrow \quad -w\frac{\partial F_1}{\partial x} = \frac{\partial w}{\partial x}F_1 - \frac{\partial}{\partial x}(wF_1) \quad \text{..... (5.11a)}$$

$$\frac{\partial}{\partial y}(wF_2) = \frac{\partial w}{\partial y}F_2 + w\frac{\partial F_2}{\partial y} \quad \Rightarrow \quad -w\frac{\partial F_2}{\partial y} = \frac{\partial w}{\partial y}F_2 - \frac{\partial}{\partial y}(wF_2) \quad \text{..... (5.11b)}$$

Using gradient theorem we convert the surface integral into line integral,

$$\int_{\Omega^e}\frac{\partial}{\partial x}(wF_1)dxdy = \oint_{\Gamma^e} wF_1 n_x ds \quad \text{..... (5.12a)}$$

$$\int_{\Omega^e}\frac{\partial}{\partial y}(wF_2)dxdy = \oint_{\Gamma^e} wF_2 n_y ds \quad \text{..... (5.12b)}$$

where n_x and n_y are the direction cosines of the unit normal vector.

$$\bar{n} = n_x\bar{i} + n_y\bar{j}$$

From equation (5.10), equation (5.11) and equation (5.12), we have:

$$0 = \int \left[w\frac{\partial S_w}{\partial t} - w[F_1]\frac{\partial}{\partial x}\left[\frac{kk_{rw}k_{ro}}{\phi(\mu_w k_{ro} + \mu_o k_{rw})}\right] + \frac{\partial w}{\partial x}\left[\frac{kk_{rw}k_{ro}}{\phi(\mu_w k_{ro} + \mu_o k_{rw})}\right][F_1]\right] dxdy$$

$$- \int \left[w[F_2]\frac{\partial}{\partial y}\left[\frac{kk_{rw}k_{ro}}{\phi(\mu_w k_{ro} + \mu_o k_{rw})}\right] - \frac{\partial w}{\partial y}\left[\frac{kk_{rw}k_{ro}}{\phi(\mu_w k_{ro} + \mu_o k_{rw})}\right][F_2]\right] dxdy$$

$$- \oint_{\Gamma^e} wMF_1 n_x ds - \oint_{\Gamma^e} wMF_2 n_y ds \text{ ……..... (5.13)}$$

Simplifying and replacing the value of forcing functions we have:

$$0 = \int \left[w\frac{\partial S_w}{\partial t} - w\left[-\left(\frac{\partial P_c}{\partial x}\right) + g\Delta\rho\sin\alpha\right]\frac{\partial}{\partial S_w}\left[\frac{kk_{rw}k_{ro}}{\phi(\mu_w k_{ro} + \mu_o k_{rw})}\right]\frac{\partial S_w}{\partial x}\right] dxdy$$

$$+ \int \frac{\partial w}{\partial x}\left[\frac{kk_{rw}k_{ro}}{\phi(\mu_w k_{ro} + \mu_o k_{rw})}\right]\left[-\left(\frac{\partial P_c}{\partial x}\right) + g\Delta\rho\sin\alpha\right] dxdy$$

$$- \int \left[w\left[-\left(\frac{\partial P_c}{\partial y}\right) + g\Delta\rho\sin\alpha\right]\frac{\partial}{\partial S_w}\left[\frac{kk_{rw}k_{ro}}{\phi(\mu_w k_{ro} + \mu_o k_{rw})}\right]\frac{\partial S_w}{\partial y}\right] dxdy$$

$$+ \int \frac{\partial w}{\partial y}\left[\frac{kk_{rw}k_{ro}}{\phi(\mu_w k_{ro} + \mu_o k_{rw})}\right]\left[-\left(\frac{\partial P_c}{\partial y}\right) + g\Delta\rho\sin\alpha\right] dxdy - \oint_{\Gamma^e} wq_n ds$$

……..... (5.14)

where,

$$q_n = \left(MF_1 n_x + MF_2 n_y\right) \text{ ……..... (5.15)}$$

Equation (5.14) is the weak form of the governing differential equation. Rearranging it and expressing it in terms of capillary potential, we get:

$$0 = \int \left[w \frac{\partial S_w}{\partial t} \right] dxdy$$

$$+ \frac{1}{\phi} \int \frac{\partial w}{\partial x} \left[\frac{k k_{rw} k_{ro}}{(\mu_w k_{ro} + \mu_o k_{rw})} \right] \left[- \left(\left(\frac{\partial \Phi_c}{\partial S_w} \right) \frac{\partial S_w}{\partial x} \right) \right] dxdy$$

$$+ \frac{1}{\phi} \int \frac{\partial w}{\partial y} \left[\frac{k k_{rw} k_{ro}}{(\mu_w k_{ro} + \mu_o k_{rw})} \right] \left[- \left(\left(\frac{\partial \Phi_c}{\partial S_w} \right) \frac{\partial S_w}{\partial y} \right) \right] dxdy$$

$$- \frac{1}{\phi} \int \left[w \left[- \left(\frac{\partial \Phi_c}{\partial S_w} \right) \right] \left\{ \frac{\partial}{\partial S_w} \left[\frac{k k_{rw} k_{ro}}{(\mu_w k_{ro} + \mu_o k_{rw})} \right] \right\} \left(\frac{\partial S_w}{\partial x} \right)^2 \right] dxdy$$

$$- \frac{1}{\phi} \int \left[w \left[- \left(\frac{\partial \Phi_c}{\partial S_w} \right) \right] \left\{ \frac{\partial}{\partial S_w} \left[\frac{k k_{rw} k_{ro}}{(\mu_w k_{ro} + \mu_o k_{rw})} \right] \right\} \left(\frac{\partial S_w}{\partial y} \right)^2 \right] dxdy - \oint_{\Gamma^e} w q_n ds$$

……..... (5.16)

Equation (5.1) is clearly a non-linear equation. Also it is not in bilinear form, which simply stated means that if we interchange the primary variable with the weight function the differential equation essentially remains the same, hence Rayleigh-Ritz method cannot be applied to it. The secondary variable is given by:

$$\oint_{\Gamma^e} w q_n ds = \oint_{\Gamma^e} \left[wM \left(\frac{\partial \Phi_c}{\partial x} \right) \right] n_x ds + \oint_{\Gamma^e} \left[wM \left(\frac{\partial \Phi_c}{\partial y} \right) \right] n_y ds$$

which upon expansion is:

$$\oint_{\Gamma^e} w q_n ds = \oint_{\Gamma^e} \left[wM \left(\frac{\partial \Phi_c}{\partial S_w} \left(\frac{\partial S_w}{\partial x} \right) \right) \right] n_x ds + \oint_{\Gamma^e} \left[wM \left(\frac{\partial \Phi_c}{\partial S_w} \left(\frac{\partial S_w}{\partial y} \right) \right) \right] n_y ds \text{ ……..... (5.17)}$$

This brings out the fact that we have to use Lagrange interpolation function for the weight function and Hermite interpolation function for the primary variable. If it is decided that we use this combination then the method is called Rayleigh-Ritz method. Otherwise Galerkin method is the way out in this case, wherein both the weight function and the primary variable are approximated by Hermite interpolating function. With this we are trying to establish the continuity of the secondary variable, both the weight function and the primary variable at the element boundaries, which is not done by Rayleigh-Ritz Method. This is the main reason why Galerkin method is computationally more intense than the Rayleigh-Ritz method. If we were to apply the approximation as discussed in the next section, then we will see that we can solve the equation (5.16) with use of Lagrange interpolation function only, thereby bringing down computational complexity of finite element method.

Also, in case of Rayleigh-Ritz method the secondary variable needs to be meaningful in order the method to be applied. This is not the case in here. What can be said is that the capillary pressure gradient curve will be zero outside the porous media and hence, at the boundary, the secondary variable will be zero. This theory can also be extended to grid / matrix block which are completely surrounded by water at all times and for such a case the capillary pressure gradient is zero at $S_w = 1.0$.

5.3.3 Formulation of Linearized Variational Weak Form – Truncated Equation

In order to further simplify the problem, we will try to covert the non-linear differential equation into a linear one. As the primary variable, which in this case is saturation varies from 0.0 to 1.0, the value of the first derivative is small compared to unity and hence $\frac{\partial S_w}{\partial x} << 1$ and $\frac{\partial S_w}{\partial y} << 1$. This means, from reference 20, the value of $\left(\frac{\partial S_w}{\partial x}\right)^2 \approx 0$ and $\left(\frac{\partial S_w}{\partial y}\right)^2 \approx 0$. If this is applied to the equation (5.16) the resulting equation is:

$$0 = \int \left[w \frac{\partial S_w}{\partial t} \right] dxdy$$

$$+ \frac{1}{\phi} \int \frac{\partial w}{\partial x} \left[\frac{k k_{rw} k_{ro}}{(\mu_w k_{ro} + \mu_o k_{rw})} \right] \left[\left(\left(\frac{\partial \Phi_c}{\partial S_w} \right) \frac{\partial S_w}{\partial x} \right) \right] dxdy$$

$$+ \frac{1}{\phi} \int \frac{\partial w}{\partial y} \left[\frac{k k_{rw} k_{ro}}{(\mu_w k_{ro} + \mu_o k_{rw})} \right] \left[\left(\left(\frac{\partial \Phi_c}{\partial S_w} \right) \frac{\partial S_w}{\partial y} \right) \right] dxdy - \oint_{\Gamma^e} w q_n ds \quad \text{…….....} \quad (5.18)$$

This is the weak form which we use to formulate the finite element model.

5.3.4 Finite Element Model

Let us assume that saturation S_w is approximated over a typical finite element as:

$$S_w(x, y) = \sum_{j=1}^{n} s_j^e(t) \psi_j^e(x, y)$$

and $$w = \psi_i^e \quad \text{…....} \quad (5.19)$$

The only requirement on this function is that it should be at least linear in both the x and y direction and it does not make any terms in the weak form as zero. Substituting in equation (5.18),

$$0 = \int \left[\psi_i^e \sum \psi_j^e \frac{\partial s_j^e}{\partial t} \right] dxdy$$

$$+ \frac{1}{\phi} \int \frac{\partial \psi_i^e}{\partial x} \left[\left(\frac{\partial \Phi_c}{\partial S_w} \right) \right] \left[\frac{k k_{rw} k_{ro}}{(\mu_w k_{ro} + \mu_o k_{rw})} \right] \sum \frac{\partial \psi_j^e}{\partial x} s_j^e dxdy$$

$$+ \frac{1}{\phi} \int \frac{\partial \psi_i^e}{\partial y} \left[\left(\frac{\partial \Phi_c}{\partial S_w} \right) \right] \left[\frac{k k_{rw} k_{ro}}{(\mu_w k_{ro} + \mu_o k_{rw})} \right] \sum \frac{\partial \psi_j^e}{\partial y} s_j^e dxdy - \oint_{\Gamma^e} \psi_i^e q_n ds$$

Rearranging the summation common and out of the parenthesis:

$$0 = \sum_{j=1}^{n} \left\{ \int \left[\psi_i^e \psi_j^e \right] dxdy \right\} \frac{\partial s_j^e}{\partial t}$$

$$+ \sum_{j=1}^{n} \left\{ \frac{1}{\phi} \int \left[\left(\frac{\partial \Phi_c}{\partial S_w} \right) \right] \left[\frac{k k_{rw} k_{ro}}{\left(\mu_w k_{ro} + \mu_o k_{rw} \right)} \right] \frac{\partial \psi_i^e}{\partial x} \frac{\partial \psi_j^e}{\partial x} dxdy \right\} s_j^e$$

$$+ \sum_{j=1}^{n} \left\{ \frac{1}{\phi} \int \left[\left(\frac{\partial \Phi_c}{\partial S_w} \right) \right] \left[\frac{k k_{rw} k_{ro}}{\left(\mu_w k_{ro} + \mu_o k_{rw} \right)} \right] \frac{\partial \psi_i^e}{\partial y} \frac{\partial \psi_j^e}{\partial y} dxdy \right\} s_j^e \qquad \text{..... (5.20)}$$

This is the finite element model. This is of the form:

$$\sum_{j=1}^{n} M_{ij}^e \left\{ \dot{s}_j^e \right\} + \sum_{j=1}^{n} K_{ij}^e s_j^e = Q_i^e \qquad \text{..... (5.21)}$$

Comparing equation (5.20) and equation (5.21), we have:

$$M_{ij}^e = \int_{\Omega_e} \left[\psi_i^e \psi_j^e \right] dxdy$$

$$Q_i^e = \oint_{\Gamma^e} \psi_i^e q_n ds$$

Here,

$$K_{ij}^e = a_{11} \left[K^{11} \right] + a_{22} \left[K^{22} \right] \qquad \text{..... (5.22)}$$

with,

$$a_{11} = \frac{1}{\phi} \int \left[\left(\frac{\partial \Phi_c}{\partial S_w} \right) \right] \left[\frac{k k_{rw} k_{ro}}{\left(\mu_w k_{ro} + \mu_o k_{rw} \right)} \right]$$

$$a_{22} = \frac{1}{\phi} \int \left[\left(\frac{\partial \Phi_c}{\partial S_w} \right) \right] \left[\frac{k k_{rw} k_{ro}}{\left(\mu_w k_{ro} + \mu_o k_{rw} \right)} \right] \qquad \text{..... (5.23)}$$

5.3.5 Decoupling of the Saturation Domain Variables

A close examination of equation (5.23) reveals that $a_{11} = a_{22}$ and both of them depend on change in saturation, S_w only. This we refer to as saturation domain. The whole idea behind this method is to solve analytically the capillary gradient equation and the mobility ratio equation which gives us the ability to apply the Rayleigh-Ritz method and increase the computational efficiency of the method. This idea is somewhat similar to streamline simulation. The theoretical basis of the decoupling operation is explained here. Integration of two functions like *u* and *v*, which depend on a primary variable such as *x*, is carried out by parts as:

$$\int udv = uv - \int vdu \qquad \text{..... (5.24)}$$

If for some reason, we assume that *u* is a constant then we can write this equation as:

$$\int uvdx = u\int vdx \qquad \text{..... (5.25)}$$

This basic assumption that functions represented by *u*, (saturation dependent variables) like relative permeabilities such as that of water, oil or gas and capillary pressure depend on saturation only and hence can be taken out of the integration process, forms the basis of this approach. In the above expression we are only interested in knowing the solution of *v* (saturation) with respect to *x* (distance). We go ahead and calculate *u* with the help of mean value theorem of definite integration which provides us with the solution in the form of average value and let FEM calculate *v* with respect to *x*.

Assuming the relative permabilities are functions of saturation as represented by Brooks and Corey[22] and given by the following equations:

$$k_{rw} = k_w S_{we}^n$$

$$k_{ro} = k_o\left(1 - S_{we}\right)^2\left(1 - S_{we}^{\gamma}\right) \qquad \text{..... (5.26a)}$$

where S_{we} is the normalized saturation of water. For our purpose, we are assuming that in the differential equation we deal with normalized saturation. The derivatives are given by:

$$\frac{\partial}{\partial S_w} k_{rw} = n k_w S_{we}^{n-2} S_{we}$$

$$\frac{\partial}{\partial S_w} k_{ro} = \frac{\partial}{\partial S_w}\left[k_o \left(\frac{1}{S_{we}} - 1 \right)^2 \left(1 - S_{we}^{\gamma}\right) \right] S_{we}^2 + 2\left[k_o \left(\frac{1}{S_{we}} - 1 \right)^2 \left(1 - S_{we}^{\gamma}\right) \right] [S_{we}] \text{..... (5.26b)}$$

Again, assuming the capillary pressure is a function of saturation given by the following:

$$P_c = -P_{c0} S_w^3 + P_{c1} S_w^2 - P_{c2} S_w + C_c$$

$$\frac{\partial}{\partial S_w} P_c = -3P_{c0} S_w^2 + 2P_{c1} S_w - 2P_{c2} \qquad \text{..... (5.26c)}$$

The various relevant expressions are:

$$S_{we} = \frac{\left(S_w - S_{wi}\right)}{\left(1 - S_{wi} - S_{oi}\right)} \qquad \text{..... (5.27)}$$

and as per the definition of exponents as given by Brooks and Corey[22] we have:

$$n = \frac{2 + 3\lambda}{\lambda} \qquad \text{..... (5.28)}$$

$$\gamma = \frac{2 + \lambda}{\lambda} \qquad \text{..... (5.29)}$$

where λ is called pore size distribution index and for typical porous rocks has a value of 2 and n is the saturation exponent. Soils which have a well developed structure have the value of λ less than 2 where as sands have a value greater than 2. These equations are

derived experimentally and take into account the distribution of the pore sizes. For simplicity we can assume $k_o = k_w = 1$.

5.3.5.1 Mean Value Theorem of Definite Integration

According to mean-value theorem of definite integration, for any function $f(x)$, the average value between the limits a and b, as given by Adams[44], is given by:

$$\overline{f} = \frac{1}{b-a}\int_a^b f(x)dx \qquad \text{…….... (5.30)}$$

The requirement of function $f(x)$ is that it should be continuous and integrable on the interval [a, b]. Applying the above concept we go ahead and calculate the various integrals of the saturation domain.

5.3.5.2 Treatment of Capillary Potential Gradient Term

From equation (5.7) we have:

$$\frac{\partial \Phi_c}{\partial x} = -\frac{\partial P_c}{\partial x} + \Delta\rho g \sin\alpha \qquad \text{…….... (5.7)}$$

From equation (5.26c) we substitute the value of capillary pressure gradient and have:

$$\frac{\partial \Phi_c}{\partial x} = 3P_{c0}S_w^2 - 2P_{c1}S_w + 2P_{c2} + \Delta\rho g \sin\alpha \qquad \text{…….... (5.31)}$$

Integrating, as per the mean value theorem, the above equation between the limits 0 and 1 leads to:

$$\int_0^1 \left(\frac{\partial \Phi_c}{\partial S_w}\right) dS_w = \Phi_c\big|_0^1 = \left(P_c + \Delta\rho g \sin\alpha\right)_0^1 = \left[P_{c0} - P_{c1} + P_{c2} + \Delta\rho g \sin\alpha\right]$$

$$\text{…….... (5.32)}$$

The variable C_c vanishes because of successive use of differentiation and integration. It could be argued that we could fit any curve with as different coefficients as possible. But if we add the coefficients P_{c0}, P_{c1} and P_{c2} we will find that these all add to C_c. So even though we are not using C_c it helps in determining the shape of the capillary pressure curve. Obviously, the results changes with different limits of saturation.

5.3.5.3 Treatment of Mobility Ratio Terms

The integration of the mobility terms are difficult process to be done analytically. There is no known exact analytical solution to the problem. Hence the only alternative is to go along numerical integration. Also, if we have to use finite element method, we have to know what the value of integrand before hand, similar to what we did for the capillary potential gradient term. The mobility ratio terms, from equation (5.23), are given by:

$$\int_a^b \frac{k_w S_w^4 k_o \left(1-S_w^2\right)\left(1-S_w\right)^2}{\left[\mu_o k_w S_w^4 + \mu_w k_o \left(1-S_w^2\right)\left(1-S_w\right)^2\right]} \qquad \text{..... (5.33)}$$

This ratio can be represented by partial fractions thus:

$$\frac{k_w S_w^4 k_o \left(1-S_w^2\right)\left(1-S_w\right)^2}{\left[\mu_o k_w S_w^4 + \mu_w k_o \left(1-S_w^2\right)\left(1-S_w\right)^2\right]} = A + 2B \times S_w + 3C \times S_w^2 + 4D \times S_w^3 + 5E \times S_w^4 + F\left(S_w\right)$$

..... (5.34)

where:

$$A = \frac{\mu_o k_w^2 k_o \left(\mu_o^3 k_w^3 + 5\mu_o^2 k_w^2 \mu_w k_o - 13\mu_o k_w \mu_w^2 k_o^2 - 9\mu_w^3 k_w^3\right)}{\left(\mu_o k_w - \mu_w k_o\right)^5}$$

$$B = -\frac{2\mu_o k_w^2 k_o \left(\mu_o^2 k_w^2 - 2\mu_o k_w \mu_w k_o - 3\mu_w^2 k_o^2\right)}{\left(\mu_o k_w - \mu_w k_o\right)^4}$$

$$C = -\frac{4\mu_o k_w^2 \mu_w k_o^2}{3\left(\mu_o k_w - \mu_w k_o\right)^3}$$

$$D = \frac{\mu_o k_w^2 k_o}{2\left(\mu_o k_w - \mu_w k_o\right)^2}$$

$$E = -\frac{k_w k_o}{5\left(\mu_o k_w - \mu_w k_o\right)}$$

$$F = \frac{\mu_o k_w^2 \mu_w k_o^2}{2\left(\mu_o k_w - \mu_w k_o\right)^5} \qquad \text{..... (5.35)}$$

The full derivation of the partial fractions was derived by *Mathematica*® and appears in Appendix A. With help of these partial fractions, we carry out the integration as:

$$\int_a^b \frac{k_w S_w^4 k_o \left(1 - S_w^2\right)\left(1 - S_w\right)^2}{\left[\mu_o k_w S_w^4 + \mu_w k_o \left(1 - S_w^2\right)\left(1 - S_w\right)^2\right]} = A \times S_w + B \times S_w^2 + C \times S_w^3 + D \times S_w^4 + E \times S_w^5 + F \int_a^b \left(S_w\right) dS_w$$

..... (5.36)

For oil-water system or for gas-water system, the typical range of viscosities is:

$$\mu_w \approx 1.0 \text{ cP}$$

$$\mu_g \approx 0.001 \text{ to } 0.02 \text{ cP and } \mu_o \approx 1.5 \text{ to } 2.5 \text{ cP} \qquad \text{..... (5.37)}$$

For gas-water system, since the value of viscosity is very low, the value of $F \to 0$ and hence we neglect this term whenever gas is present. For oil-water system, we have to use sound judgment before we go ahead and truncate this term. The only constrain on this type of solution is that we should get a positive value of the integrand, represented by equation (5.33), for this method to be applied.

5.4 Multiphase Flow in Porous Media through Rayleigh-Ritz Finite Element Method

We begin by reproducing equation (3.39) which was derived previously for one dimension as:

$$\left(1+\frac{\rho_w}{\rho_o}\right)\frac{\partial S_w}{\partial t}=\frac{\partial}{\partial x}\left[\frac{kk_{rw}k_{ro}}{\phi\left(\mu_w k_{ro}+\mu_o k_{rw}\right)}\right]\left[-\left(\frac{\partial P_c}{\partial S_w}\frac{\partial S_w}{\partial x}\right)+g\Delta\rho\sin\alpha\right]$$

$$+\left[\frac{kk_{rw}k_{ro}}{\phi\left(\mu_w k_{ro}+\mu_o k_{rw}\right)}\right]\frac{\partial}{\partial x}\left[-\left(\frac{\partial P_c}{\partial S_w}\frac{\partial S_w}{\partial x}\right)+g\Delta\rho\sin\alpha\right]+\left(\frac{k_{ro}\mu_w}{\mu_w k_{ro}+\mu_o k_{rw}}\right)\frac{q_{ws}}{\phi A}$$

…....(3.39)

5.4.1 Formulation of the Governing Differential Equation in Two-Dimension

Extending the above equation from one dimension to two dimensional flow this equation converts to:

$$\left(1+\frac{\rho_w}{\rho_o}\right)\frac{\partial S_w}{\partial t}=\frac{\partial}{\partial x}\left[\frac{kk_{rw}k_{ro}}{\phi\left(\mu_w k_{ro}+\mu_o k_{rw}\right)}\right]\left[-\left(\frac{\partial P_c}{\partial S_w}\frac{\partial S_w}{\partial x}\right)+g\Delta\rho\sin\alpha\right]$$

$$+\left[\frac{kk_{rw}k_{ro}}{\phi\left(\mu_w k_{ro}+\mu_o k_{rw}\right)}\right]\frac{\partial}{\partial x}\left[-\left(\frac{\partial P_c}{\partial S_w}\frac{\partial S_w}{\partial x}\right)+g\Delta\rho\sin\alpha\right]$$

$$+\frac{\partial}{\partial y}\left[\frac{kk_{rw}k_{ro}}{\phi\left(\mu_w k_{ro}+\mu_o k_{rw}\right)}\right]\left[-\left(\frac{\partial P_c}{\partial S_w}\frac{\partial S_w}{\partial y}\right)+g\Delta\rho\sin\alpha\right]$$

$$+\left[\frac{kk_{rw}k_{ro}}{\phi\left(\mu_w k_{ro}+\mu_o k_{rw}\right)}\right]\frac{\partial}{\partial y}\left[-\left(\frac{\partial P_c}{\partial S_w}\frac{\partial S_w}{\partial y}\right)+g\Delta\rho\sin\alpha\right]$$

$$+\left(\frac{k_{ro}\mu_w}{\mu_w k_{ro}+\mu_o k_{rw}}\right)\frac{2q_{ws}}{\phi A}\ \text{…….....}\ (5.38)$$

Again, as per previous definition, we have:

$$F_1 = \left[-\left(\frac{\partial P_c}{\partial x} \right) + g\Delta\rho \sin\alpha \right] = \frac{\partial \Phi_c}{\partial x}$$

$$F_2 = \left[-\left(\frac{\partial P_c}{\partial y} \right) + g\Delta\rho \sin\alpha \right] = \frac{\partial \Phi_c}{\partial y} \qquad \text{…….... (5.8)}$$

Substitution of equation (5.8) in equation (5.38) reduces it to:

$$0 = \left(1 + \frac{\rho_w}{\rho_o} \right) \frac{\partial S_w}{\partial t} - \frac{\partial}{\partial x} \left[\frac{k k_{rw} k_{ro}}{\phi(\mu_w k_{ro} + \mu_o k_{rw})} \right] [F_1] - \left[\frac{k k_{rw} k_{ro}}{\phi(\mu_w k_{ro} + \mu_o k_{rw})} \right] \frac{\partial}{\partial x} [F_1]$$

$$- \frac{\partial}{\partial y} \left[\frac{k k_{rw} k_{ro}}{\phi(\mu_w k_{ro} + \mu_o k_{rw})} \right] [F_2] - \left[\frac{k k_{rw} k_{ro}}{\phi(\mu_w k_{ro} + \mu_o k_{rw})} \right] \frac{\partial}{\partial y} [F_2]$$

$$- \left(\frac{k_{ro} \mu_w}{\mu_w k_{ro} + \mu_o k_{rw}} \right) \frac{2 q_{ws}}{\phi A} \qquad \text{…….... (5.39)}$$

which is the governing differential equation used to formulate the finite element model.

5.4.2 Formulation of the Variational Weak Form

Following the previous footsteps, we construct the weak form by multiplying the governing equation with weight function w, and integrating over the domain to get:

$$0 = \int_{\Omega_e} w \left\{ \left(1 + \frac{\rho_w}{\rho_o} \right) \frac{\partial S_w}{\partial t} - \frac{\partial}{\partial x} \left[\frac{k k_{rw} k_{ro}}{\phi(\mu_w k_{ro} + \mu_o k_{rw})} \right] [F_1] - \left[\frac{k k_{rw} k_{ro}}{\phi(\mu_w k_{ro} + \mu_o k_{rw})} \right] \frac{\partial}{\partial x} [F_1] \right\} dxdy$$

$$- \int_{\Omega_e} w \left\{ \frac{\partial}{\partial y} \left[\frac{k k_{rw} k_{ro}}{\phi(\mu_w k_{ro} + \mu_o k_{rw})} \right] [F_2] + \left[\frac{k k_{rw} k_{ro}}{\phi(\mu_w k_{ro} + \mu_o k_{rw})} \right] \frac{\partial}{\partial y} [F_2] \right\} dxdy$$

$$- \int_{\Omega_e} w \left\{ \left(\frac{k_{ro} \mu_w}{\mu_w k_{ro} + \mu_o k_{rw}} \right) \frac{2 q_{ws}}{\phi A} \right\} dxdy \qquad \text{…….... (5.40)}$$

Replacing the operators from previous equations,

$$\frac{\partial}{\partial x}(wF_1) = \frac{\partial w}{\partial x}F_1 + w\frac{\partial F_1}{\partial x} \quad \Rightarrow \quad -w\frac{\partial F_1}{\partial x} = \frac{\partial w}{\partial x}F_1 - \frac{\partial}{\partial x}(wF_1) \quad \text{..... (5.11a)}$$

$$\frac{\partial}{\partial y}(wF_2) = \frac{\partial w}{\partial y}F_2 + w\frac{\partial F_2}{\partial y} \quad \Rightarrow \quad -w\frac{\partial F_2}{\partial y} = \frac{\partial w}{\partial y}F_2 - \frac{\partial}{\partial y}(wF_2) \quad \text{..... (5.11b)}$$

and using gradient theorem we convert the surface integral into line integral,

$$\int_{\Omega^e} \frac{\partial}{\partial x}(wF_1)dxdy = \oint_{\Gamma^e} wF_1 n_x ds \quad \text{..... (5.12a)}$$

$$\int_{\Omega^e} \frac{\partial}{\partial y}(wF_2)dxdy = \oint_{\Gamma^e} wF_2 n_y ds \quad \text{..... (5.12b)}$$

From equation (5.40), equation (5.11) and equation (5.12), we have:

$$0 = \int \left[w\left(1 + \frac{\rho_w}{\rho_o}\right)\frac{\partial S_w}{\partial t} - w[F_1]\frac{\partial}{\partial x}\left[\frac{kk_{rw}k_{ro}}{\phi(\mu_w k_{ro} + \mu_o k_{rw})}\right] + \frac{\partial w}{\partial x}\left[\frac{kk_{rw}k_{ro}}{\phi(\mu_w k_{ro} + \mu_o k_{rw})}\right][F_1]\right]dxdy$$

$$- \int \left[w[F_2]\frac{\partial}{\partial y}\left[\frac{kk_{rw}k_{ro}}{\phi(\mu_w k_{ro} + \mu_o k_{rw})}\right] - \frac{\partial w}{\partial y}\left[\frac{kk_{rw}k_{ro}}{\phi(\mu_w k_{ro} + \mu_o k_{rw})}\right][F_2] - wf\right]dxdy$$

$$- \oint_{\Gamma^e} wMF_1 n_x ds - \oint_{\Gamma^e} wMF_2 n_y ds \quad \text{..... (5.41)}$$

Simplifying and replacing the value of forcing functions we have:

$$0=\int\left[w\left(1+\frac{\rho_w}{\rho_o}\right)\frac{\partial S_w}{\partial t}-w\left[-\left(\frac{\partial P_c}{\partial x}\right)+g\Delta\rho\sin\alpha\right]\frac{\partial}{\partial S_w}\left[\frac{kk_{rw}k_{ro}}{\phi\left(\mu_w k_{ro}+\mu_o k_{rw}\right)}\right]\frac{\partial S_w}{\partial x}\right]dxdy$$

$$+\int\frac{\partial w}{\partial x}\left[\frac{kk_{rw}k_{ro}}{\phi\left(\mu_w k_{ro}+\mu_o k_{rw}\right)}\right]\left[-\left(\frac{\partial P_c}{\partial x}\right)+g\Delta\rho\sin\alpha\right]dxdy$$

$$-\int\left[w\left[-\left(\frac{\partial P_c}{\partial y}\right)+g\Delta\rho\sin\alpha\right]\frac{\partial}{\partial S_w}\left[\frac{kk_{rw}k_{ro}}{\phi\left(\mu_w k_{ro}+\mu_o k_{rw}\right)}\right]\frac{\partial S_w}{\partial y}\right]dxdy$$

$$+\int\frac{\partial w}{\partial y}\left[\frac{kk_{rw}k_{ro}}{\phi\left(\mu_w k_{ro}+\mu_o k_{rw}\right)}\right]\left[-\left(\frac{\partial P_c}{\partial y}\right)+g\Delta\rho\sin\alpha\right]dxdy-\int wfdxdy-\oint_{\Gamma^e}wq_n ds$$

……..... (5.42)

$$f=\left(\frac{k_{ro}\mu_w}{\mu_w k_{ro}+\mu_o k_{rw}}\right)\frac{2q_{ws}}{\phi A}$$

$$q_n=\left(MF_1 n_x+MF_2 n_y\right)$$ ……..... (5.43)

Equation (5.42) is the weak form of the governing differential equation. Rearranging:

$$0=\int\left[w\left(1+\frac{\rho_w}{\rho_o}\right)\frac{\partial S_w}{\partial t}\right]dxdy+\frac{1}{\phi}\int\frac{\partial w}{\partial x}\left[\frac{kk_{rw}k_{ro}}{\left(\mu_w k_{ro}+\mu_o k_{rw}\right)}\right]\left[-\left(\left(\frac{\partial\Phi_c}{\partial S_w}\right)\frac{\partial S_w}{\partial x}\right)\right]dxdy$$

$$+\frac{1}{\phi}\int\frac{\partial w}{\partial y}\left[\frac{kk_{rw}k_{ro}}{\left(\mu_w k_{ro}+\mu_o k_{rw}\right)}\right]\left[-\left(\left(\frac{\partial\Phi_c}{\partial S_w}\right)\frac{\partial S_w}{\partial y}\right)\right]dxdy$$

$$-\frac{1}{\phi}\int\left[w\left[-\left(\frac{\partial\Phi_c}{\partial S_w}\right)\right]\left\{\frac{\partial}{\partial S_w}\left[\frac{kk_{rw}k_{ro}}{\left(\mu_w k_{ro}+\mu_o k_{rw}\right)}\right]\right\}\left(\frac{\partial S_w}{\partial x}\right)^2\right]dxdy$$

$$-\frac{1}{\phi}\int\left[w\left[-\left(\frac{\partial\Phi_c}{\partial S_w}\right)\right]\left\{\frac{\partial}{\partial S_w}\left[\frac{kk_{rw}k_{ro}}{\left(\mu_w k_{ro}+\mu_o k_{rw}\right)}\right]\right\}\left(\frac{\partial S_w}{\partial y}\right)^2\right]dxdy-\int wfdxdy-\oint_{\Gamma^e}wq_n ds$$

……..... (5.44)

Equation (5.44) is more general weak form than equation (5.42).

5.4.3 Formulation of Linearized Variational Weak Form – Truncated Equation

To further simplify the problem, we apply the same justification to the above equation as was used with equation (5.18) to yield the following equation:

$$0 = \int \left[w\left(1 + \frac{\rho_w}{\rho_o}\right)\frac{\partial S_w}{\partial t}\right] dxdy$$

$$+ \frac{1}{\phi}\int \frac{\partial w}{\partial x}\left[\frac{kk_{rw}k_{ro}}{(\mu_w k_{ro} + \mu_o k_{rw})}\right]\left[\left(\left(\frac{\partial \Phi_c}{\partial S_w}\right)\frac{\partial S_w}{\partial x}\right)\right] dxdy$$

$$+ \frac{1}{\phi}\int \frac{\partial w}{\partial y}\left[\frac{kk_{rw}k_{ro}}{(\mu_w k_{ro} + \mu_o k_{rw})}\right]\left[\left(\left(\frac{\partial \Phi_c}{\partial S_w}\right)\frac{\partial S_w}{\partial y}\right)\right] dxdy$$

$$- \int wfdxdy - \oint_{\Gamma^e} wq_n ds \quad \text{…….....} \quad (5.45)$$

This is the weak form which we use to formulate the finite element model.

5.4.4 Finite Element Model

Again, assume that saturation S_w is approximated over a typical finite element by:

$$S_w(x,y) = \sum_{j=1}^{n} s_j^e(t)\psi_j^e(x,y)$$

and

$$w = \psi_i^e \quad \text{…….....} \quad (5.19)$$

Substituting in equation (5.45),

$$0 = \left(1 + \frac{\rho_w}{\rho_o}\right)\int \left[\psi_i^e \sum \psi_j^e \frac{\partial s_j^e}{\partial t}\right] dxdy$$

$$+ \frac{1}{\phi}\int \frac{\partial \psi_i^e}{\partial x}\left[\left(\frac{\partial \Phi_c}{\partial S_w}\right)\right]\left[\frac{kk_{rw}k_{ro}}{(\mu_w k_{ro} + \mu_o k_{rw})}\right]\sum \frac{\partial \psi_j^e}{\partial x} s_j^e dxdy$$

$$+ \frac{1}{\phi}\int \frac{\partial \psi_i^e}{\partial y}\left[\left(\frac{\partial \Phi_c}{\partial S_w}\right)\right]\left[\frac{kk_{rw}k_{ro}}{(\mu_w k_{ro} + \mu_o k_{rw})}\right]\sum \frac{\partial \psi_j^e}{\partial y} s_j^e dxdy - \int f\psi_i^e dxdy - \oint_{\Gamma^e} \psi_i^e q_n ds$$

Rearranging the summation common and out of the parenthesis:

$$0 = \sum_{j=1}^{n} \left\{ \left(1 + \frac{\rho_w}{\rho_o} \right) \int \left[\psi_i^e \psi_j^e \right] dxdy \right\} \frac{\partial s_j^e}{\partial t}$$

$$+ \sum_{j=1}^{n} \left\{ \frac{1}{\phi} \int \left[\left(\frac{\partial \Phi_c}{\partial S_w} \right) \right] \left[\frac{k k_{rw} k_{ro}}{\left(\mu_w k_{ro} + \mu_o k_{rw} \right)} \right] \frac{\partial \psi_i^e}{\partial x} \frac{\partial \psi_j^e}{\partial x} dxdy \right\} s_j^e$$

$$+ \sum_{j=1}^{n} \left\{ \frac{1}{\phi} \int \left[\left(\frac{\partial \Phi_c}{\partial S_w} \right) \right] \left[\frac{k k_{rw} k_{ro}}{\left(\mu_w k_{ro} + \mu_o k_{rw} \right)} \right] \frac{\partial \psi_i^e}{\partial y} \frac{\partial \psi_j^e}{\partial y} dxdy \right\} s_j^e$$

$$- \int f \psi_i^e dxdy - \oint_{\Gamma^e} \psi_i^e q_n ds \qquad \text{…….....} \quad (5.46)$$

This is the finite element model. This is of the form:

$$\sum_{j=1}^{n} M_{ij}^e \left\{ \dot{s}_j^e \right\} + \sum_{j=1}^{n} K_{ij}^e s_j^e = f_i^e + Q_i^e \qquad \text{…….....} \quad (5.47)$$

Comparing equation (5.46) and equation (5.47), we have:

$$M_{ij}^e = \left(1 + \frac{\rho_w}{\rho_o} \right) \int_{\Omega_e} \left[\psi_i^e \psi_j^e \right] dxdy$$

$$f_i^e = \int f \psi_i^e dxdy$$

$$Q_i^e = \oint_{\Gamma^e} \psi_i^e q_n ds$$

and,

$$K_{ij}^e = a_{11} \left[K^{11} \right] + a_{22} \left[K^{22} \right]$$

CHAPTER VI

VERIFICATION TASKS OF THE NUMERICAL MODELS

After having formulated the numerical model, we applied it to the experiments which were conducted in the laboratory. Equation (4.3) has been used by many researchers such as Babadagli and Ershaghi[4], Li and Horne[5], etc. to describe spontaneous imbibition. For FEM numerical simulation we modified FEM2DV2 code by Reddy[45].

6.1 Handy's Experiment of Spontaneous Imbibition

One of the earliest attempts with air-water system was made by Handy[2] who assumed that the capillary term varied linearly with distance. This is true as long as we assume a piston type displacement of the non-wetting phase by the wetting phase and the potential, generated by the capillary forces, provides the driving force. With these assumptions, equation (4.3) for cylindrical cores reduces to the following form:

$$Q_w^2 = \left(\frac{2P_c k_w \phi A^2 S_w}{\mu_w} \right) t \qquad \text{…….... (6.1)}$$

This is the equation of a line and on a plot of squared of the water imbibed versus time, will pass through the origin.

6.1.1 Results of Finite Difference Method Code

We chose Handy's data to verify our finite difference (FDM) numerical code. The reason for doing this is to prove that our simulator could exactly match that data as well as bring forth the limitation of the initial assumption that capillary pressure varies linearly with distance. This is true for early time but the relationship breaks down as time progresses. If imbibition is allowed to prolong into late time, it levels off and stops. This is shown in **fig. 6.1** which shows the results of our numerical simulation run. One of the important points, which come out of this plot, is the shape of the various curves. For sandstone cores, which are represented by the first two curves on the left hand side in

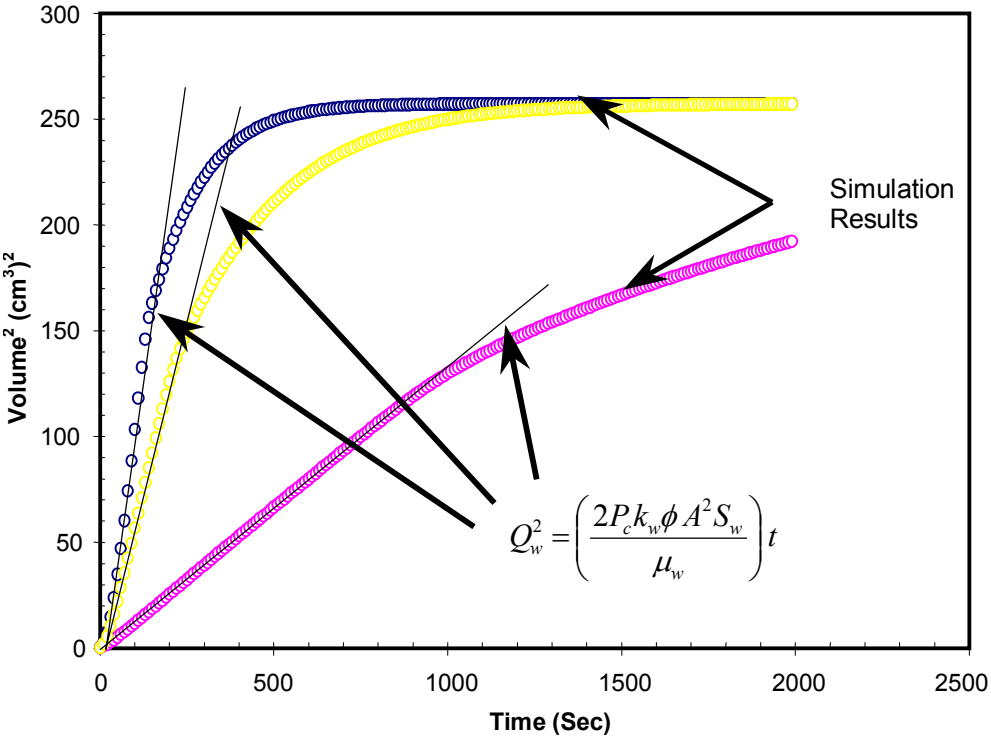

Figure 6.1 – Comparison of Handy's Data with Numerical Simulation (FDM)

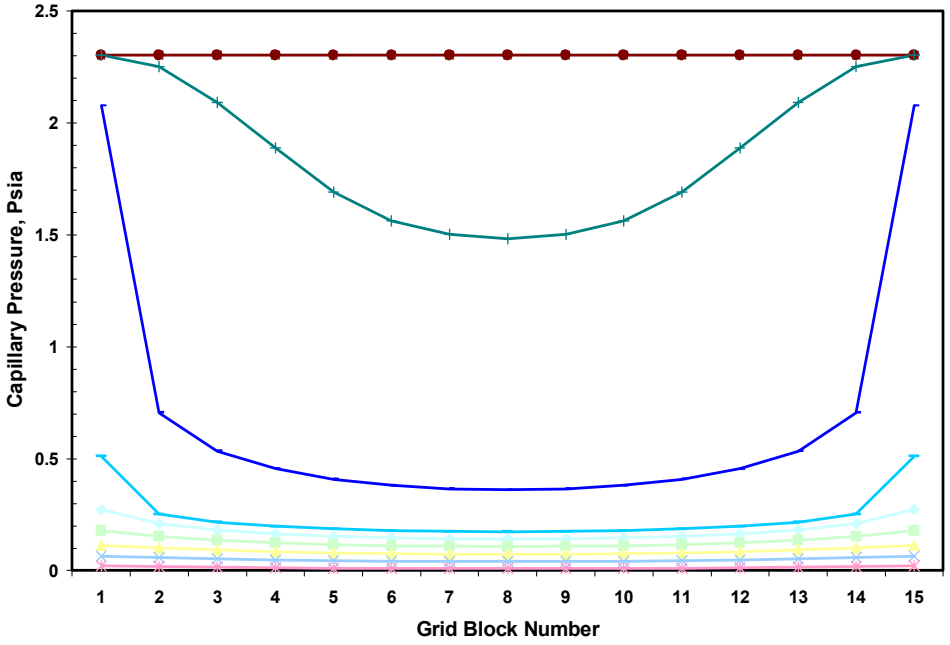

Figure 6.2 – Capillary Pressure versus Distance (FDM)

fig. 6.1, the slope of the linear portion of the curve is very steep. The difference in the two curves is the fact that one, which is on to the left and follows the linear trend to a greater degree, is of more permeable sandstone as compared to the curve on the right. The extreme right hand side curve is that of a limestone core, the slope of the linear portion of the curve is not that steep as compared to the sandstone cores. Also there is a point to realize that we can numerically simulate fluid flow both of sandstone cores as well as limestone cores. We plotted one of the outputs of our simulator, a plot of capillary pressure versus distance and as it is clear from **fig. 6.2**, the relationship is a not a linear one. Most researchers simplify the capillary pressure gradient to a linear relationship and then solve the above equation (6.1). In this simulator we have not assumed such a linear relation between capillary pressure and saturation.

6.1.2 Results of Finite Element Method Code

Similar kinds of results were obtained by finite element (FEM) code. Here we ran a simulation on Berea core. Although Berea core can be assumed to be a sandstone core for all practical purposes, this core was not a highly permeable one and this fact is brought out in **fig. 6.3**. The linearity of the spontaneous imbibition data breaks down early and then it tapers off at a relatively slow rate. In order to illustrate the linearity of the initial part of the data, we plotted the data on a semi-log plot as shown in **fig. 6.4**. The initial point all fall on a straight line which is accordance with Handy's assumption.

6.2 Spontaneous Imbibition Experiment of Unfractured Core

Garg *et al*[3] solved eqn. (4.2) for one-dimensional saturation data measured with the help of X-ray CT. They setup a mechanism with which they could simultaneously measure the weight of the water imbibed and measure the water saturation with the help of CT scanner.

6.2.1 Verification Through Finite Difference Code

We chose to compare the validity of our FDM code with the help of two simultaneously varying data, the first being weight gain of the imbibed water expressed as a fraction of total water imbibed and the other being water saturation measured with

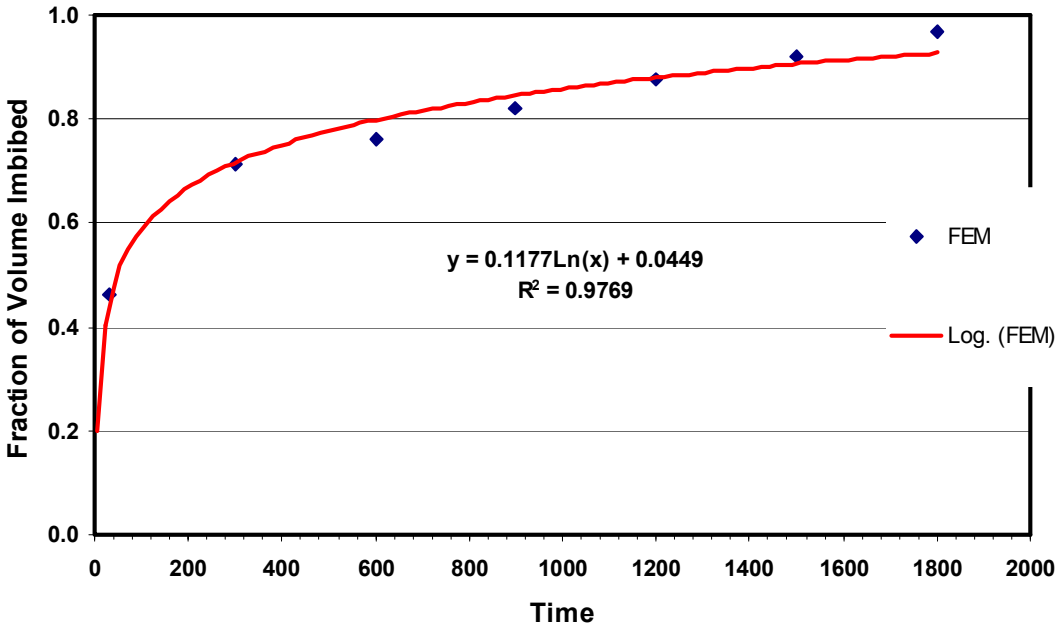

Figure 6.3 – Comparison of Handy's Data with Numerical Simulation (FEM) – Linear Fit

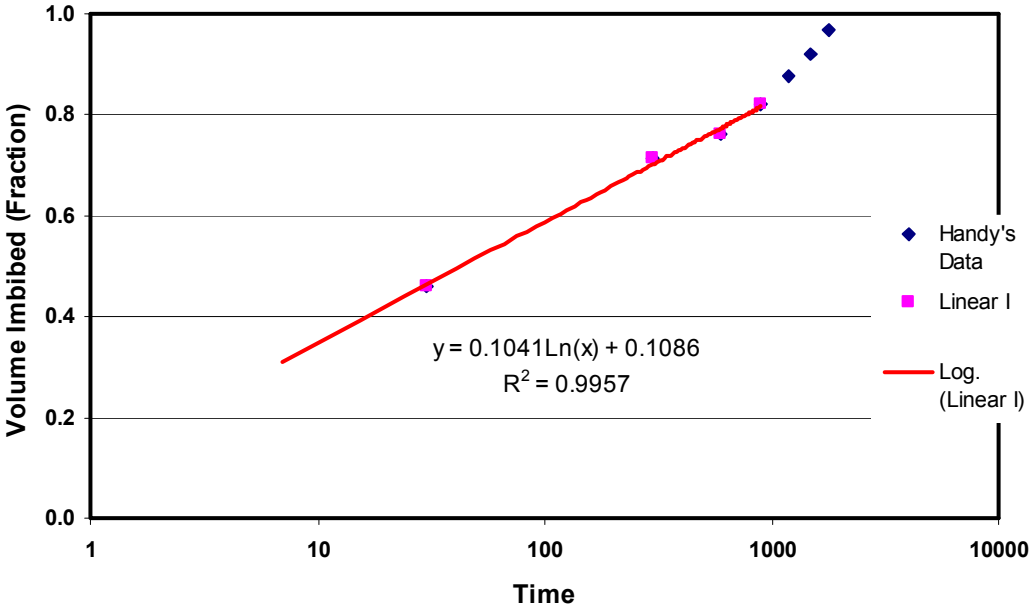

Figure 6.4 – Comparison of Handy's Data with Numerical Simulation (FEM) – Logarithmic Fit

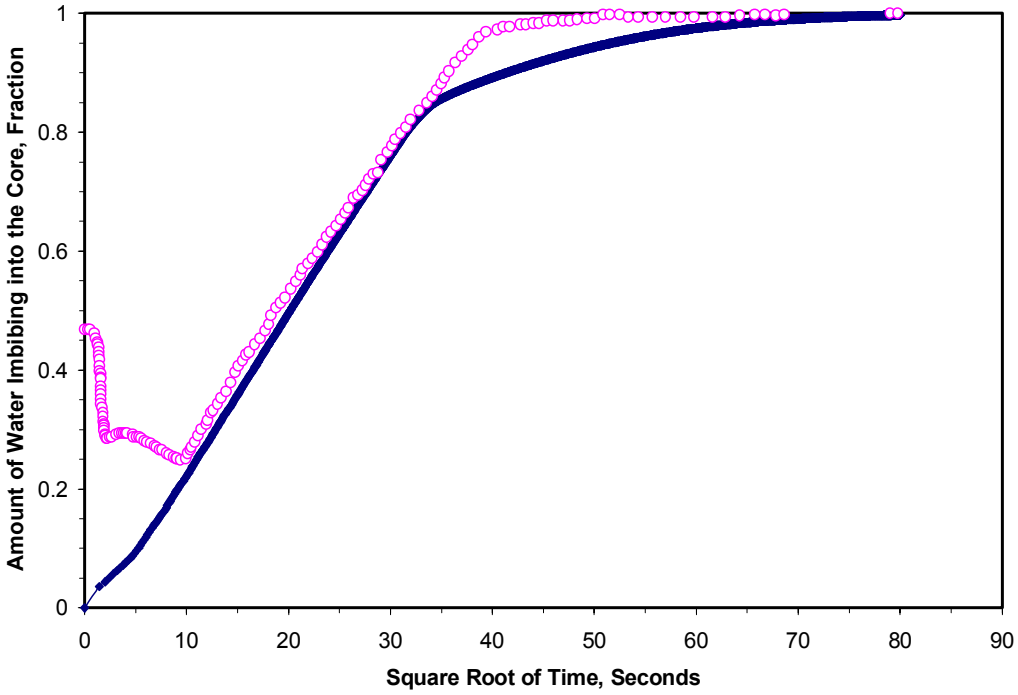

Figure 6.5 – Weight Gain versus Square Root of Imbibition

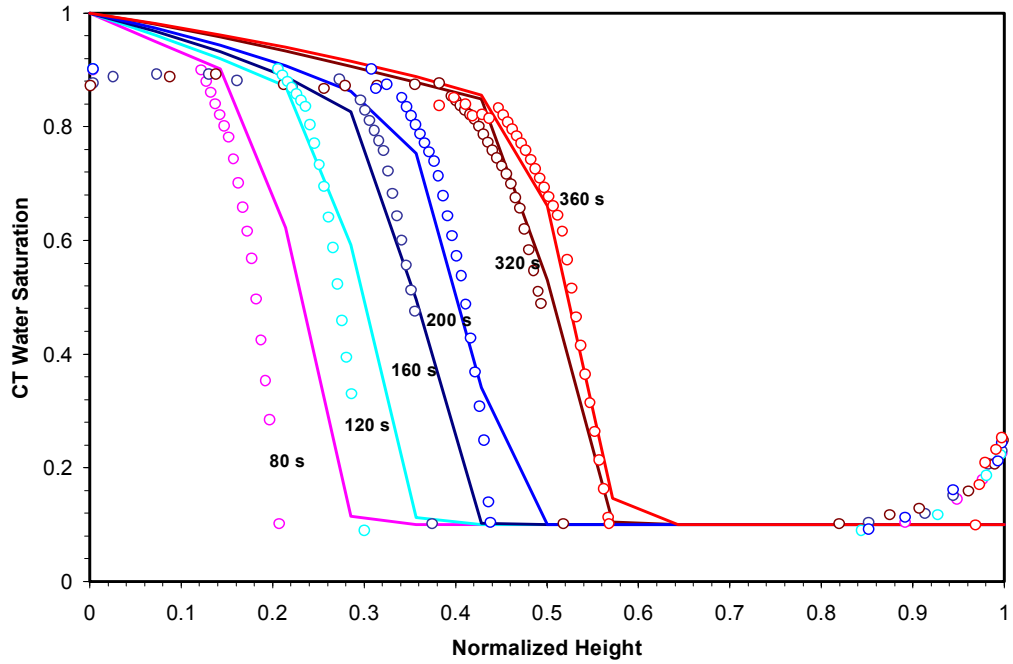

Figure 6.6 – CT Water Saturation versus Normalized Height (FDM)

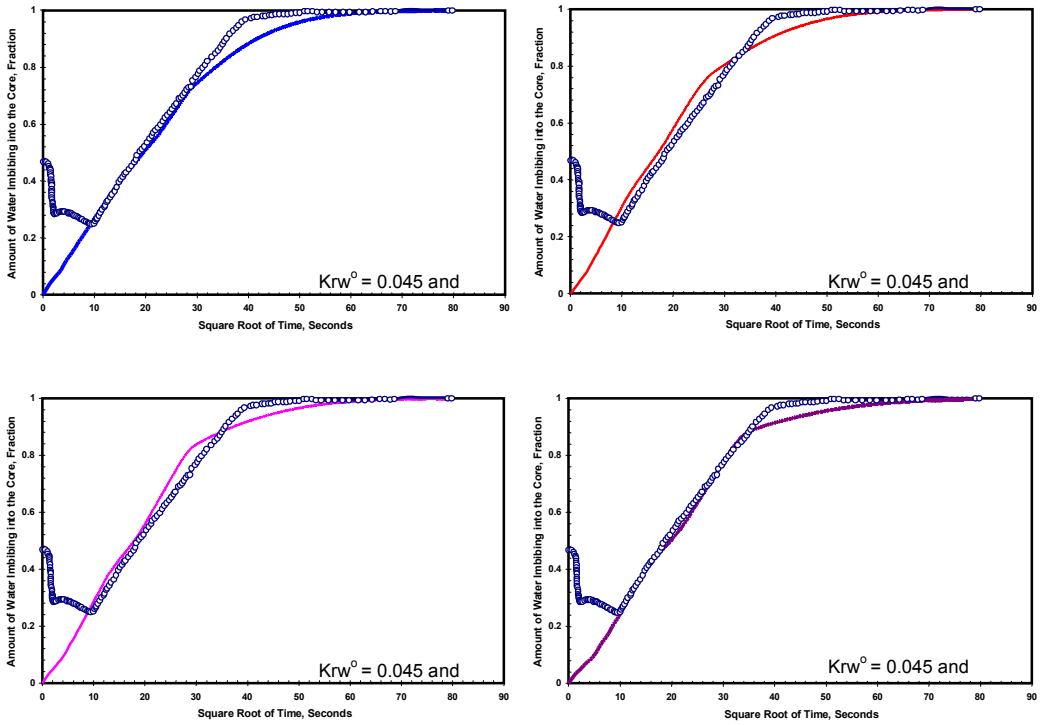

Figure 6.7 – Sensitivity Study on Weight Gain Data for Constant End-Point Saturation

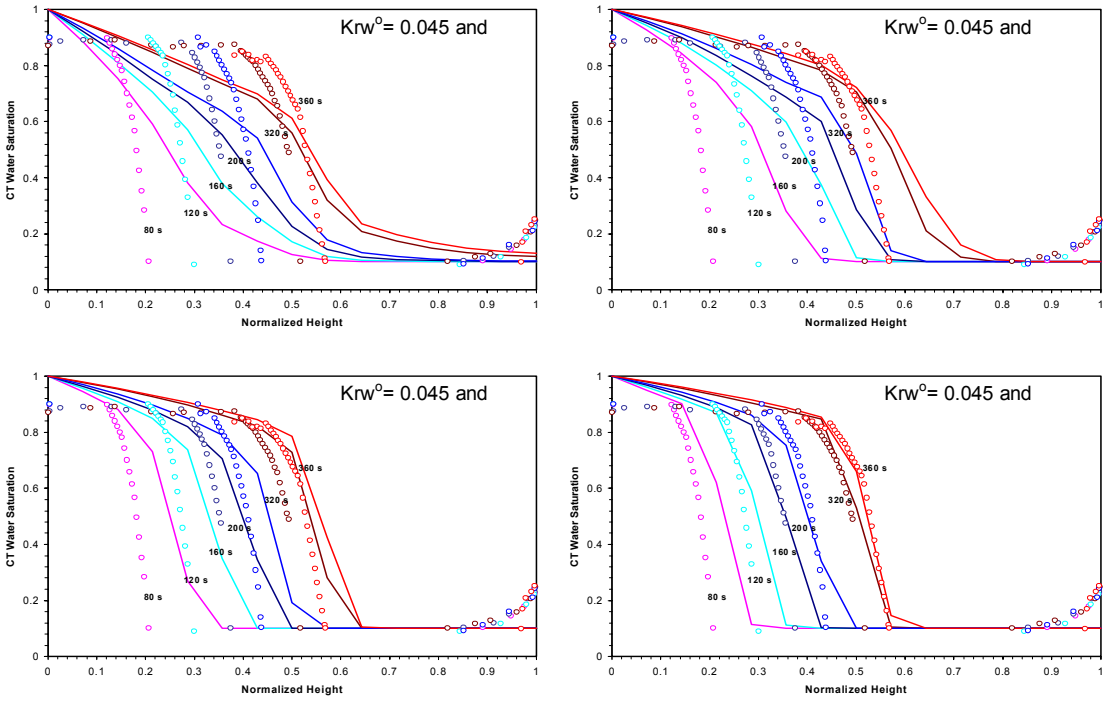

Figure 6.8 – Sensitivity Study on Saturation Data for Constant End-Point Saturation

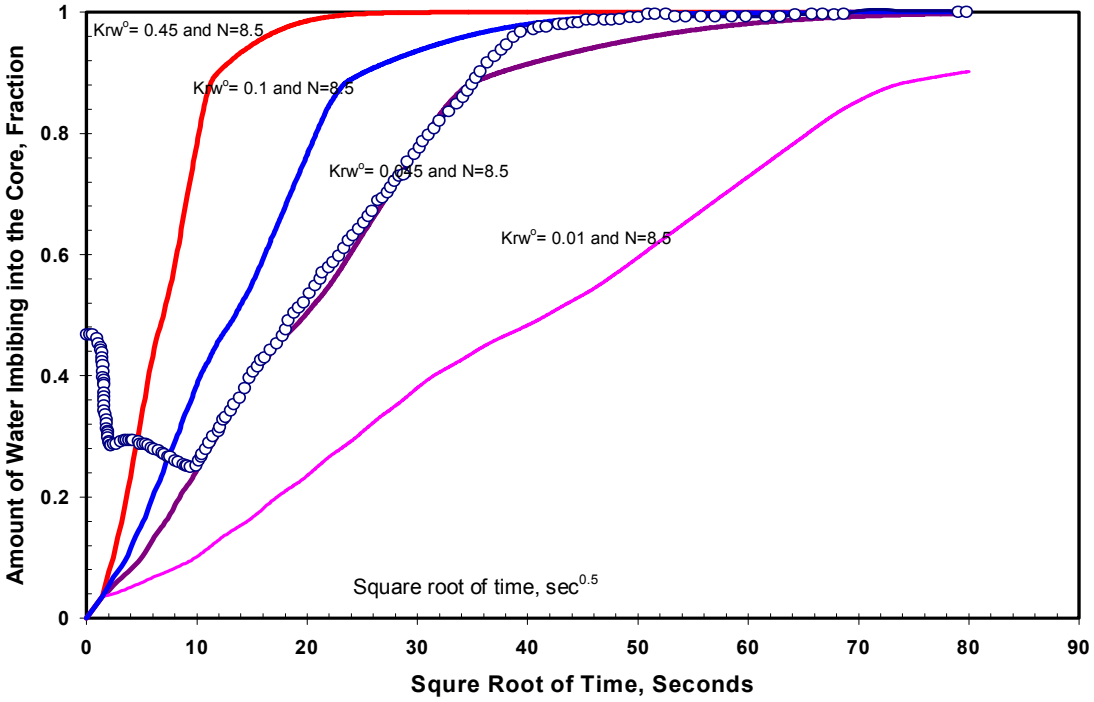

Figure 6.9 – Sensitivity Study on Weight Gain Data for Constant Saturation Exponent

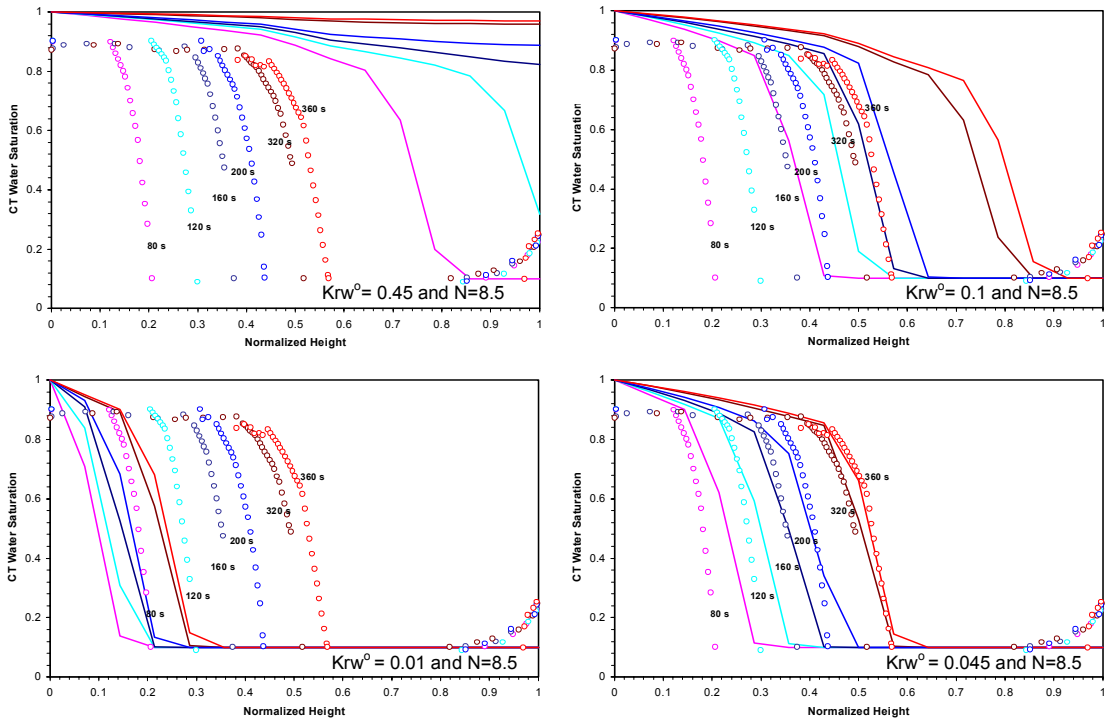

Figure 6.10 – Sensitivity Study on Saturation Data for Constant Saturation Exponent

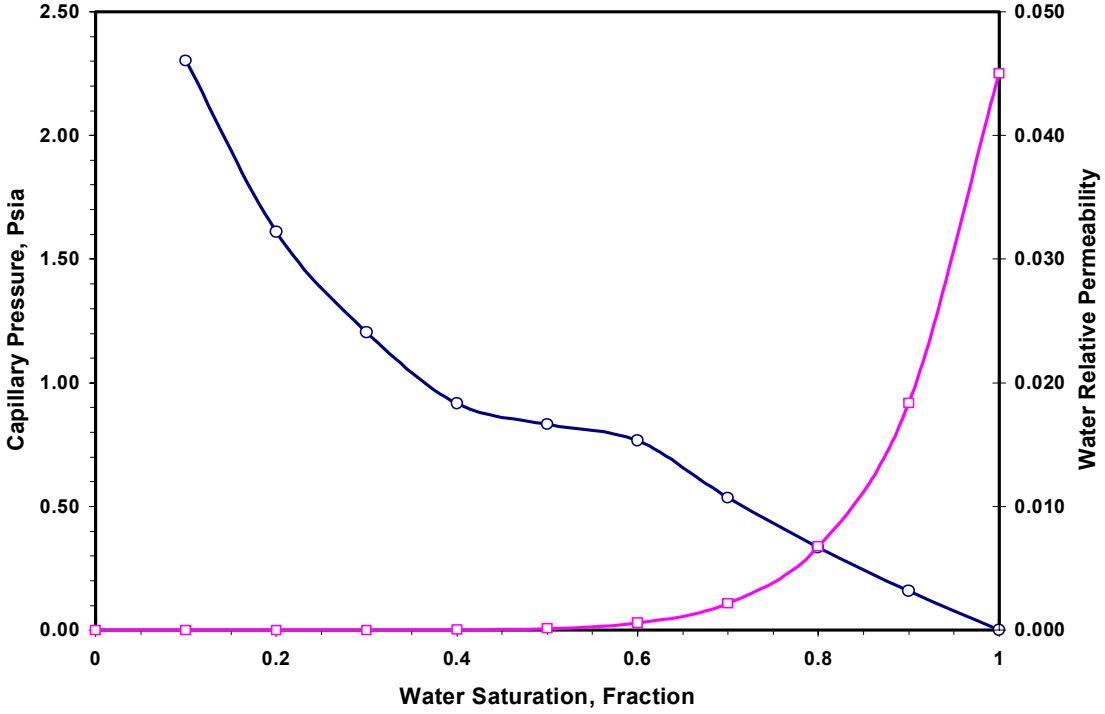

Figure 6.11 – Final Capillary Pressure and Relative Permeability Data Used in Simulation

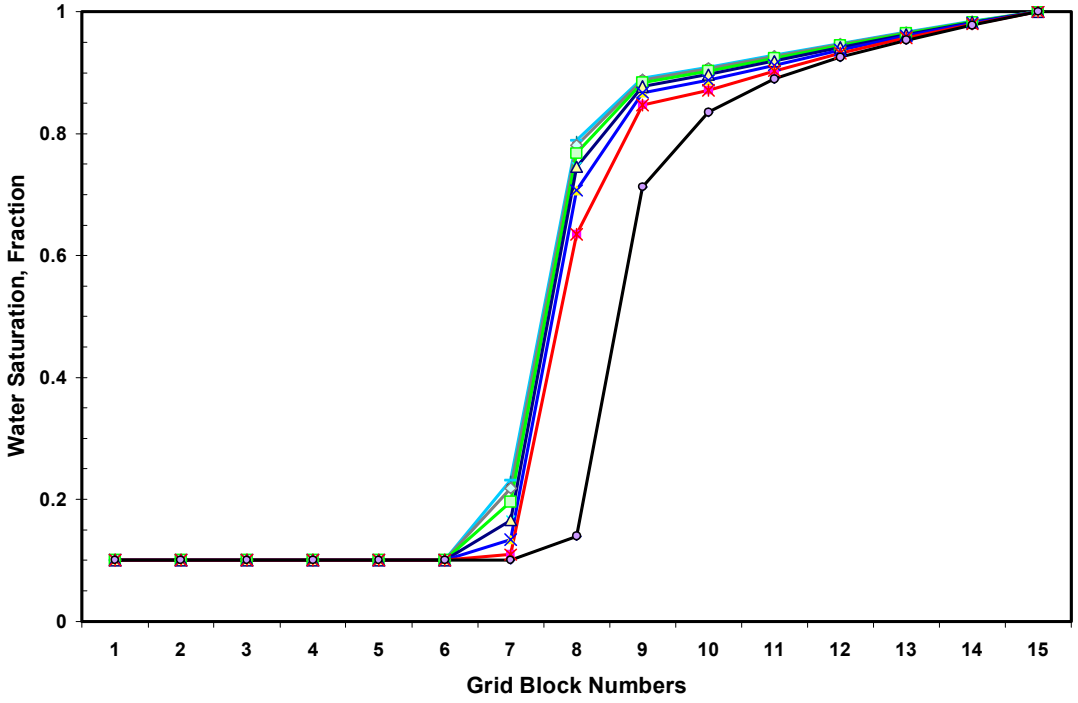

Figure 6.12 – Saturation versus Distance (Front is Moving from Left to Right)

X-ray CT scanner. As is with all multiple parameters, a match with one does not necessarily guarantee match with the other and this leads to lot of iterative effort before both can be matched. The out of the two, the data collected for weight gain was a tricky one as, at the initial stages, buoyancy forces had to be contended with as it does not start from the origin. We started with a power expression for relative permeability and found that an exponent of n = 8.5, gave us a close match as can be seen in **fig. 6.5**. Next we varied the different values of end-point relative permeability to arrive at an adequate match for saturation. We found that this value had more sensitive to saturation than the amount of water imbibed, which was almost the same in all cases of different exponents. **Fig. 6.7** and **fig. 6.8** shows the effect of various values of saturation exponent and **fig. 6.9** and **fig. 6.10** gives shows the effect of various values of end-point relative permeability values. Hence:

$$k_{rw} = 0.045 S_w^{8.5} \qquad \text{…….....} \quad (6.2)$$

We used a variable capillary pressure curve as shown in **fig. 6.11** as input. We also did the sensitivity study on gridblock size and the time steps used in the simulation and found that 15 gridblocks and time step of 2 seconds were enough to adequately run our model. The output from the code can track the saturation front in one-dimension as shown in **fig. 6.12**, where saturation for each grid block in a section are plotted. There is a difference in the methodologies between our experimental study and experimental work conducted by Garg *et al*[3]. They used the following logarithmic capillary pressure relation:

$$P_c = P_c^o \ln S \qquad \text{…….....} \quad (6.3)$$

where P_c^o is the threshold capillary pressure and S is the normalized saturation. They have used a power expression for air-water relative permeability as given by:

$$k_{rw} = k_{rw}^o S^n, \qquad n \geq 1 \qquad \text{…….....} (6.4)$$

Again k_{rw}^{o} is the end point relative permeability and they matched the experimental data with n = 2.5. We have gone further than this and our code can incorporate both variable capillary pressure data and variable relative permeability data. The departure from the experimental data initially, in **fig. 6.5**, is on account of high imbibition rate. The anomaly at the top of the core, we believe, is due to diffraction of X-rays which produces artifacts. The sides of the core were covered by epoxy and hence shielded from this effect. Summarily, we used the following parameters given in **Table 6.1.**

TABLE 6.1 – Summary of Key Parameters Used to Match CT Water Saturation

Parameters	Value
k	300 md
k_{rw}^{o}	0.045
P_c^{o}	2.5 psi
ϕ	0.22
n	0.5
S_{wi}	0.1

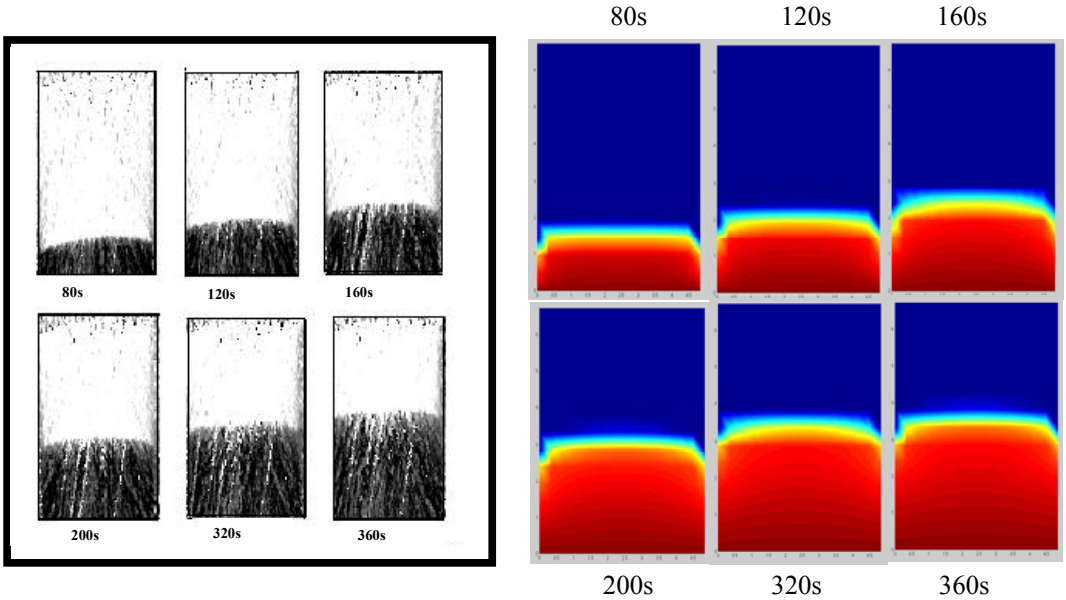

Figure 6.13 – Two-Dimensional CT Water Saturation Front Movement (FDM)

Garg *et al*[3] have incorporated the effect of gravity which we have neglected due to the small size of the core. We had to alter horizontal permeability as well, at normalized height of 0.6 to 80 md so as to match the experimental results at 360 seconds. Having matched the one-dimensional data, we went ahead and compared the two-dimensional saturation front pictures with our simulator output. Here also we got an adequate match on a picture-by-picture basis, as shown in **fig. 6.13**. To the left are the pictures appearing in Garg *et al*[3] paper and to the right are our simulator results.

6.2.2 Verification Through Finite Element Code

Our approach to verify the validity of the finite element code was the same as the finite difference code. The results of this are presented in **fig. 6.14**. The input capillary pressure and relative permeability curve are given in **fig. 6.17** and **fig. 6.18**. As was encountered in the FDM code as well, the match in case of 200 to 360 seconds range was the best. The data at 40 sec is considered as an anomalous data since it is in the region were buoyancy effect is still predominant. Here, as with FDM code, we had to put a streak of 10 md low permeability layer to get the output as shown in **fig. 6.14**. The weight gain data match is given in **fig. 6.15** and the trendline fit is given in **fig. 6.16**.

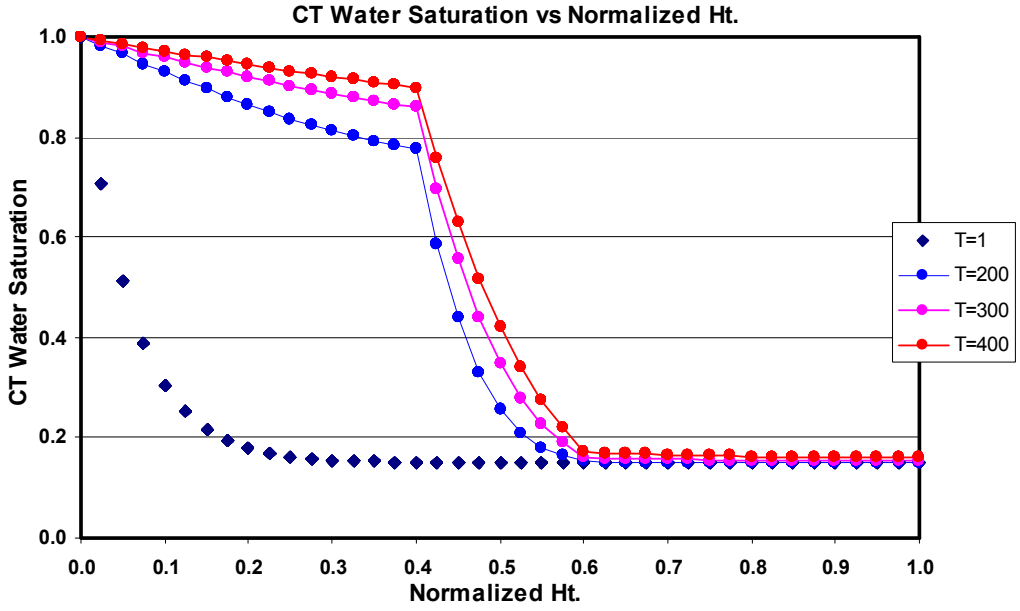

Figure 6.14 – Two-Dimensional Water Saturation Front Movement (FEM)

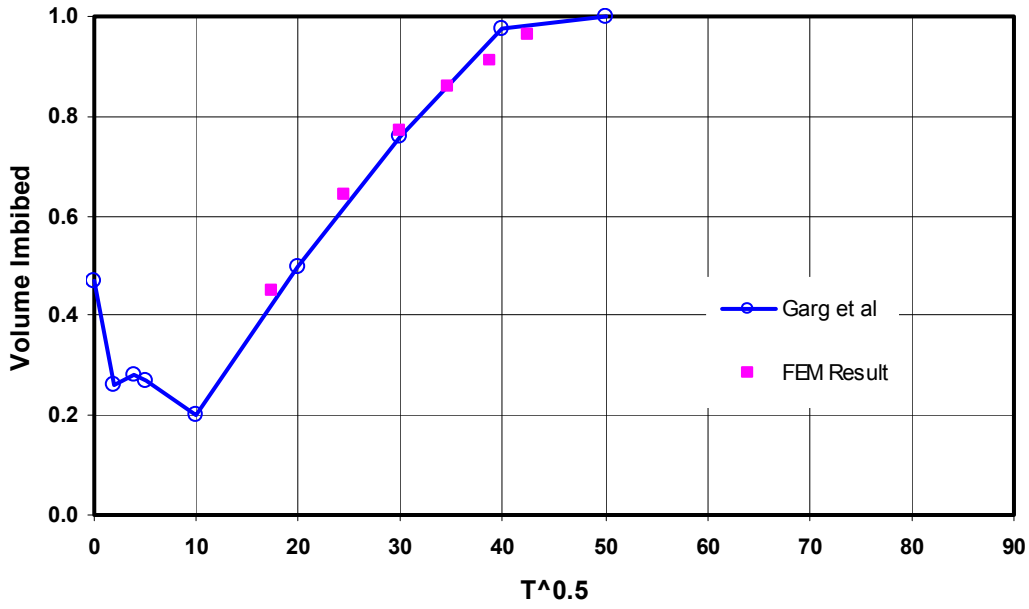

Figure 6.15 – Weight Gain Data Match Using FEM Code

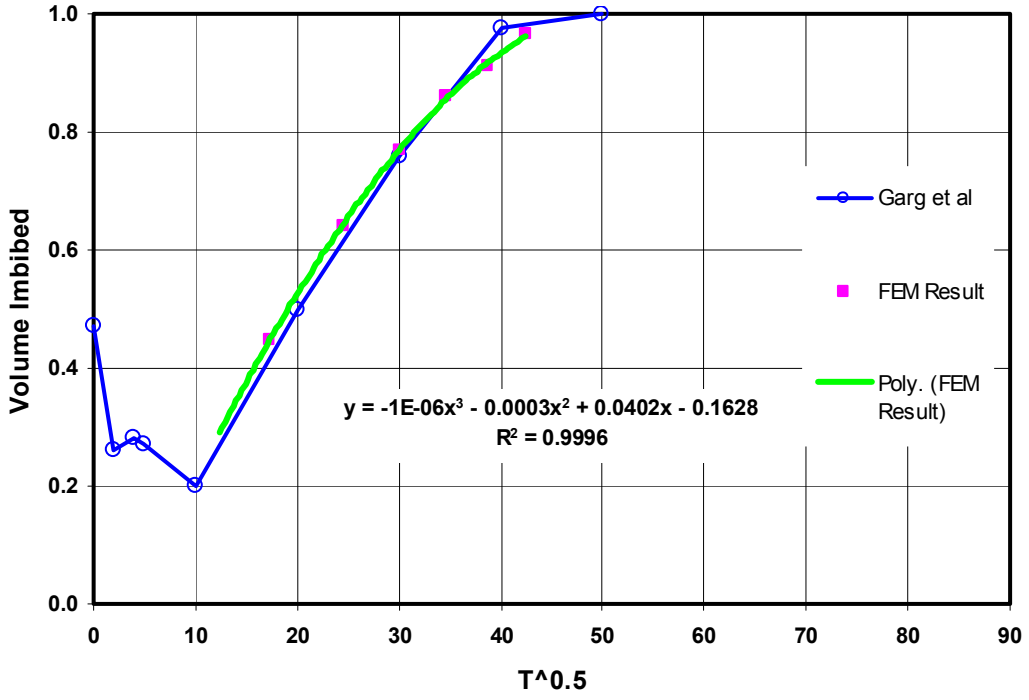

Figure 6.16 – Weight Gain Data Fit Using FEM Code

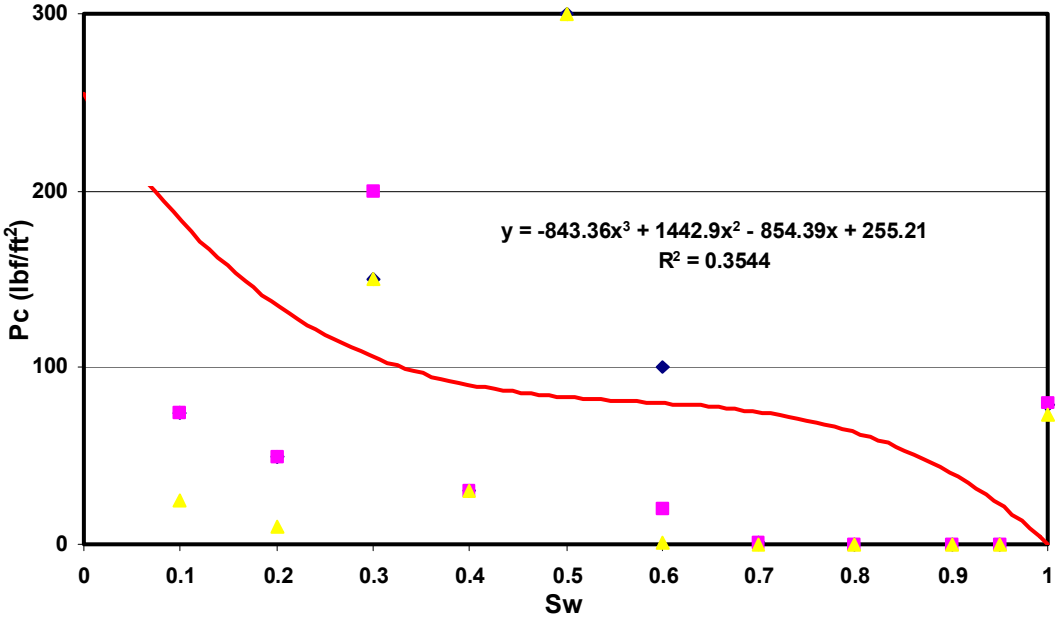

Figure 6.17 – Capillary Pressure Curve Used in FEM Code

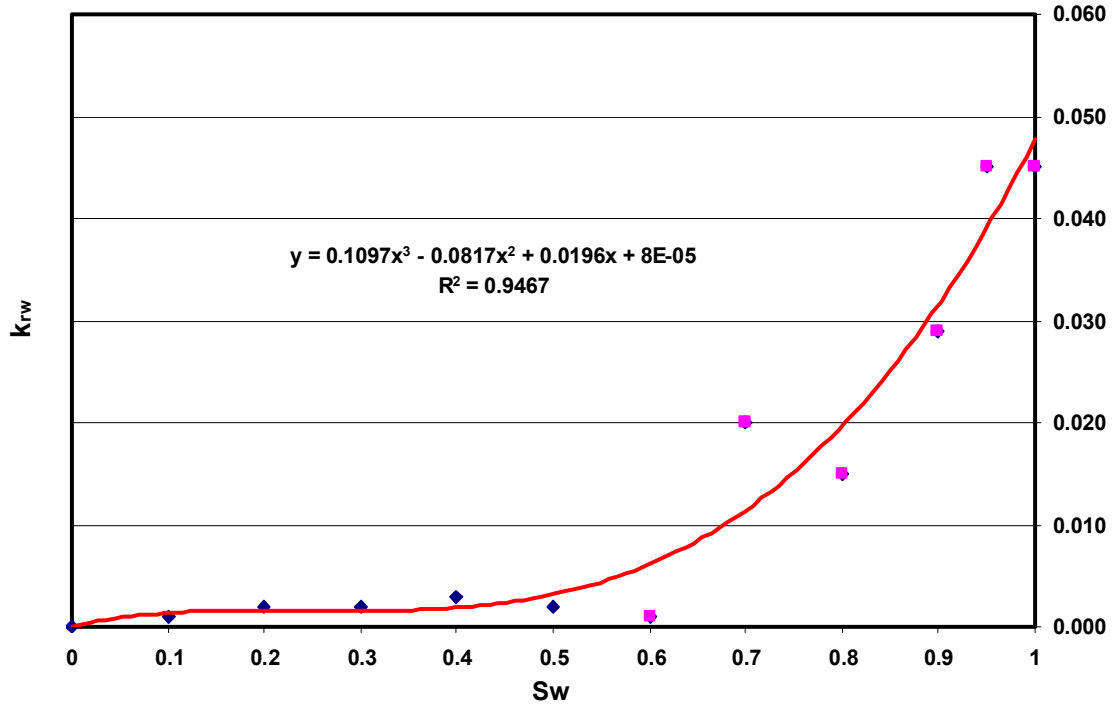

Figure 6.18 – Relative Permeability Curve Used in FEM Code

We did not perform the sensitivity test with the finite element code as it would have been a needless repetition of the FDM data.

6.3 Spontaneous Imbibition Experiments with Fractured Core

We also carried out our own experiments with fractured Berea core. The aim was to again put to test the validity of the FDM code and for its faithful reproduction of the experiment. For the experiment we used Berea core, 1.5 inches in diameter and 2.5 inches in height with an average permeability of around 200 md. It was first dried for 24 hours and then put in a water bath at the beginning of the experiment. Great care was taken so that the constant level of water was maintained at the bottom. The experiment was conducted at room temperature and normal tap water was used in the water bath. As can be seen from **fig. 6.19**, as soon as experiment was started the clock reported the actual time of the experiment. It took close to half an hour for the imbibition saturation front to travel from bottom to top. Initially, CT images were taken at one-minute time interval subsequently to be increased near the end of the experiment, as shown in **fig. 6.19**. The energy level used was 120 keV that gave us the best resolution. The step-by-step match is shown in **fig. 6.20**. The obvious point to be noticed here is that both **fig. 6.19** and **fig. 6.20** have the same number of time steps. Once again we used a variable capillary pressure curve and a variable relative permeability curve and obtained an adequate match. We did not reproduce this experiment with FEM code. For validation of the FEM code we went ahead with a field case which is discussed in subsequent section.

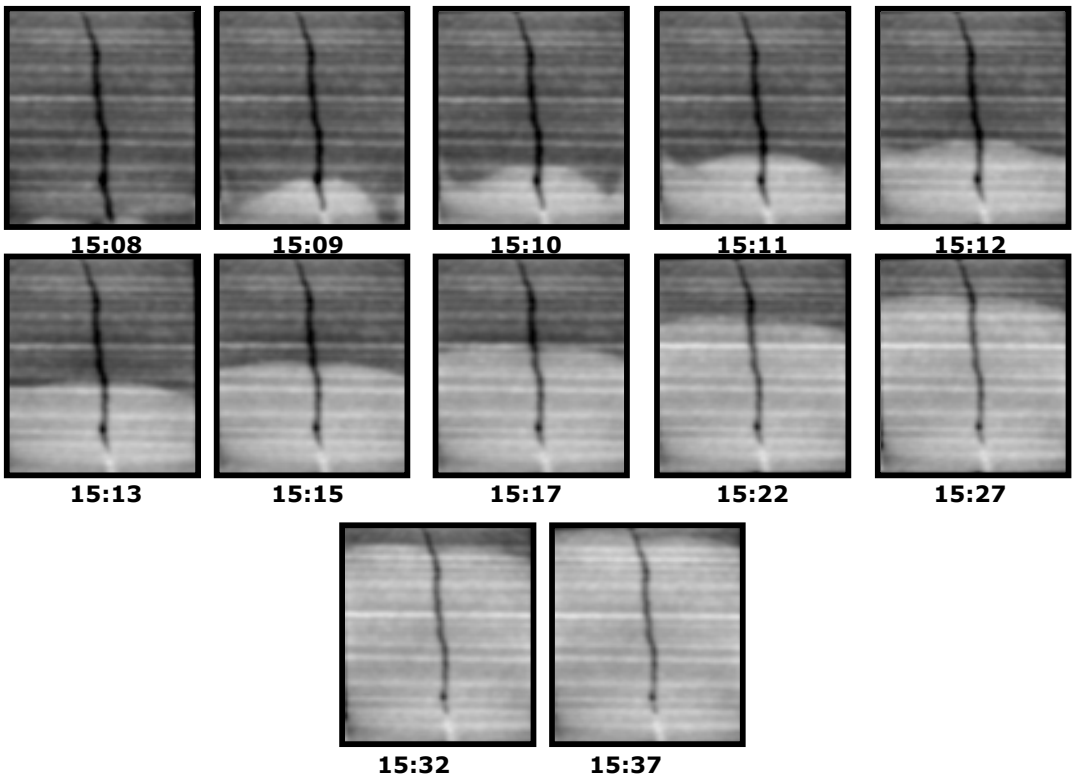

Figure 6.19 – Two-Dimensional CT Water Saturation Front Movement in Fractured Core

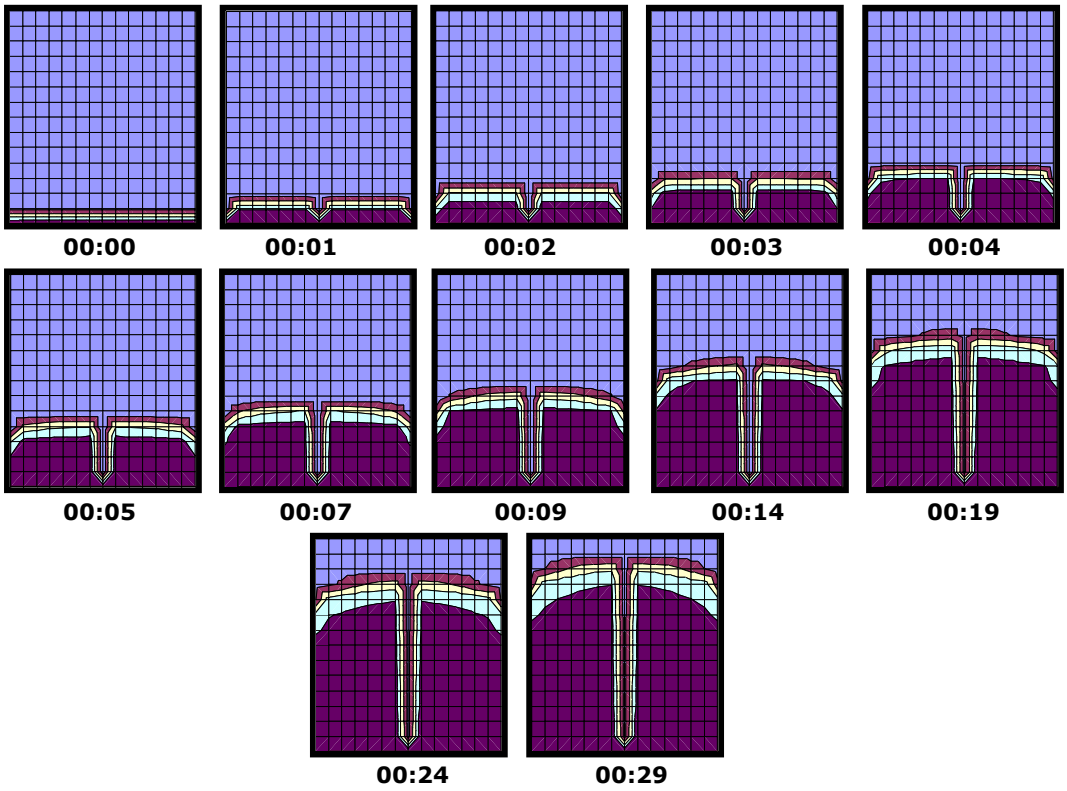

Figure 6.20 – Two-Dimensional Simulation Water Saturation Front Movement

6.4 Field-Size Spontaneous Imbibition Simulation

We extended this idea to spontaneous imbibition to field size imbibition study. This way we could prove the strength and the weaknesses of our approach. We generated a data set of a field sized 10 ft. X 10 ft. matrix block, represented in **Table 6.2** and ran the case as a CMG® dual porosity sub domain method simulation. **Fig. 6.21** and **fig. 6.22** give the capillary pressure and relative permeability used in simulation. The output of the simulation run is given in **fig. 6.23**.

TABLE 6.2 – Summary of Key Parameters Used in Dual Porosity Simulation

Parameters	Value
k	1 md
μ_W	0..35 cP
μ_o	0.275 cP
ϕ	0.29
n	0.5
S_{wi}	0.0

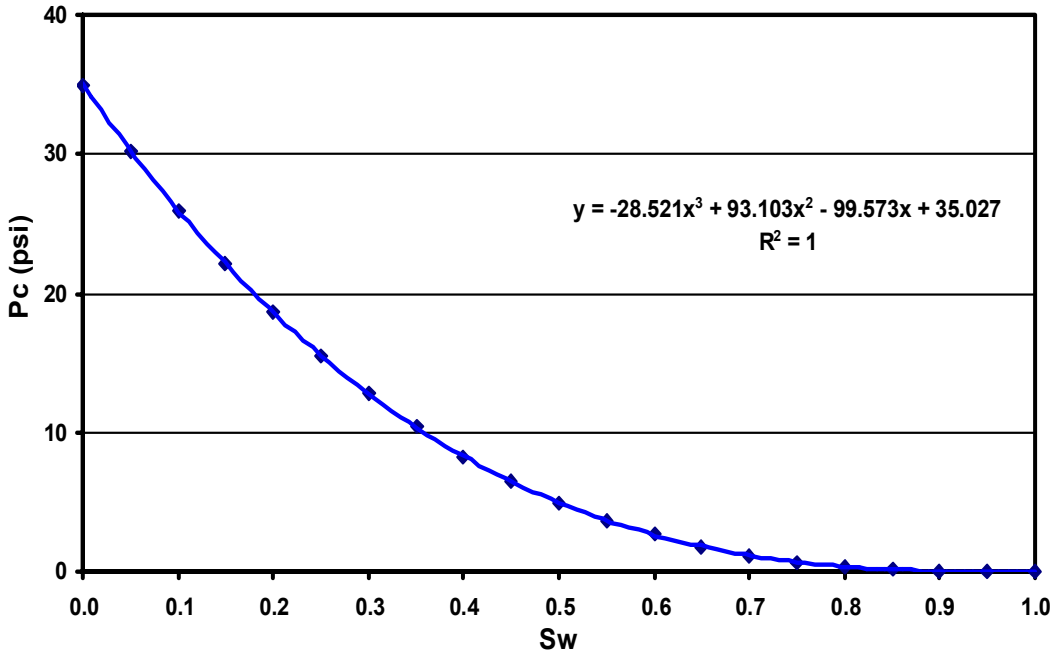

Figure 6.21 – Capillary Pressure Input Used in CMG

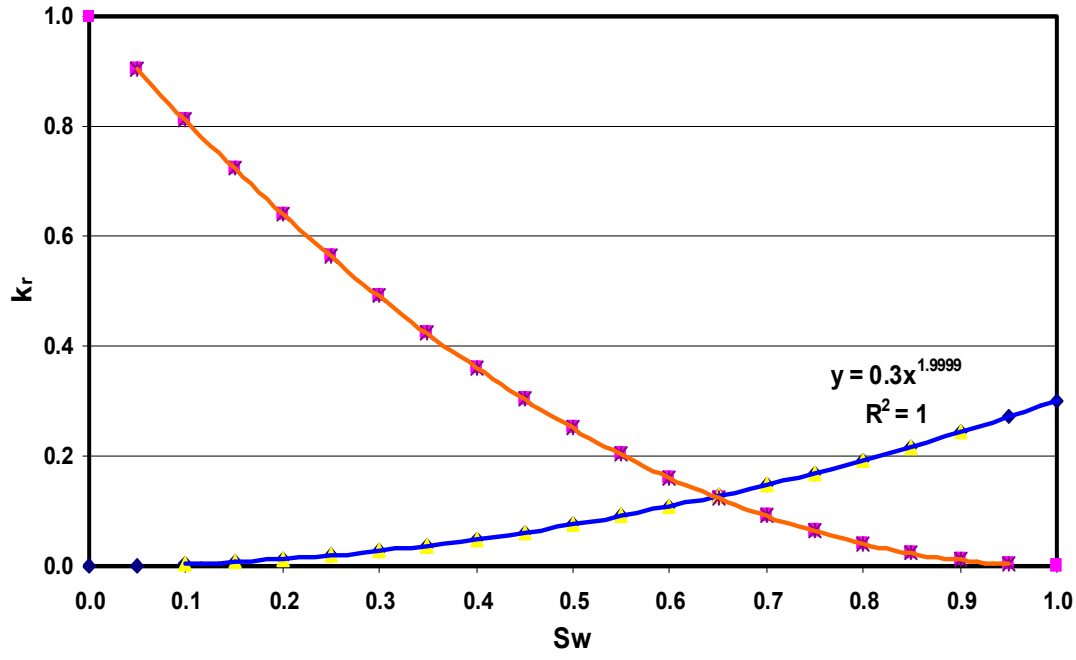

Figure 6.22 – Relative Permeability Input Used in CMG

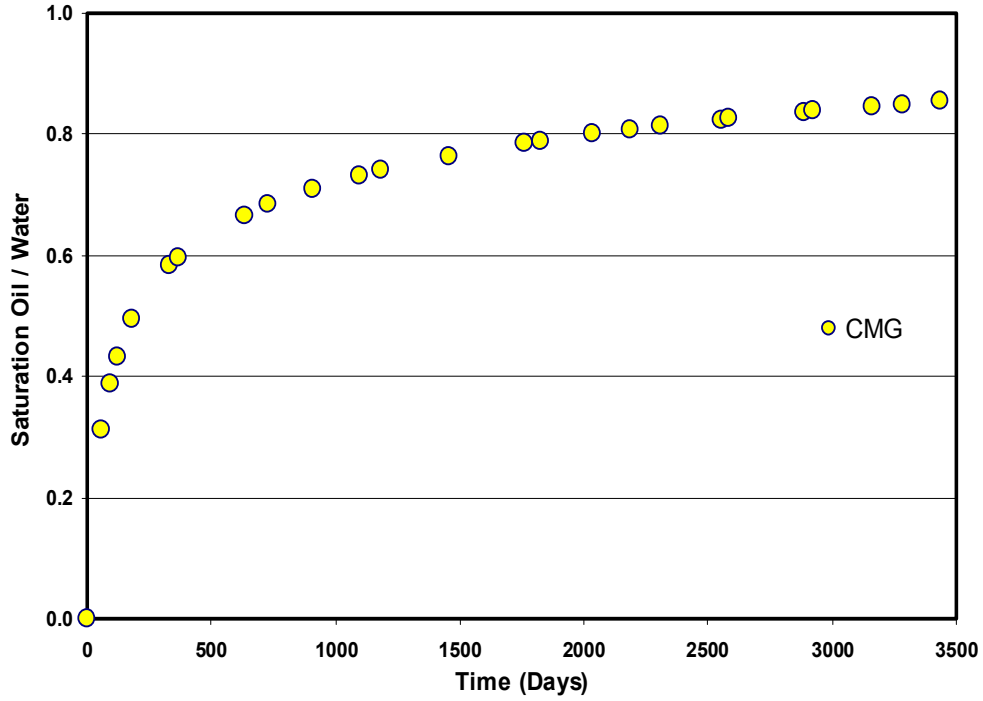

Figure 6.23 – Change of Average Saturation with Time Output of CMG

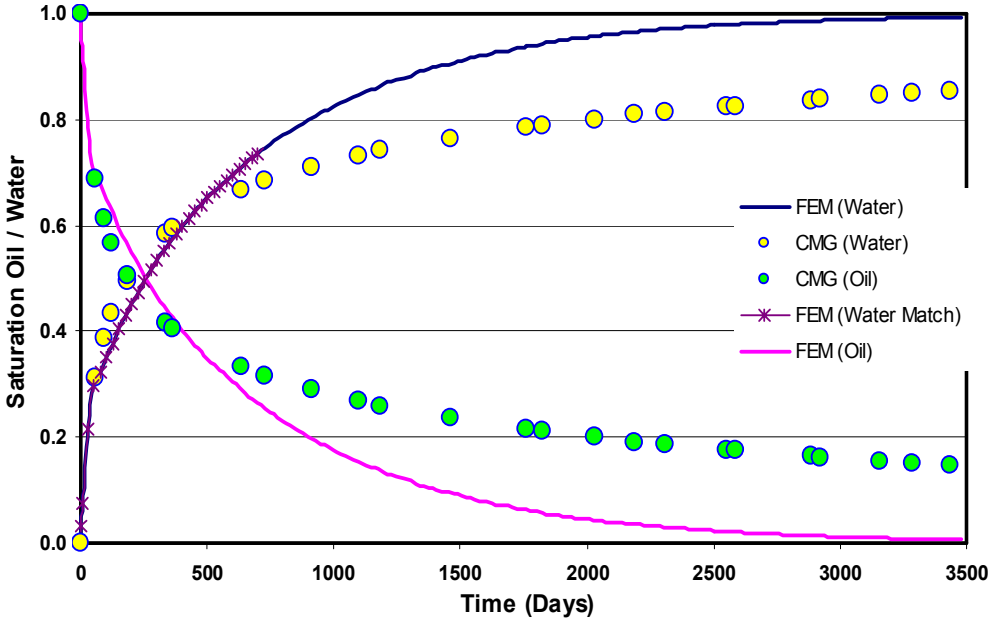

Figure 6.24 – Change of Average Saturation with Time Output of FEM vs. CMG

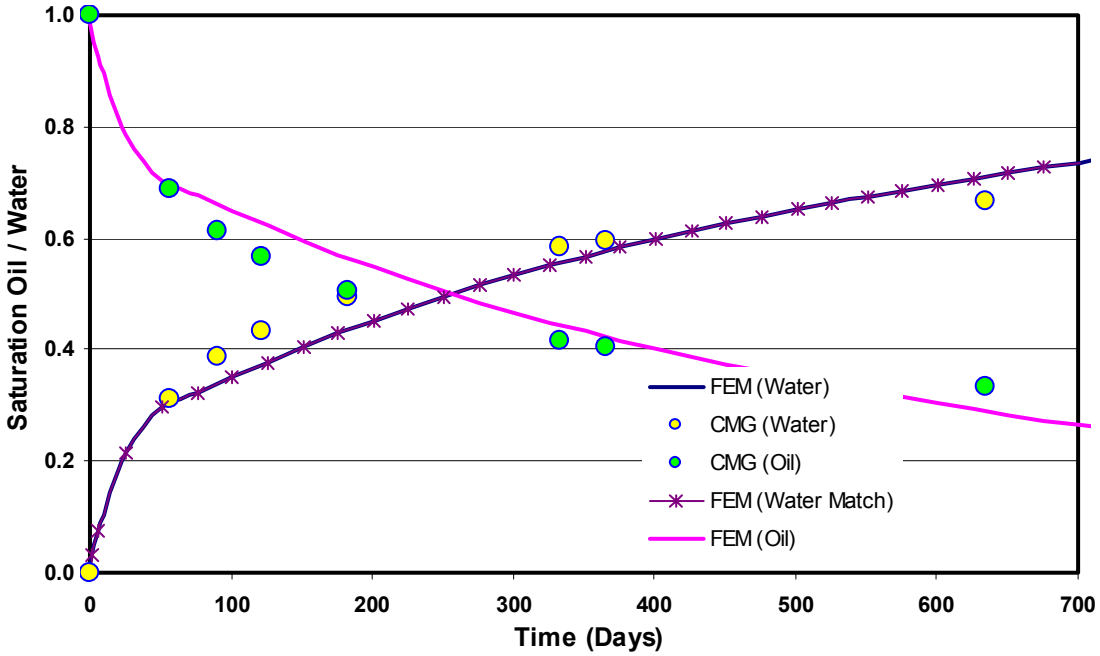

Figure 6.25 – Change of Average Saturation with Time Output of FEM vs. CMG

This is superposed with the results of FEM code are shown in **fig. 6.24** and **fig. 6.25**. It can be seen that there is a good match up to nearly 500 days after which the results diverge and clearly shows that our assumption has broken down. From that point onwards the validity of Rayleigh-Ritz method breaks down and we definitely have to use Galerkin methods with all its disadvantages.

CHAPTER VII

DISCUSSION AND CONCLUDING REMARKS

From the previous chapter we have come to conclusion that beyond a certain point our assumptions breakdown. It is interesting to know, according to our thinking, why the formulation breaks down. The spontaneous imbibition equation derived in the previous chapter was for one dimension. Rewriting this equation here:

$$\frac{\partial S_w}{\partial t} = \frac{\partial}{\partial x}\left[\frac{kk_{rw}k_{ro}}{\phi(\mu_w k_{ro} + \mu_o k_{rw})}\right]\left[-\left(\frac{\partial P_c}{\partial S_w}\frac{\partial S_w}{\partial x}\right) + g\Delta\rho\sin\alpha\right]$$

$$+\left[\frac{kk_{rw}k_{ro}}{\phi(\mu_w k_{ro} + \mu_o k_{rw})}\right]\frac{\partial}{\partial x}\left[-\left(\frac{\partial P_c}{\partial S_w}\frac{\partial S_w}{\partial x}\right) + g\Delta\rho\sin\alpha\right]$$

……..... (3.30)

Integrating both sides of this equation, we have:

$$\int\frac{\partial S_w}{\partial t} = \int\left\{\frac{\partial}{\partial x}\left[\frac{kk_{rw}k_{ro}}{\phi(\mu_w k_{ro} + \mu_o k_{rw})}\right]\left[-\left(\frac{\partial P_c}{\partial S_w}\frac{\partial S_w}{\partial x}\right) + g\Delta\rho\sin\alpha\right]\right\}dx$$

$$+\int\left\{\left[\frac{kk_{rw}k_{ro}}{\phi(\mu_w k_{ro} + \mu_o k_{rw})}\right]\frac{\partial}{\partial x}\left[-\left(\frac{\partial P_c}{\partial S_w}\frac{\partial S_w}{\partial x}\right) + g\Delta\rho\sin\alpha\right]\right\}dx$$

……..... (7.1)

The mobility ratio terms on the right hand side can be rearranged and written as:

$$k\int\left(\frac{\left(\frac{k_{rw}}{\mu_w}\right)}{\left(\frac{\mu_o}{\mu_w}\frac{k_{rw}}{k_{ro}} + 1\right)}\left[\left(\frac{dP_c}{dS}\right)\frac{dS}{dx} + \Delta\rho g\frac{dz}{dx}\right]\right)dx \qquad \text{……..... (7.2)}$$

This equation is of the form as given by the equation (7.3) which has a logarithmic solution.

$$\int \frac{s}{as+1} ds = \frac{s}{a} - \frac{1}{a^2} \ln[as+1] \qquad \text{…….... (7.3)}$$

When we apply the assumption that the saturation domain variables are not dependent on spatial coordinates and take them out of spatial integration, as shown in equation (7.4) we arrive at an expression of the form given by equation (7.5) which has a polynomial form solution.

$$k \left(\frac{\left(\frac{k_{rw}}{\mu_w} \right)}{\frac{\mu_o}{\mu_w} \frac{k_{rw}}{k_{ro}} + 1} \right) \int \left[\left(\frac{dP_c}{dS} \right) \frac{dS}{dx} + \Delta \rho g \frac{dz}{dx} \right] dx \qquad \text{…….... (7.4)}$$

$$a \int s ds = a \frac{s^2}{2} + C \qquad \text{…….... (7.5)}$$

This is the equation of parabola. Depending on the powers of variables used, this can be a higher order parabola as well. This is the reason why Rayleigh-Ritz method diverges from the actual solution. The proof of this can be seen in **fig. 7.1** where using the initial data we try to fit a logarithmic curve and subsequently extend the trendline. Almost all the points fall onto this line. Thus the decoupling of the saturation domain with spatial and temporal domain is not the reason for the break down of the solution. The reason is that the formulation after the decoupling process does not imitate the physical phenomenon. What can be done as a next step is to use oil and water equations separately so that the integrity of the original formulation is maintained.

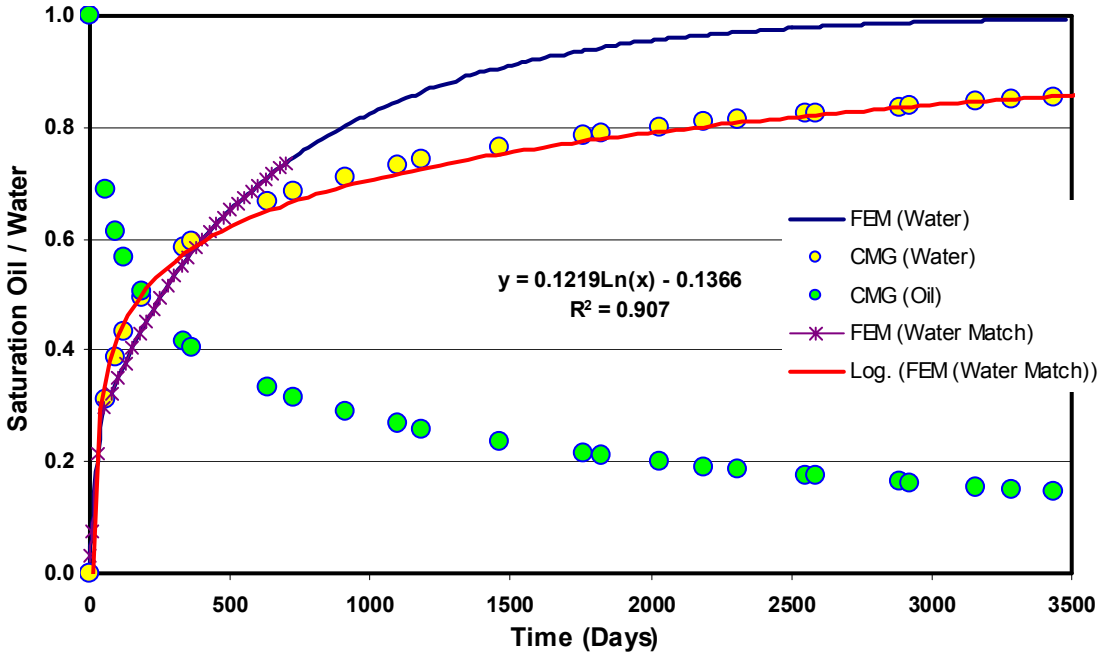

Figure 7.1 – Fitting of Logarithmic Trendline to Initial Part of FEM Solution

Hence we reach the following conclusions:

1. Proved Handy's equation (1960) with results from numerical simulation.
2. Matched weight-gain and CT water saturation obtained from Garg *et al.* experiment.
3. Modeled air-water spontaneous experiments in a fractured core.

NOMENCLATURE

A = matrix area (cm^2, ft^2)

A_{ma} = matrix face area (cm^2, ft^2)

B = bilinear part of weighted integral

C = constant

d_{ma} = distance of matrix face from the center of matrix block (cm, ft)

e = constant, 2.7182

g = acceleration due to gravity, ft^2 /sec

I = weighted integral

k_r = relative permeability (mD)

L = length (cm, ft)

l = linear part of weighted integral

N_{maRu}= total recovery from matrix

N_{CT} = CT number

n = saturation exponent

Δp = pressure drop across the core (psi, lbf /ft^2)

P_c = capillary pressure (psi, lbf /ft^2)

Q_w = amount of water imbibed

q_n = secondary variable of finite element equation

R = recovery of oil from matrix

S = Saturation

t = time of imbibition (seconds, hrs., days)

V = volume (cm^3, ft^3)

V_{ma} = volume of matrix block (cm^3, ft^3)

W'_{Iu} = amount of water imbibed

μ = viscosity (cp)

ϕ = porosity

σ = shape factor, ft^2

λ = exponential decline imbibition constant

w = effective fracture width (cm)

τ = shear stress

τ_I = matrix block imbibition time, time to produce $1-\frac{1}{e}=0.63$ of total oil

ρ = density (gm/cm^3, lbf/ft^3)

θ = integration parameter

γ = saturation exponent, Corey

Φ = fluid potential, psia

ψ = lagrange interpolation function

Subscripts

D = dimensionless variables

f = fracture

i = initial value

m = matrix

o = oil phase

w = water phase

x = x-direction

y = y-direction

z = z-direction

REFERENCES

1. Craig. Jr., F. F., *The Reservoir Engineering Aspect of Waterflooding*, Monograph Series, SPE, Vol. 3, 1993, 12-22.
2. Handy, L. L.: "Determination of Effective Capillary Pressures for Porous Media from Imbibition Data," *SPEJ Petroleum Transactions*, AIME, 1960, Vol. 219, 75-80.
3. Garg, A., Zwahlen, E. and Patzek, T.W.: "Experimental and Numerical Studies of One-Dimensional Imbibition in Berea Sandstone," presented at the 16th Annual American Geophysical Union Hydrology Days, Fort Collins, Colorado, (15-18 Apr, 1996).
4. Babadagli, T. and Ershaghi, I.: "Imbibition Assisted Two-Phase Flow in Natural Fractures," paper SPE 24044 presented at the 1992 SPE Western Regional Meeting, Bakersfield, California, Mar 30-Apr 1.
5. Li, K. and Horne, R.N.: "Characterization of Spontaneous Water Imbibition into Gas-Saturated Rocks," paper SPE 62552 presented at the 2000 SPE/AAPG Western Regional Meeting, Long Beach, California, 19-23 June.
6. Akin, S. and Kovscek, A. R.: "Imbibition Studies of Low-Permeability Porous Media," paper SPE 54590 presented at the 1999 SPE Western Regional Meeting, Anchorage, Alaska, 26-27 May.
7. Reis, J.C. and Cil, M.: "A Model for Oil Expulsion by Counter-Current Water Imbibition into Gas-Saturated Matrix Blocks," *J. Pet. Sci. & Eng.*, 10, 1998, 97-107.
8. Zhou, D., Kamath, J., and Kovscek, A. R.: "An Investigation of Counter-Current Imbibition Process in Diatomite," paper SPE 68837 presented at the 2001 SPE Western Regional Meeting, Bakersfield, California, 26-30 Mar.
9. Barenblatt, G. I., Zheltov, I. P., and Kochina, I.N.: "Basic Concepts in the Theory of Seepage of Homogeneous Liquids in Fissured Rocks," Prikl. Mat. Mekh., 24, 1960, 852-864. (English Translation: *J. Appl. Mech.*, 24, 1960, 1286-1303.
10. Warren, J. E., and Root, P. J.: "The Behavior of Naturally Fractured Reservoirs," *SPEJ Petroleum Transactions*, AIME, 1963, Vol. 228, 245-255.
11. Mattax, C. C., and Kyte, J. R.: "Imbibition Oil Recovery from Fractured, Water-Drive Reservoirs," *SPEJ Petroleum Transactions*, AIME, 1962, Vol. 225, 175-184.
12. de Swaan, A.: "Theory of Waterflooding in Fractured Reservoirs," *SPEJ Petroleum Transactions*, AIME, 1978, Vol. 219, 117-122.

13. Kazemi, H., Merrill. Jr., L. S., Porterfield, K. L, and Zeman, P. R.: "Numerical Simulation of Water-Oil Flow in Naturally Fractured Reservoirs," *SPEJ Petroleum Transactions*, AIME, 1976, Vol. 219, 317-325.

14. Firoozabadi, A., and Hauge, J.: "Capillary Pressure in Fractured Porous Media," paper SPE 18747 presented at the 1989 SPE California Regional Meeting, Bakersfield, California, 5-7 Apr.

15. Kazemi, H., Gilman, J. R., and Elsharkawy, A. M.: "Analytical and Numerical Solution of Oil Recovery from Fractured Reservoirs with Empirical Transfer Functions," *SPERE*, (May 1992), 219-227.

16. Guzman, R. E., and Aziz, K.: "Fine Grid Simulation of Two-Phase Flow in Fractured Porous Media," paper SPE 24916 presented at the 1992 SPE Annual Technical Conference and Exhibition, Washington D. C., 4-7 Oct.

17. Civan, F.: "Waterflooding of Naturally Fractured Reservoirs: An Efficient Simulation Approach," paper SPE 25449 presented at the 1993 Production Operations Symposium, Oklahoma City, Oklahoma, 21- 23 Mar.

18. Schechter, D. S. and Guo, B.: "An Integrated Investigation for Design of a CO_2 Pilot in the Naturally Fractured Spraberry Trend Area," paper SPE 39881 presented at the 1998 SPE International Petroleum Conference and Exhibition, Villahermosa, Mexico, 3-5 Mar.

19. Wattenbarger, R. A.: *PETE* 603-601: *Advanced Reservoir Simulation*, Class Notes, Texas A&M University, 2002.

20. Reddy, J. N., *An Introduction to Finite Element Method*, McGraw-Hill Inc., New York (1993).

21. Reddy, J. N. and Gartling, D.K., *The Finite Element Method in Heat Transfer and Fluid Dynamics*, CRC Press, Boca Raton, Florida (2001).

22. Corey, A. T.: *Mechanics of Immiscible Fluids in Porous Media*, Water Resources Publications, Denver, Colorado (1994).

23. Javandel, I., and Witherspoon, P. A.: "Application of the Finite Element Method to Transient Flow in Porous Media," *SPEJ Petroleum Transactions*, AIME, 1968, Vol. 243, 241-252.

24. Spivak, A., Price, H. S., and Settari, A.: "Solution of the Equations for Multidimensional, Two-Phase, Immiscible Flow by Variational Methods," paper SPE 5723 presented at the 1977 SPE Numerical Simulation of Reservoir Performance Symposium, Houston, Texas, 10-12 Jan.

25. Young, L. C.: "A Finite Element Method for Reservoir Simulation," ," paper SPE 7413 presented at the 1978 SPE Annual Technical Conference and Exhibition, Houston, Texas, 1-4 Oct.

26. McMicheal, C. L., and Thomas, G. W.: "Reservoir Simulation by Galerkin's Method," *SPEJ* (June 1973) 125-138.

27. Darlow, B. L., Ewing, R. E., and Wheeler, M. F.: "Mixed Finite Element Method for Miscible Displacement Problems in Porous Media," paper SPE 10501 presented at the 1982 Reservoir Simulation Symposium, New Orleans, Louisiana, 31 Jan – 3 Feb.

28. Chavent, G., Cohen, G., Jaffre, J., Eymard, R., Guerillot, D. R., and Weill, L.: Discontinuous and Mixed Finite Element Method for Two-Phase Incompressible Flow," paper SPE 16018 presented at the 1987 Reservoir Simulation Symposium, San Antonio, Texas, 1- 3 Feb.

29. Ewing, R. E., Russell, T. F., and Wheeler, M. F.: "Simulation of Miscible Displacement Using Mixed Methods and a Modified Method of Characteristics," paper SPE 12241 presented at the 1983 Reservoir Simulation Symposium, San Francisco, California, 15- 18 Nov.

30. Asfari, A., and Witherspoon, P. A.: "Numerical Simulation of Naturally Fractured Reservoirs," paper SPE 4290 presented at the 1973 SPE Numerical Simulation of Reservoir Performance Symposium, Houston, Texas, 10-12 Jan.

31. Bhatia, K. S., Advani, S. H., and Lee, J. K.: "Finite Element Representation of Two-Phase Flow Through a Naturally Fracture Reservoir," paper SPE 19069 presented at the 1989 SPE Gas Technology Symposium held in Dallas, Texas, 7-9 Jun.

32. Naji, H. S., and Kazemi, H.: "A Fully Implicit, Three Dimensional, Two Phase, Control Volume Finite Element Model for the Simulation of Naturally Fractured Reservoirs," paper SPE 71615 presented at the 1996 SPE Abu Dhabi International Petroleum Exhibition and Conference, Abu Dhabi, U.A.E., 13-16 Oct.

33. Sutopo, and Arihara, N.: "Accurate and Effective Simulation of Reservoirs of Complex Geological Features," paper SPE 77903 presented at the 2002 SPE Asia Pacific Oil and Gas Conference and Exhibition held in Melbourne, Australia, 8-10 Oct.

34. Karimi-Fard, M., and Firoozabadi, A.: "Numerical Simulation of Water Injection in 2D Fractured Media Using Discrete-Fracture Model" paper SPE 71615 presented at the 2001 SPE Annual Technical Conference and Exhibition held in New Orleans, Louisiana, 30 September-3 October.

35. Iqbal, G. M. and Civan, F.: "Reservoir Simulation Based on the Finite Analytic Method," paper SPE 15625 presented at the 1986 Annual Technical Conference and Exhibition, New Orleans, Louisiana, 5-8 Oct.

36. Dalen, V.: "Simplified Finite Element Models for Reservoir Flow Problems," *SPEJ Petroleum Transactions*, AIME, 1979, 333-343.

37. Huang, H. K., *Elements of Digital Radiology: A Professional Handbook and Guide*, Prentice-Hall Inc., Englewood Cliffs, New Jersey (1987).

38. Snow, D.T.: "A Parallel Plate Model of Fractured Permeable Media," Ph.D. Dissertation, University of California, Berkeley, (1965).

39. Bird, R. B., Stewart, W. E., and Lightfoot, E. N., *Transport Phenomena*, John Wiley & Sons, Inc., New York (1960).

40. Iwai, K.: "Fundamental Studies of Fluid Flow Through a Single Fracture," Ph.D. Dissertation, University of California, Berkeley, (1976).

41. Cornwell D.K., and Murphy, H. D.: "Experiments with non-darcy flow in joints with large scale roughness," *Proc.* Int. Symp. on Fundamentals of Rock Joints, Centek, Lulea, France (1985), 323–334.

42. Qadeer, S., Dehghani, K., Ogbe, D. O., Ostermann, R. D.: "Correcting Oil/Water Relative Permeability Data for Capillary End Effect in Displacement Experiments," paper SPE 17423 presented at the 1988 SPE California Regional Meeting, Long Beach, California, , 23-25 March.

43. Sahimi, M.: *Flow and Transport in Porous Media and Fractured Rock*, VCH, New York (1995), 158 - 161.

44. Adams, R. A.: *Calculus – A Complete Course*, Addison Wesley, Don Mills, Ontario (1999), 317-321.

45. Reddy, J. N.: "FEM2DV1 Finite Element Program," *An Introduction to Finite Element Method*, McGraw-Hill Inc., New York (1993).

APPENDIX A

SOLUTION OF SATURATION DOMAIN VARIABLES INTEGRATION THROUGH MAPLE ®

```
> int(s^4*(1-s^2)*(1-s)^2/(a*s^4+(1-s^2)*(1-s)^2),s);
```

$$-\frac{s^5}{5(a-1)}+\frac{a\,s^4}{2(a-1)^2}-\frac{4\,a\,s^3}{3(a-1)^3}-\frac{a^3\,s^2}{(a-1)^4}+\frac{2\,a^2\,s^2}{(a-1)^4}+\frac{3\,a\,s^2}{(a-1)^4}+\frac{a^4\,s}{(a-1)^5}$$
$$+\frac{5\,a^3\,s}{(a-1)^5}-\frac{13\,a^2\,s}{(a-1)^5}-\frac{9\,a\,s}{(a-1)^5}-a\left(\sum_{\_R=\mathrm{RootOf}(1+(a-1)\_Z^4+2\_Z^3-2\_Z)}\left(\right.\right.$$
$$(-12+4\,a^3+12\,a^2-36\,a)\,\_R^3+(4\,a^3+8-16\,a^2+4\,a)\,\_R^2$$
$$+(12-4\,a^3-4\,a^2+28\,a)\,\_R+a^3+5\,a^2-13\,a-9)\ln(s-\_R)\Big/\Big($$
$$\left.\left.4\,\_R^3\,a-2+6\,\_R^2-4\,\_R^3\right)\right)\Big/(a-1)^5$$

```
> int(c*s^4*d*(1-s^2)*(1-s)^2/(a*c*s^4+b*d*(1-s^2)*(1-
s)^2),s);
```

$$-\frac{c\,d\,s^5}{5(a\,c-b\,d)}+\frac{c^2\,d\,a\,s^4}{2(a\,c-b\,d)^2}-\frac{4\,c^2\,d^2\,a\,b\,s^3}{3(a\,c-b\,d)^3}-\frac{c^4\,d\,a^3\,s^2}{(a\,c-b\,d)^4}+\frac{2\,c^3\,d^2\,a^2\,s^2\,b}{(a\,c-b\,d)^4}$$
$$+\frac{3\,c^2\,d^3\,a\,s^2\,b^2}{(a\,c-b\,d)^4}+\frac{c^5\,d\,a^4\,s}{(a\,c-b\,d)^5}+\frac{5\,c^4\,d^2\,a^3\,s\,b}{(a\,c-b\,d)^5}-\frac{13\,c^3\,d^3\,a^2\,s\,b^2}{(a\,c-b\,d)^5}-\frac{9\,c^2\,d^4\,a\,s\,b^3}{(a\,c-b\,d)^5}$$
$$-c^2\,d^2\,a\,b\left(\sum_{\_R=\mathrm{RootOf}((a\,c-b\,d)\_Z^4+2\,b\,d\,\_Z^3-2\,b\,d\,\_Z+b\,d)}\left(\right.\right.$$
$$(-12\,b^3\,d^3+4\,a^3\,c^3+12\,a^2\,c^2\,b\,d-36\,b^2\,d^2\,a\,c)\,\_R^3$$
$$+(4\,b^2\,d^2\,a\,c+8\,b^3\,d^3-16\,a^2\,c^2\,b\,d+4\,a^3\,c^3)\,\_R^2$$
$$+(28\,b^2\,d^2\,a\,c-4\,a^3\,c^3-4\,a^2\,c^2\,b\,d+12\,b^3\,d^3)\,\_R+a^3\,c^3+5\,a^2\,c^2\,b\,d$$
$$\left.\left.-13\,b^2\,d^2\,a\,c-9\,b^3\,d^3)\ln(s-\_R)\Big/(4\,\_R^3\,a\,c-2\,b\,d+6\,\_R^2\,b\,d-4\,b\,d\,\_R^3)\right)\right.$$
$$\Big/(a\,c-b\,d)^5$$

>

APPENDIX B

DISCUSSION ON ALTERNATIVE APPROACH – IMBIBITION BOUNDARY CONDITION

We begin with equation (5.45) which is reproduced below:

$$0 = \int \left[w\left(1 + \frac{\rho_w}{\rho_o}\right)\frac{\partial S_w}{\partial t} \right] dxdy$$

$$+ \frac{1}{\phi}\int \frac{\partial w}{\partial x}\left[\frac{kk_{rw}k_{ro}}{(\mu_w k_{ro} + \mu_o k_{rw})} \right]\left[\left(\left(\frac{\partial \Phi_c}{\partial S_w} \right)\frac{\partial S_w}{\partial x} \right) \right] dxdy$$

$$+ \frac{1}{\phi}\int \frac{\partial w}{\partial y}\left[\frac{kk_{rw}k_{ro}}{(\mu_w k_{ro} + \mu_o k_{rw})} \right]\left[\left(\left(\frac{\partial \Phi_c}{\partial S_w} \right)\frac{\partial S_w}{\partial y} \right) \right] dxdy$$

$$- \int wfdxdy - \oint_{\Gamma^e} wq_n ds \quad \text{…….....} \quad (5.45)$$

where the boundary term is given by the secondary variable represented by:

$$\oint_{\Gamma^e} wq_n ds = \oint_{\Gamma^e}\left[wM\left(\frac{\partial \Phi_c}{\partial S_w}\left(\frac{\partial S_w}{\partial x} \right) \right) \right] n_x ds + \oint_{\Gamma^e}\left[wM\left(\frac{\partial \Phi_c}{\partial S_w}\left(\frac{\partial S_w}{\partial y} \right) \right) \right] n_y ds \quad \text{…….....} \quad (5.17)$$

Our discussion is mainly centered on this secondary variable. If we recall, here;

$$M = \frac{kk_{rw}k_{ro}}{\phi(\mu_w k_{ro} + \mu_o k_{rw})}$$

and

$$u_w = \left(\frac{kk_{rw}k_{ro}}{\mu_w k_{ro} + \mu_o k_{rw}} \right) \left(\frac{\partial P_c}{\partial x} - g\Delta\rho \sin\alpha \right) \qquad \text{…….....} \quad (3.27)$$

Thus,

$$u_w = M\left(\frac{\partial P_c}{\partial x} - g\Delta\rho \sin\alpha \right) = -M\left(\frac{\partial \Phi_c}{\partial x} \right) = -M\left(\left(\frac{\partial \Phi_c}{\partial S_w} \right) \frac{\partial S_w}{\partial x} \right) \text{…….....} \quad (B.1)$$

This expression, when integrated along a line, tells us that the secondary variable is the flux at the boundary because of the viscous forces represented by *M*, capillary forces represented by $\left(\frac{\partial \Phi_c}{\partial S_w} \right)$, and gravity forces represented by $g\Delta\rho \sin\alpha$ are being integrated along a line. In our case, as we are assuming that $\left(\frac{\partial \Phi_c}{\partial S_w} \right)_{S_w=1.0} = 0$, the whole of secondary variable becomes zero. If spontaneous imbibition is occurring at the boundary there is no way we can account for this phenomenon by equation (5.17) alone. Thus there arises the need to modify the secondary variable to include this.

We go back to the theory of spontaneous imbibition and reproduce the following equation:

$$u_w = -u_o \qquad \text{…….....} \quad (3.26)$$

This phenomenon is happening only on the boundary of the porous media where the fracture borders the matrix. In order to quantify it, we follow a dual porosity approach as proposed by Warren and Root and extended by Kazemi *et al* that the matrix block is in pseudo-steady state condition and the flow from the outside into it can be quantified by the following equations for water and oil:

$$\tilde{u}_w = \frac{kk_{rw}}{\mu_w} \left(\Delta\Phi_{wm} - \Delta\Phi_{wf} \right) \qquad \text{…….....} \quad (B.2a)$$

$$\widetilde{u}_o = \frac{kk_{ro}}{\mu_o}\left(\Delta\Phi_{om} - \Delta\Phi_{of}\right) \qquad \text{..... (B.2b)}$$

Combining equations (B.2a) and (B.2b) we have:

$$\frac{\widetilde{u}_o\mu_o}{kk_{ro}} - \frac{\widetilde{u}_w\mu_w}{kk_{rw}} = \left(\Delta\Phi_{cm} - \Delta\Phi_{cf}\right) \qquad \text{..... (B.3)}$$

Using equation (3.26) we have and assuming capillary pressure potential is zero in the fracture, we have:

$$\widetilde{u}_w = -\left(\frac{kk_{ro}k_{rw}}{\mu_o k_{rw} + \mu_w k_{ro}}\right)\Delta\Phi_{cm} \qquad \text{..... (B.4)}$$

which can be rewritten as:

$$\widetilde{u}_w = -\left(\frac{kk_{ro}k_{rw}}{\mu_o k_{rw} + \mu_w k_{ro}}\right)\left(\frac{\Delta\Phi_{cm}}{\Delta S_w}\right)\Delta S_w \qquad \text{..... (B.5)}$$

This is the additional boundary condition term that must be added in equation (5.17). Here A_s is the area of each face of control volume through which imbibition is taking place and V is the volume. Hence taking into account this condition we modify the boundary variable and have:

$$\left[wM\left(\frac{\partial\Phi_c}{\partial S_w}\left(\frac{\partial S_w}{\partial x}\right)\right)\right]n_x + \left[wM\left(\frac{\partial\Phi_c}{\partial S_w}\left(\frac{\partial S_w}{\partial y}\right)\right)\right]n_y = q_n + \widetilde{u}_w \qquad \text{..... (B.6)}$$

The negative sign indicates that the spontaneous imbibition process takes place in opposite direction to q_n, which happens from the porous media to the boundary.

Let us assume $\left(S_w\right)_\infty$ as the saturation outside the boundary, then:

$$\Delta S_w = \left[S_w - \left(S_w \right)_\infty \right] \qquad \text{..... (B.7)}$$

Thus the final form of finite element equation is:

$$0 = \int \left[w \left(1 + \frac{\rho_w}{\rho_o} \right) \frac{\partial S_w}{\partial t} \right] dxdy$$

$$+ \frac{1}{\phi} \int \frac{\partial w}{\partial x} \left[\frac{k k_{rw} k_{ro}}{\left(\mu_w k_{ro} + \mu_o k_{rw} \right)} \right] \left[\left(\left(\frac{\partial \Phi_c}{\partial S_w} \right) \frac{\partial S_w}{\partial x} \right) \right] dxdy$$

$$+ \frac{1}{\phi} \int \frac{\partial w}{\partial y} \left[\frac{k k_{rw} k_{ro}}{\left(\mu_w k_{ro} + \mu_o k_{rw} \right)} \right] \left[\left(\left(\frac{\partial \Phi_c}{\partial S_w} \right) \frac{\partial S_w}{\partial y} \right) \right] dxdy$$

$$- \int w f dxdy - \oint_{\Gamma^e} w \left[q_n - \left(\frac{k k_{ro} k_{rw}}{\phi \left(\mu_o k_{rw} + \mu_w k_{ro} \right)} \right) \left(\frac{\Delta \Phi_{cm}}{\Delta S_w} \right) \left[S_w - \left(S_w \right)_\infty \right] \right] ds$$

..... (B.8)

VITA

SANDEEP KAUL
1502 – 34th Street, S. E.
Calgary, AB T2A 1A1, Canada
Tel: (403) 265-0512

EDUCATION

Texas A&M University, College Station, TX	Master of Science (Petroleum Engineering)	2001 - 03
Southern Alberta Institute of Technology	Bachelor of Applied Petroleum Engineering Technology (Honors)	1996 - 97
G. B. Pant University, Pantnagar, India	Bachelor of Technology (Civil Engineering)	1983 - 87

CITIZENSHIP

Canadian

CAREER HISTORY

TEXAS A&M UNIVERSITY, College Station, TX	2001 - Present
POLAR COMPLETIONS ENGINEERING INC., Calgary, AB	1999 - 2001
BAKER OIL TOOLS, BAKER HUGHES CANADA INC., Red Deer, AB	1997 - 1999
OIL & NATURAL GAS CORPORATION LTD., INDIA	1989 - 1996
CONSULTANT (Self Employed)	1987 - 1989